Scuola di Dottorato di Ricerca in Scienze Molecolari
XXXI ciclo Università degli Studi di Padova
Dipartimento di Scienze Chimiche

GRAPHENE-BASED DONOR ACCEPTOR SYSTEMS

DIRETTORE DELLA SCUOLA: *Prof.* Leonard Prins

SUPERVISORE: *Prof.* Michele Maggini

DOTTORANDA: Meng Zheng

MAY 2019

Fondazione
Cassa di Risparmio
di Padova e Rovigo

Acknowledgement

I would like to express my sincere gratitude to my supervisor Prof. Michele Maggini, for giving me an opportunity to carry out my Ph.D under his supervision. In the past three years, he firmly supported and kindly encouraged me on my research. I appreciated his efforts, and I respect his patience, motivation and immense knowledge.

Sincerely, I give many thanks to Prof. Enzo Menna, Prof. Tommaso Carofiglio and Prof. Miriam Mba Blazquez in our group, with whom I enjoyed a free work atmosphere. I also would like to thank my colleagues Dr. Teresa Gatti, Mr. Nicola Vicentini and Mr. Andrea Faresin, for their kindly help and support. I extend sincere thanks to Ms. Sushmitha Chandrabhas for her efforts on my English improvement.

Thanks to the CARIPARO scholarship for funding my three years Ph.D. study in the University of Padua, and thanks to my schoolmates Ms. Xiaohuan Sun, Mr. Chuanyu Sun, Mr. Yan Hu, Mr. Yanchao Lyu, Ms. Rui Chen, Ms. Jiaying Yu, et al. and all the people who have helped me in the past three years.

I extend my sincere thanks to my best friends that I met in Padua: Ms. Xue Li, Dr. Qianqian Li & Dr. Riccardo Spolaor, Ms. Huijing Yin & Dr. Lei Chang, with their accompany I spent a wonderful time in Padova.

Finally, I gave my great thanks to my family. Thanks to my parents Mr. Zhongdong Zheng and Mrs. Shujuan Chen for their kindness upbring and support, thanks to my grandparents Mr. Guixin Zheng and Mrs. Shulan Chen for their meticulous care and love, thanks to my little brother Mr. Qun Zheng for nothing in particular. I love you all.

2019. 05.01 Padua

致谢

衷心地感谢我的导师 MICHELE MAGGINI 教授，感谢他给我机会在他的指导下完成我的博士学位。在过去的三年里，他十分坚定地支持我的研究计划，并在我感到迷茫时给予及时的鼓励。我感激他为我花费的精力，敬重他的谆谆教诲，砥砺奋进和渊博学识。

非常感谢我们实验团队的 Enzo Menna 教授，Tommaso Carofiglio 教授和 Miriam Mba Blazquez 教授，他们营造了一个自由的科研氛围。同时，我要郑重感谢我的同事 Teresa Gatti 博士， Nicola Vicentini 先生和 Andrea Farsin 先生，感谢他们对我日常学习工作的帮助。感谢 Sushmitha Chandrabhas 帮助我辅导英文。

感谢 CARIPARO 奖学金资助我在帕多瓦大学攻读三年博士学位，感谢我的同窗好友孙晓环，孙传禹，胡言，吕艳超，陈蕤，蔚佳莹等，以及所有在过去三年里帮助过我的人。

同时，我真诚地感谢我在帕多瓦遇到的最好的小伙伴儿们：雪，倩倩博士和 Riccardo 博士，小静和畅磊博士，谢谢你们陪我一起在帕多瓦度过的快乐时光。

最后，我感谢我的家人。叩谢我的父母郑中东先生和陈述娟夫人的养育之恩，拜谢我的祖父母郑桂欣先生和陈述兰女士的惦念之情，感谢我的小弟群崴然而并没有什么要多说的。我爱你们。

<div align="right">2019 年 5 月 1 日 于帕多瓦</div>

Abstract

An efficient method to exfoliate graphite to prepare exfoliated few-layer graphene (**EXG**) was carried out in this thesis. Through proper centrifugation at different rounds per minute (rpm), three kinds of exfoliated graphene flakes (**EXG 800**, **EXG 1500** and **EXG 3000**) with different qualities were obtained. The qualities of these **EXG** flakes were characterized by TEM, TGA and Raman spectroscopy. Raman spectra also states that the **EXG 3000** flakes were of good quality and can be highly functionalized. Further research was focussed on the functionalization of **EXG 3000** with charge donating π-centre based on diketopyrollopyrrole (**DPP**). The resulting hybrids graphene material has good solubility in organic solvent and wide light absorption (500 nm ∼ 800 nm) features. Electron or energy transfer from **DPP** chromophores to **EXG** flakes was confirmed by the efficient fluorescence quenching of **DPP** chromophores. The new hybrid materials are under investigation as a third component in **P3HT**: **PCBM** bulk-heterojunction blends for organic photovoltaic applications.

Abbreviation

EXG…………………………………………………………………………… Exfoliated Few-layer Graphene

DPP…………………………………………………………………………………. Diketopyrollopyrrole

P3HT……………………………………………………………………………. Poly(3-hexylthiophene)

PCBM……………………………………………………………… Phenyl-C61-butyric acid methyl ester

GO…………………………………………………………………………………….Graphite Oxide

rGO ……………………………………………………………………………Reduced Graphite Oxide

PSS……………………………………………………………………………..Poly(styrenesulfonate)

DC………………………………………………………………………………….Direct Current

CNTs………………………………………………………………………… Carbon Nanotubes

SiC ……………………………………………………………………………Silicon Carbide

UHV……………………………………………………………………………Ultra High Vacuum

CVD………………………………………………………………………Chemical Vapour Deposition

AFM ……………………………………………………………………..Atomic Force Microscopy

TEM………………………………………………………………Transmission Electron Microscopy

SEM…………………………………………………………………Scanning Tunneling Microscopy

UV-vis………………………………………………………………Ultra Violet-visible spectroscopy

FTIR…………………………………………………………Fourier transform infrared spectroscopy

PVC……………………………………………………………………………….. Poly(vinyl chloride)

TGA……………………………………………………………………Thermo-Gravimetric Analysis

aC…………………………………………………………………………….amorphous Carbon

1LG……………………………………………………………………………….1 Layer Graphene

3LG……………………………………………………………………………….3 Layer Graphene

SWCNTs………………………………………………………………Single-Walled Carbon Nanotubes

NMP……………………………………………………………………….N-Methyl-2–Pyrrolidone

TDPP………………………………… 3,6-Di(thiophen-2-yl)pyrrolo[3,4-c]pyrrole-1,4(2H,5H)-dione

GNFs…………………………………………………………………………. Graphene Nanoflakes

HRXPS……………………………………… High Resolution X-ray Photoelectron Spectroscopy

TCNQ…………………………………………………………………….. 7,7,8,8-Tetracyanoquinodimethane

PCA……………………………………………………………………….. Phenanthrene-9-Carboxaldehyde

EDNB…………………………………………………………………………… Ethylenedinitrobenzoyl

DFT…………………………………………………………………………. Density Functional Theory

HOMO……………………………………………………………………… Highest Occupied Molecular 0rbital

LUMO……………………………………………………………………Lowest Unoccupied Molecular Orbital

D-A……………………………………………………………………………. Donor–Acceptor

DLS……………………………………………………………………….. Dynamic Light Scattering

NIR……………………………………………………………………………. Near Infrared

NMR…………………………………………………………………………. Nuclear Magnetic Resonance

ESI-MS……………………………………………………………………. Electrospray ionization Mass Spectroscopy

DMSO……………………………………………………………………………Dimethyl Sulphoxide

DMF………………………………………………………………………………… Dimethylformamide

DCM……………………………………………………………………………….. Dichloromethane

$CHCl_3$…………………………………………………………………………… Chloroform

MeOH……………………………………………………………………………. Methanol

ACN…………………………………………………………………………………. Acetonitrile

ICT……………………………………………………………………………. Intramolecular Charge Transfer

FRET…………………………………………………………………. Fluorescent Resonance Energy Transfer

BHJ………………………………………………………………………………….Bulk Heterojunction

OPV………………………………………………………………………………………Organic Photovoltaics

CHAPTER 1 INTRODUCTION

Graphene materials have aroused great research interest in the recent years for their outstanding properties and potential applications in the development of innovative organic electronic devices. An essential technological challenge that graphene faces is the controlled production of large sheets and possible exploitation of graphene-based devices. In this introduction chapter, a general description of graphene is presented; it includes production, chemical functionalization and physical-chemical properties characterization of pristine materials and derivatives. An overview of graphene-based donor/acceptor systems is also provided.

1. INTRODUCTION

Graphene is one monoatomic layer of carbon atoms which are hybridized in the sp² form and arranged to form hexagons extending to give a honeycomb lattice (shown in Figure 1.1). Graphene can be stacked to form 3D graphite, rolled to form 1D nanotubes, and wrapped to form 0D fullerenes.[1] The history of graphene can be traced back to 70+ years,[2] and it was believed that such a structure should not exist as it would be thermodynamically unstable.[3] In 2004, the isolation and characterization of single layer graphene by the Manchester group[4] led to an explosion of interest in the research of isolated graphene.
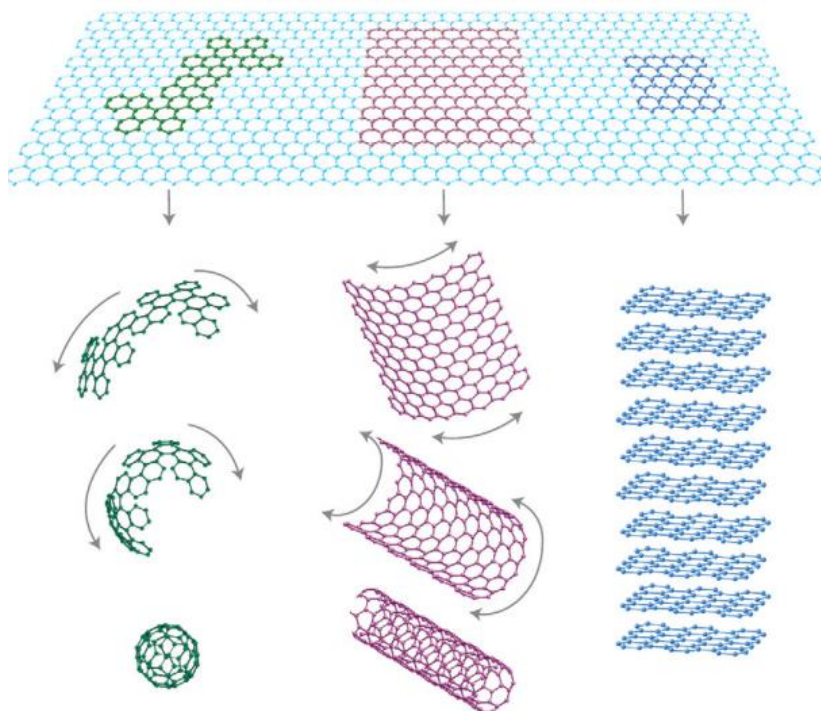
Figure 1.1 Graphene is a 2D building material for carbon materials of all other dimensionalities. It can be wrapped (at least in principle) up into 0D buckyballs, rolled into 1D nanotubes or stacked into 3D graphite. (ref. 1)

1.1 Chemistry of graphene

Graphene is among the thinnest compounds known with a thickness of one atom. The monolayer graphene has a reported lattice constant of 2.46 Å. [5] Carbon atoms form a hexagonal lattice on a two-dimensional plane, as shown in Figure 1.2. Each carbon atom is

at a distance of about a = 1.42 Å from its three neighbors, with each of which it shares one σ bond. The fourth bond is a π-bond, which is oriented in the z-direction (out of the plane). One can visualize the π orbital as a pair of symmetric lobes oriented along the z-axis and centered on the nucleus. Each atom has one of these π-bonds, which are then hybridized together to form what are referred to as the π-band and π∗-bands, these bands are responsible for most of the peculiar electronic properties of graphene, [6,7] which have long been the interest of many theoretical studies on high electron transfer mobilities. For instance, a fabrication of electrically contacted suspended graphene resulted in a tenfold improvement in electron mobility of up to 200,000 $cm^2\,V^{-1}\,s^{-1}$, reported by K.I. Bolotin.[8]
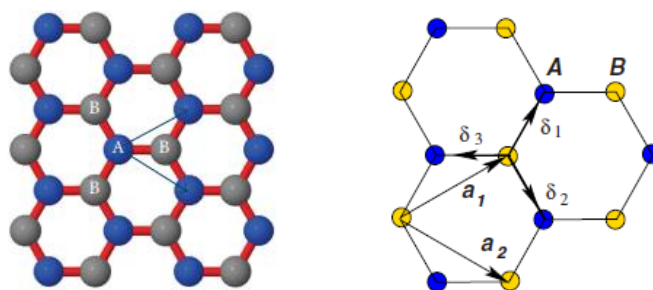
Figure 1.2 Lattice structure of graphene, each atom A in one sublattice has 3 nearest neighbors B in sublattice, a1 and a2 are the lattice unit vectors, and δ_i (i=1,2,3) are the nearest-neighbor vectors (ref. 5)

Graphene is practically transparent (97.7% of the light).[9] It is the most resistant material known and, at the same time, it is very flexible. Since the theoretical strength is commonly defined as the maximum stress that the material can sustain in the absence of any defects,[10] it is found that graphene is the strongest material, with a strength as high as 130 GPa (assuming a thickness of ∼0.335 nm) [11] making it an ideal candidate for many potential applications. However, although graphene is just one atom thick, it was found to be capable of absorbing only 2.3% of the radiation uniformly over almost the entire optical spectrum.[12] In Figure 1.3 a), the line scan profile shows the intensity of transmitted white light along the yellow line of single-layer graphene, which is a consequence of graphene's unique electronic structure. Inset of Figure 1.3 a) were samples prepared on a 20-µm-thick metal support structure which have several apertures of 20, 30, and 50 µm in diameter with graphene crystallites placed over them. In this case, the opacities of different areas can be compared. Further measurements yield graphene's opacity of 2.3 ± 0.1% and negligible reflectance (<0.1%), whereas optical spectroscopy

shows that the opacity is practically independent of the wavelength. The opacity is found to increase with increase in membrane thickness; hence, each graphene layer adds another 2.3% (Figure 1.3 b inset). Meanwhile, transmittance spectrum shows slightly lower transmittance for $\lambda < 500$ nm, this could probably be due to hydrocarbon contamination. The red line is the transmittance $T = (1 + 0.5\pi\alpha)^{-2}$ expected for two-dimensional Dirac fermions, whereas the green curve considers a nonlinearity and triangular warping of graphene's electronic spectrum.
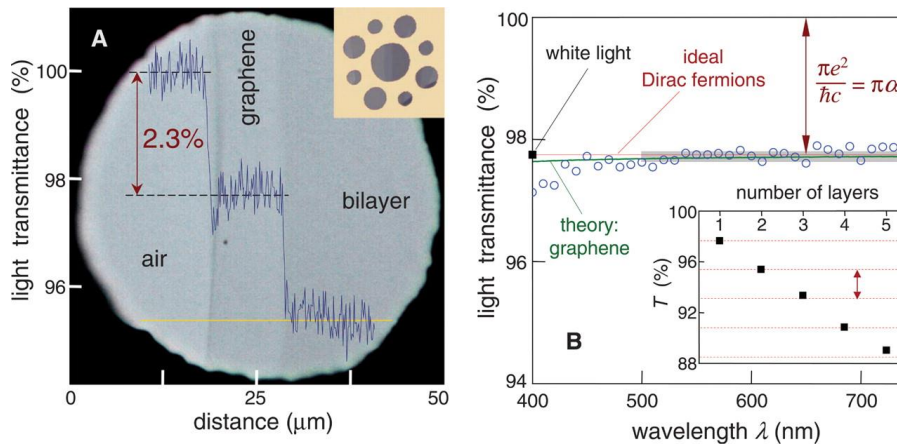
Figure 1.3 a) Image of single layer graphene in transmitted white light. b) transmittance spectrum of single layer graphene. (ref. 11)

Graphene is an excellent thermal conductor even though carbon by itself does not conduct heat.[13] Recently, the room-temperature thermal conductivity of graphene was measured by using a non-contact optical-based technique. It was shown that the conductivity reaches values at a range of $(4.84\pm0.44) \times 10^3$ to $(5.30\pm0.48) \times 10^3$ W·m^{-1}·K^{-1} at room temperature.[13] The extremely high values of the thermal conductivity suggest that graphene can outperform carbon nanotubes in heat conduction. As two-dimensional materials, quantum-mechanically enhanced transport phenomena such as the quantum Hall effect can also be observed in graphene. However, because of the unique electronic properties of graphene, which exhibits electron–hole degeneracy and vanishing carrier mass near the point of charge neutrality,[14] the quantum Hall effect was theoretically predicted to a distinctive half-integer quantum Hall effect.[5a, 15] Philip Kim reported an experimental investigation of magneto-transport in a high-mobility single layer graphene (Figure 1.4).[16] Through adjusting the chemical potential with the use of the electric field effect, an unusual half-integer quantum Hall effect for both electron and hole carriers in graphene was observed. The relevance of Berry's phase to these experiments is confirmed

by magneto-oscillations. In addition to their purely scientific interest, these unusual quantum transport phenomena may lead to new applications in carbon-based electronic and magneto-electronic devices.
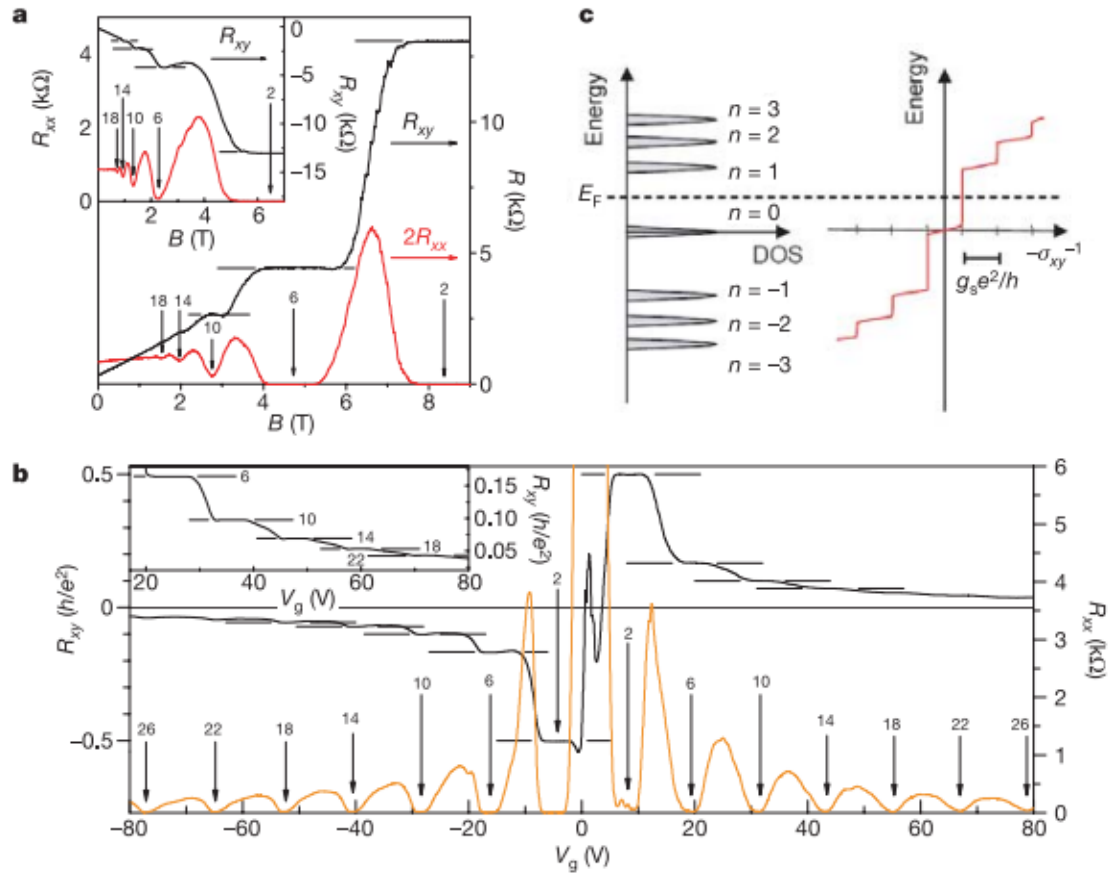
Figure 1.4 Quantized magnetoresistance and Hall resistance of a graphene device reported in ref. 16.

1.2 Production of graphene

Graphene is a single-layer material which can be seen as flat with ripples. However, graphene samples with bi-layers or few-layers are also being investigated with equal interest. Although single-layer graphene and bilayer graphene were first obtained by micro-mechanical cleavage,[4] several methods have been developed for generating graphene. Generally, the preparation of graphene samples can be carried out through a Top-Down or a Bottom-Up approach.[17] These methods have their own pros and cons depending on the final applications. Many researchers have proved that graphene produced by the bottom-up method is of high quality, but this method unfortunately suffers from low scalability. Therefore, precise control over graphene synthesis is required

for testing their fundamental physical properties and introducing them into promising device applications.

1.2.1 Mechanical scotch tape exfoliation

Geim and coworkers prepared few layer-graphene including single layer graphene by mechanical exfoliation (repeated peeling) of small mesas from highly oriented pyrolytic graphite.[4] In this micromechanical method, graphene is detached from a graphite crystal using adhesive tape. After peeling it off from the graphite, multiple layer-graphene remains on the tape. By repeated peeling, the multiple layer-graphene is cleaved into various flakes of few layer-graphene. Afterwards, the tape is attached to the substrate and the glue is dissolved, e.g. by acetone, in order to detach the tape. Finally, one last peeling with tape is performed. Through this approach, they observed few layer-graphene in the form of high-quality crystallites with an average size up to 100 μm^2.[4] However, it is difficult to obtain large amounts of graphene materials through this method, which is labor intensive and required skilled expert.[4]
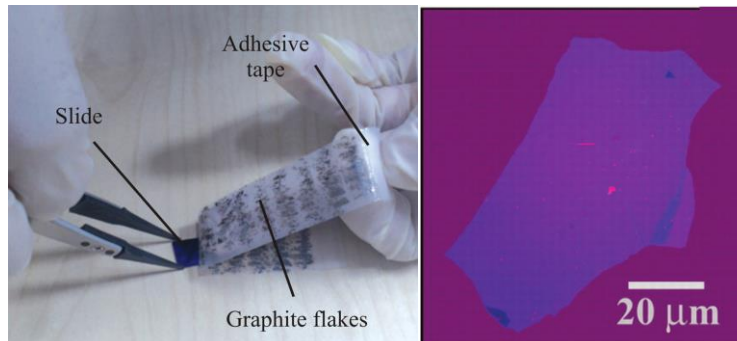
Figure 1.5 Few layers graphene achieved by Geim research group through adhesive tape (ref. 4).

1.1.2 Solvent-based exfoliation from graphite

A reliable method to produce graphene is the exfoliation of graphite in an organic solvent.[18] The energy barrier is reduced when the graphite is dispersed in a solvent with similar surface energy, the suspension is sonicated in an ultrasound bath for several hours or a voltage is applied [19] and centrifuged to dispose thicker flakes. Such exfoliation occurs because the energy required to exfoliate graphite is balanced by the solvent–graphene interaction, for solvents whose surface energies match that of graphene. [20-24] In ref 20 c),

a rapid and potentially scalable method for the liquid-phase exfoliation of natural graphite with the aid of microwaves is reported. With this protocol, exfoliated graphene materials were obtained in 93% yield, with a high selectivity (95%) towards single-layer graphene.

Figure 1.6 Microwave-assisted liquid-phase exfoliation of graphite in ionic liquids. (ref. 20c)

1.2.3 Exfoliation from graphite oxide

Graphene also can be prepared starting from graphite oxide.[25] Generally, graphite oxide (GO) can be prepared by three methods: the Brodie method, [25a] the Staudenmaier method, [25c] or the Hummers method. [25d] These three methods involve oxidation of graphite in the presence of strong acids and oxidants. GO consists of a layered structure of 'graphene oxide' sheets that are strongly hydrophilic resulting in intercalation of water molecules between the layers.[26] The interlayer distance between the GO sheets increases reversibly from 6 to 12 Å, with increasing relative humidity. Notably, graphite oxide can be completely exfoliated to produce aqueous colloidal suspensions of GO sheets by sonication of a water/graphite oxide mixture, followed by stirring.[27] After centrifugation, GO sheets can be reduced to graphene by thermal or chemical methods. The performance of this method is similar to liquid-phase exfoliation of pristine graphene. However, its complexity is higher because chemical transformations are involved. During the reduction process, it is hardly possible to remove all oxygen.[28] Over the past years, many other approaches have been pursued.[29-31] Syed Nasimul Alam synthesized few layers GO by using a modified Hummers method,[31] which is successful in increasing reaction yield and

6

the overall safety of the process by using different proportion of KMnO₄ and H₂SO₄ if compared to those required by the Hummers method. Firstly, natural flake graphite (NFG) was oxidized to graphite oxide. Thereafter, GO was prepared by the exfoliation of the graphite oxide in distilled water in an ultrasonicator. The obtained GO was later reduced thermally to obtain reduced graphene oxide (rGO). The process schematics is shown in Figure 1.7; the produced GO sheets were found to have a thickness of about 1 - 2 μm.

NFG (4 gm), K₂S₂O₈ (8 gm), and P₂O₅ (8 gm) were added into solution of concentrated (98%) H₂SO₄ (12 ml) is magnetic ally stirred

Themixture is diuted with 300 ml of distilled waterand kept in a muffle furnace at 60°C to remove moisture

A solution of 2 gm of pre-oxidised grap hite powder, 92 ml H₂SO₄, 12 gm KMnO₄ and 2 gm of NaNO₃ is prepared and the solution and stirred. 560 ml of distilled water and 10 ml of H₂O₂ (30%) is finally added to the solution and stirred. The filtrate obtained is washed with HCl (10%)

The yellow brown powder is washed with warm water to remove inpurities and finally dried at 60°C to get GO

The filtrete is sonicatedin H₂O₂

The filtrate is heated in a muffle furnace at 60°C and allowed to cool overnight in air

The brown filtrate after being washed with HCl (10%)

GO after complete drying

The beaker was placed on a hot plate set at 350°C for a period of 10 min in a hood. Thermal reduction of GO to form rGO

rGO

Figure 1.7 Schematic diagram showing the steps undertaken for the modified Hummers method synthesis of GO and rGO. (ref. 31)

1.2.4 Electrochemical exfoliation

The electrochemically-assisted exfoliation of graphite has aroused great interest[32] with contributions by several research groups.[33-35] In 2009, the group of Wang Guoxiu reported an efficient electrochemical preparation of graphene with the use of poly(styrenesulfonate) (PSS) as electrolyte/stabilizer and two graphite rods as cathode and anode electrodes (Figure 1.8).[34] By applying a constant potential (5 V, DC voltage) to the electrodes, a black product gradually appeared at the positive electrode and after four hours processing, a colloidal graphene–PSS dispersion was taken from the electrolysis cell

and centrifuged to remove large agglomerates. This suspension was very stable, showing no precipitation within a six months storage. The electrolytic exfoliation of graphite gives graphene materials at a yield of about 15 wt.%.
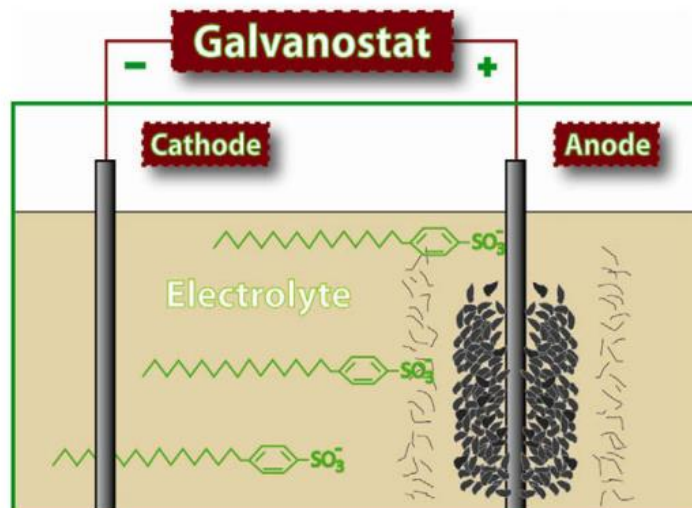
Figure 1.8 Diagram of the apparatus for synthesis of graphene via electrolytic exfoliation. (ref. 33)

1.2.5 Unzipping carbon nanotubes

An alternative approach to produce graphene is by unzipping carbon nanotubes (CNTs).[36] Narrow carbon nanoribbons, that can be considered as graphene stripes, could be produced by unzipping carbon nanotubes. James M. Tour reported an interesting oxidative, solution processing method to prepare carbon nanoribbons in nearly quantitative yields.[37] The opening of the nanotubes appears to occur along a line, similar to the unzipping of graphite oxide. [38-40] The proposed mechanism is reported in Figure 1.9.[39] The first step is a manganate ester formation (**2**, Fig. 1.9) that evolves to give dione **3**. The buttressing ketones induce strain in the alkenes (marked in red), making them more prone to $KMnO_4$ attack. As the oxidation continues, the buttressing-induced strain on the alkenes lessens because there is more space for carbonyl projection; however, the bond-angle strain induced by the enlarging hole would make the aligned alkenes (**4**, Fig. 1.9) increasingly reactive. Hence, once an opening has been initiated, its further opening is enhanced relative to an unopened tube. The ketones are then further converted to carboxylic acids that constitute the edges of the nanoribbons. Finally, relief of the bond-angle strain when the nanotube opens to the graphene ribbon (**5**, Fig. 1.9) slows down

further dione formation and cutting. The sequential bond cleavage, over random opening and cutting, occurs for the concerted attack to neighboring carbon atoms by KMnO$_4$.
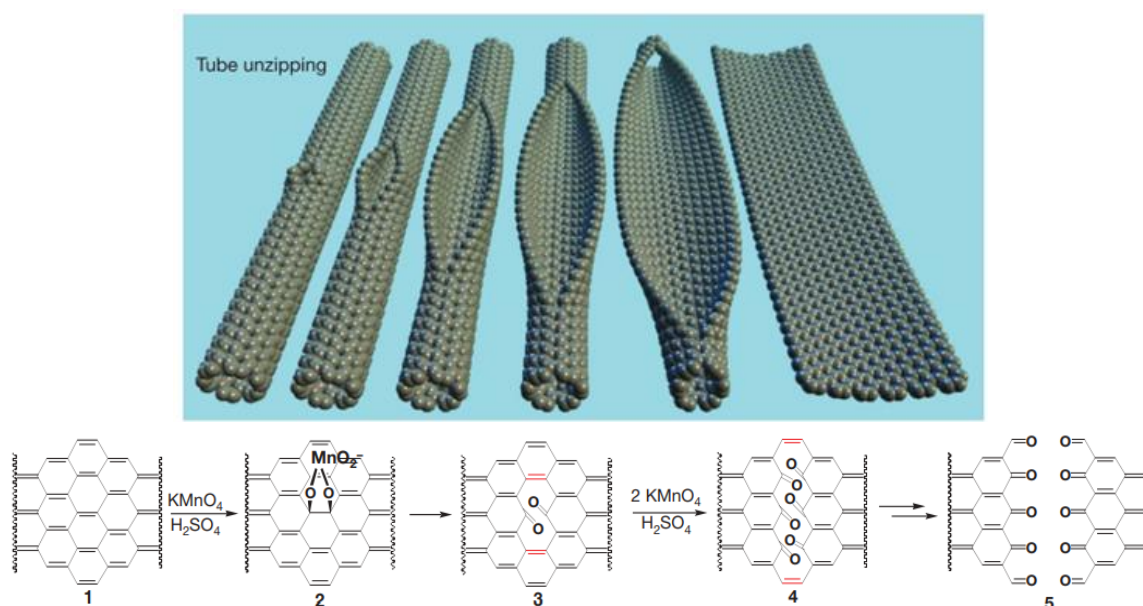
Figure 1.9 Carbon nanotubes oxidative unzipping. (ref. 30)

1.2.6 Epitaxial growth on Silicon Carbide (SiC)

Graphene can be prepared by thermal annealing of silicon carbide (SiC) crystals. [41] The formation of crystalline graphite layers on SiC via thermal heating at high temperatures in ultra-high vacuum (UHV) was first observed by van Bommel et al. in 1975. [42] The main advantage of thermal decomposition of SiC to give graphene over other techniques is that graphene layers can be directly obtained on a commercially available semiconducting or semi-insulating substrate, so no transfer is required before processing electronic devices. [43] Since the vapor pressure of carbon is negligible if compared to silicon and silicon clusters, at high temperature silicon evaporate, leaving carbon atoms on the surface, which subsequently rearrange to form graphene layers (Figure 1.10).[44]
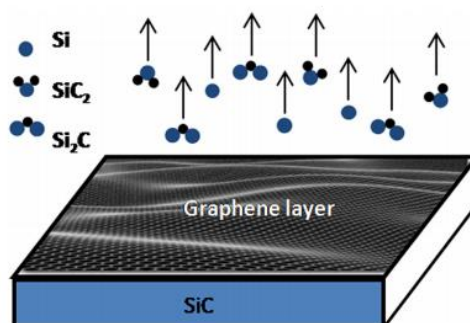
Figure 1.10 Growth of epitaxial graphene on a silicon carbide wafer (ref. 44).

9

1.2.7 Chemical Vapor Deposition (CVD) on metal catalysts

Compared with the aforementioned epitaxial growth on SiC method, chemical vapor deposition (CVD) is a more efficient method to give graphene materials. Generally, the CVD method was explored mainly on Co, Ni and Cu substrates, which are exposed to gaseous compounds. [45, 46] Jingquan Liu and coworkers developed a thermo-responsive graphene-polymer films with modified CVD graphene. [47] As shown in Figure 1.11, a copper foil was inserted into a quartz tube and then annealed at high temperatures. After cooling down to room temperature, a tape was put in contact with the surface of the graphene-on-Cu. Graphene was removed from Cu by etching in an aqueous solution of iron nitrate. Compared to epitaxial growth on SiC, the CVD method requires low temperatures, making it more versatile to obtain single-layer graphene.
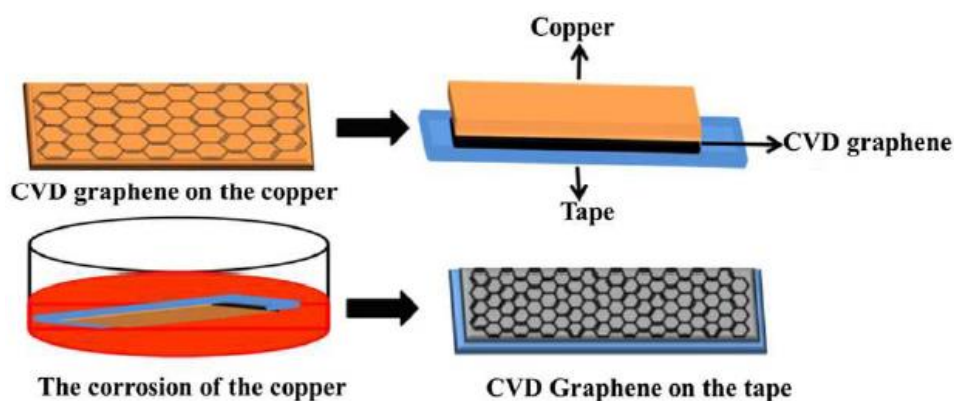
Figure 1.11 Synthesis of CVD graphene (ref. 47)

1.2.8 Organic synthesis

Although graphene is mostly prepared by physical methods, organic synthesis represents an alternative to access graphene-type structures in a selective and reproducible manner. Generally, graphene/graphene-type structures can be achieved by organic synthesis through cross-coupling, Diels–Alder, and polymerization reactions.[48]

Mullen and coworkers[48b] prepared a 3-fold symmetric, graphene-like disk consisting of 55 rings by iterating a series of Diels–Alder/dehydrogenation synthetic steps, using ethynyl-substituted tetraphenylcyclopentadienones and a tetraethynylbiphenyl core. A large nanographene was synthesized by combining cross-coupling, Diels–Alder, and dehydrogenation reactions (Figure 1.12). [48c] A building block containing two acetylene

units were prepared and subjected to Diels–Alder cycloaddition with a functionalized cyclopentadienone. A Ni-promoted coupling gave a dendrimer-like aromatic nanostructure that was planarized into a graphene ribbon upon aromatization.
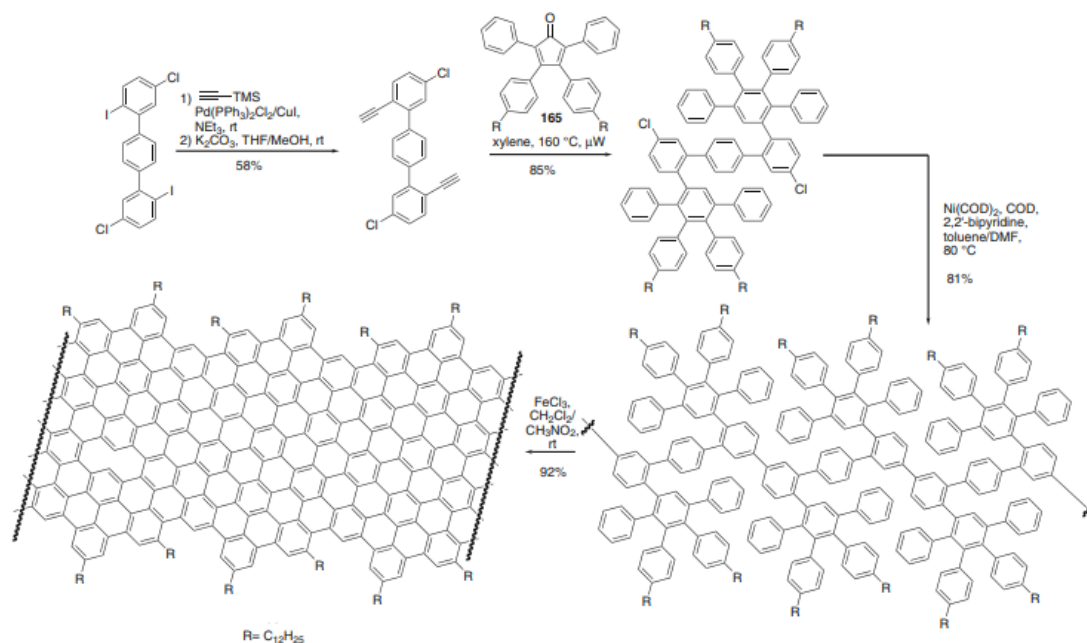
Figure 1.12. Iterative Diels–Alder/deprotection strategy for the synthesis of nano-graphene. (ref. 48)

1.3 Characterization of graphene

To characterize graphene, a variety of techniques were reported, including atomic force microscopy (AFM), transmission electron microscopy (TEM), scanning electron microscopy (SEM), Raman spectroscopy, Ultra Violet-Visible spectroscopy (UV-Vis), Fourier transform infrared spectroscopy (FTIR), thermo-gravimetric analysis (TGA). [49]

1.3.1 Scanning Probe Microscopy

Scanning probe microscopy methods allow to observe and characterize graphene samples directly. Atomic force microscopy (AFM) is regarded as the leading approach for thickness measurements and graphene layers number counting. Yang and coworkers, for example, designed a monolayer graphene-based Fe/N/C model catalyst.[50] Through AFM, it was possible to confirm the successful synthesis of the desired catalyst (Figure 1.13) and measure the thickness of the supporting graphene layer of about 0.5 nm.
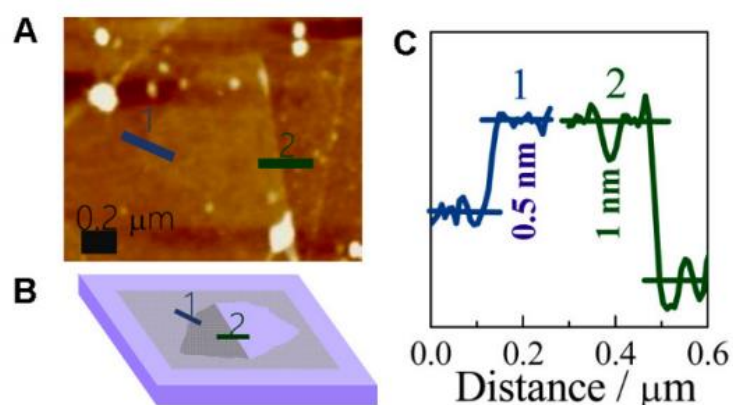
Figure 1.13 a) AFM image of the graphene-based catalyst; b) Bright spot morphology schematic; c) Height profile showing the thickness of graphene-based catalyst. (ref. 50)

SEM and TEM are other microscopy techniques that are commonly used to characterize the morphology and the structure of graphene materials. [51] Through SEM and TEM, the transparency of graphene sheets gives indications about the thickness of the graphene samples. For example, Lu and coworkers used graphene–MnO_2 hybrid nanostructures as catalysts for formaldehyde oxidation (Figure 1.14). [52] SEM and TEM characterization demonstrated the 2D planar structure of the nanohybrids with a well-defined and interconnected porous network. SEM and TEM were also used to analyze the MnO_2 control sample which is constituted of flower-like nanospheres (Figure 1.14 C, G) with a significantly different morphology of the graphene-supported MnO_2.
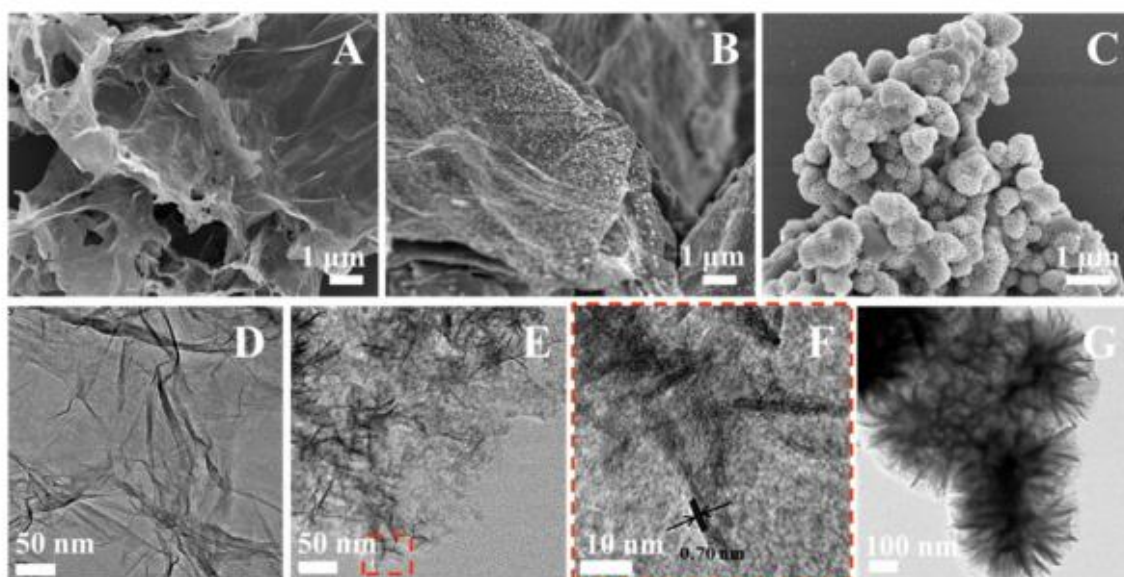
Figure 1.14 SEM and TEM images of graphene (A, D), graphene-MnO_2 (B, E), and MnO_2 samples (C, G); (F) HRTEM image of graphene–MnO_2 (ref. 52).

1.3.2 Raman spectroscopy

Raman spectroscopy is a widely used tool to gain structural information and judge the number of layers of exfoliated few layers graphene samples. Generally, graphene has six normal modes and two atoms per unit cell at the so-called Brillouin zone center (Γ), where (Γ) = A_{2u} + B_{2g} + E_{1u} + E_{2g}.[53] Main features are the defected graphite D peak, the graphite G peak and graphene 2D peak.[54] As reported, [55,56] the D peak at 1350 cm^{-1} reveals defects in the sample, which is due to the first order resonance and cannot be observed in the pristine graphite and graphene (Figure 1.15a). The G band results from in-plane vibration of sp^2 carbon atoms and is the most prominent feature of most graphitic materials. It is the result of in-plane optical vibrations and corresponds to the optical E_{2g} phonons at the Brillouin zone center resulting from the bond stretching of sp^2 carbon pairs in both, rings and chains. Since the D band is induced by defects in the graphene lattice, its intensity is therefore used to characterize the number of defects in a graphene sample. [54]
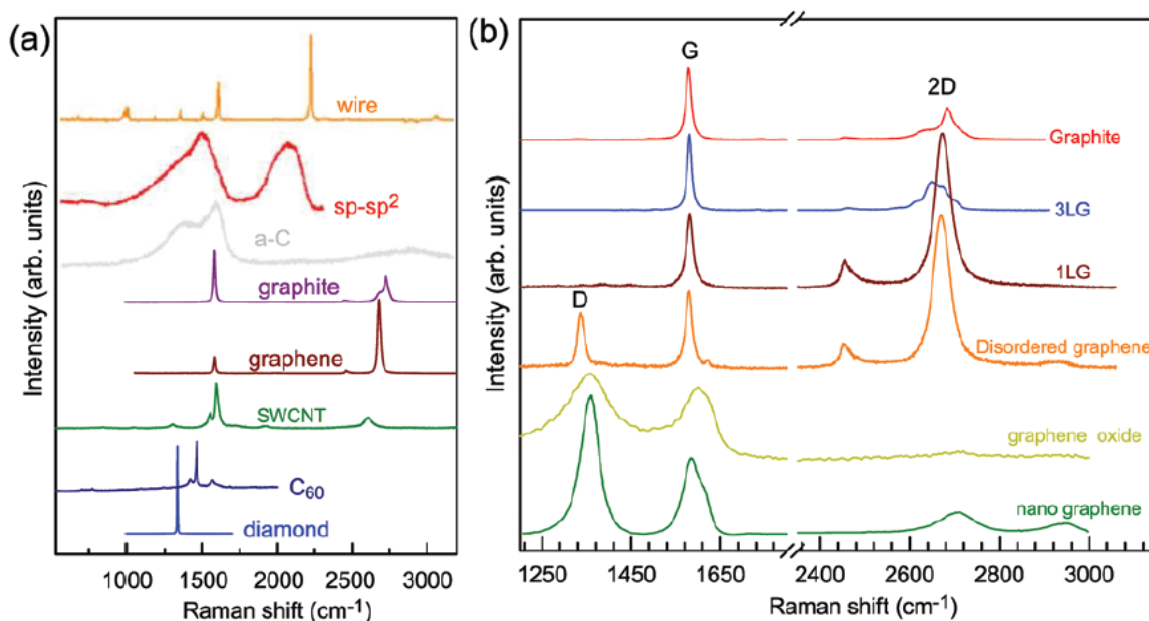
Fig. 1.15 (a) Raman spectra of carbon solids and different nanostructures. (b) Raman spectra of graphene-based materials. (ref. 49)

Figure 1.15(a) shows the Raman spectra of carbon solids and different nanostructures, [49] including 1d carbon wires, sp–sp^2 carbon, amorphous carbon (aC), graphite, graphene, single-walled carbon nanotubes, C_{60}, and diamond. Figure 1.15(b) shows the Raman spectra of graphene-based materials, including graphite, 1-layer graphene (1LG), 3-layer graphene (3LG), disordered graphene, graphene oxide and nanographene. According to

Ferrari, [54, 57] the electronic structure of graphene is captured in its Raman spectrum that clearly evolves with the number of layers. The D peak second order changes in shape, width, and position for an increasing number of layers, reflecting the change in the electron bands while the G peak slightly down-shifts. Figure 1.16(a) compares the 514 nm Raman spectra of graphene and bulk graphite. No D peak is observed in the center of graphene layers. This proves the absence of a significant number of defects. It also shows a significant change in shape and intensity of the 2D peak of graphene compared to bulk graphite. Figure 1.16 (b) and (c) show that a further increase in layers leads to a significant decrease of the relative intensity of the lower frequency 2D peaks. For more than 5 layers, the Raman spectrum becomes hardly distinguishable from that of bulk graphite. Thus, Raman spectroscopy can clearly distinguish a single layer, from a bilayer from few (less than 5) layers. Meanwhile, when the numbers of graphene layers increase, a Raman shift (about 30 cm^{-1}) to higher frequency can be observed from the 2D band shown in Figure 1.16 (b) and (c).
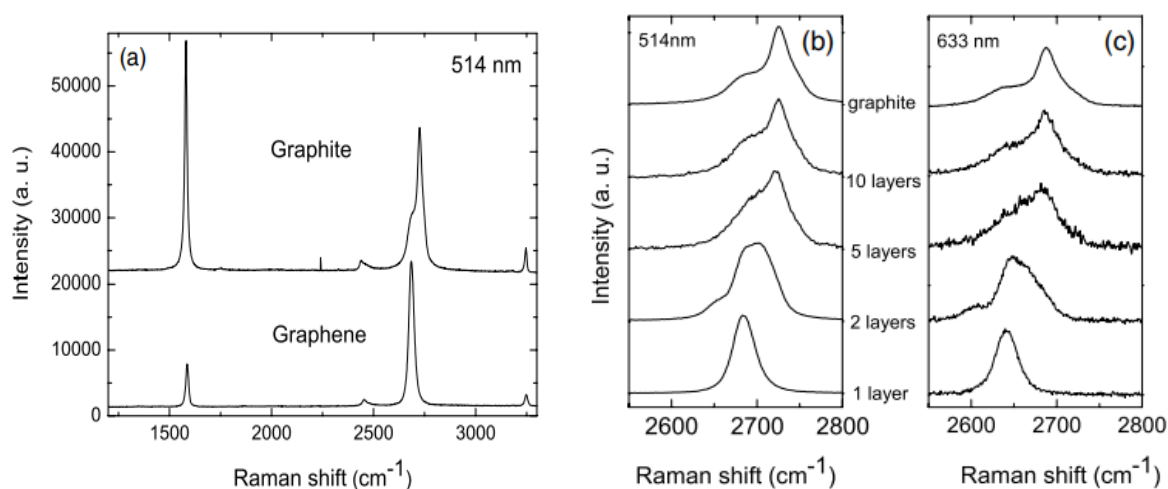
Figure 1.16 (a) Comparison of Raman spectra at 514 nm for bulk graphite and graphene. (b) Evolution of the spectra at 514 nm with the number of layers. (c) Evolution of the Raman spectra at 633 nm with the number of layers. (ref. 57)

1.3.3 Ultra Violet-Visible spectroscopy (UV-Vis)

The UV-vis spectroscopy is a convenient technique to confirm a sample graphitic structure, with an absorption peak at ~260 nm, which is attributed to the π–π* transitions of aromatic C–C bonds. Functionalized graphene samples, such as for instance graphene oxide, show a significant shift of the main absorption band of pristine graphene. For example, Zhou and coworkers [58] used UV-vis spectroscopy to distinguish graphene from

graphene oxide samples (Fig. 1.17) through the shift of the 254 nm graphene absorption to 227 nm.
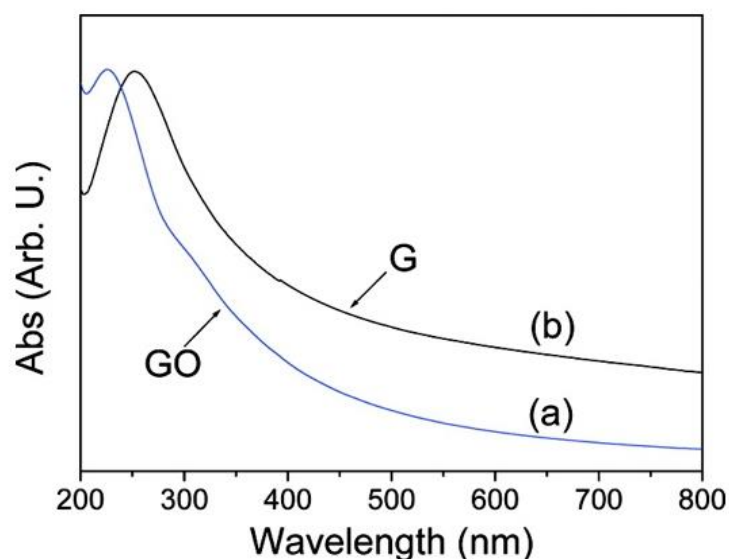
Figure 1.17. UV-vis spectra of the (a) graphene oxide (GO) and (b) graphene (ref 58).

1.3.4 Fourier Transform Infrared spectroscopy (FTIR)

FTIR is a powerful technique to characterize functional groups installed on graphene samples. [59] As reported by Baoli Ou, [60] a covalent functionalized graphene with phenol was prepared through 1,3-dipolar cycloaddition reaction. Figure 1.18 shows the FTIR spectra of pristine graphene and phenol-functionalized graphene (graphene-*f*-OH).
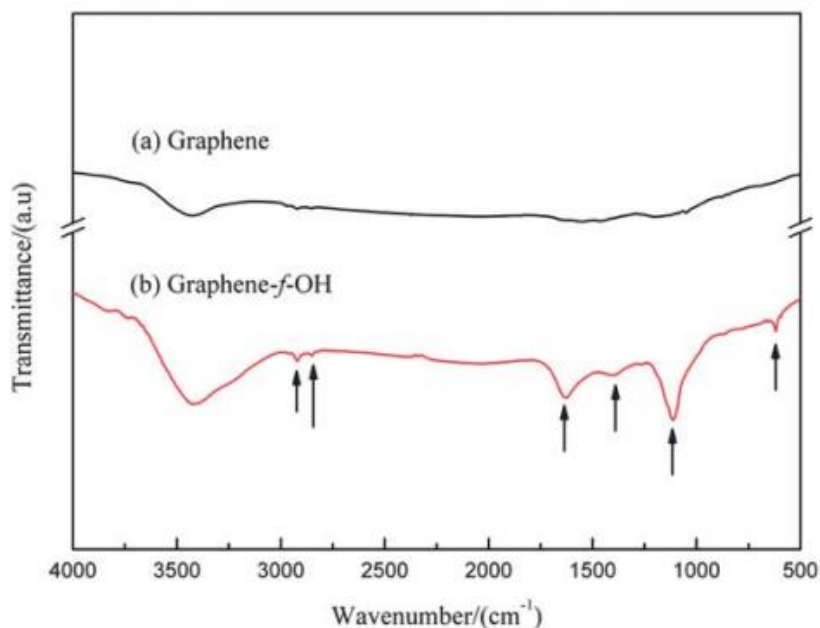
Figure 1.18 FTIR spectra of (a) pristine graphene and (b) phenol-functionalized graphene (graphene-*f*-OH). (ref 60)

15

As illustrated in Figure 1.18, the FTIR spectrum of graphene-*f*-OH (curve b) shows C–H stretch features at 2950 cm^{-1}, 2922 cm^{-1} and 2852 cm^{-1} that do not appear in the spectrum of pristine graphene (curve a). Also, apparent C–C stretch bands and a weak aromatic C–H band are observed at 1100–1700 cm^{-1}, 618 cm^{-1} and 3040 cm^{-1}, respectively. The C–O stretch band at 1120 cm^{-1} and the O–H stretch band at 3600–3700 cm^{-1}, both of which are characteristic of phenols. The FTIR spectra analysis provides support for successful covalent functionalization by 1,3 dipolar cycloaddition reaction.

1.3.5 Thermo-Gravimetric Analysis (TGA)

TGA is another important technique to characterize graphene-based materials, particularly in terms of thermal stability or degree of functionalization.[59] Ben L. Feringa [61] and coworkers prepared two kinds of functionalized graphene (**1** and **2** functionalized graphene) through a zwitterion cycloaddition onto exfoliated graphene flakes. Figure 1.19 shows the TGA curves of graphene, **1** and **2** functionalized graphene. The weight loss of graphene is about 5% between 200 °C and 450 °C, which is due to the defects caused by sonication, and also residual solvents. In the same temperature range, **1** and **2** functionalized graphene show about 54% and 36% weight loss, respectively. This weight loss is attributed to the decomposition of organic functional groups attached onto graphene. The degree of functionalization was estimated to be one functional group per 10 carbon atoms for 1 functionalized graphene, and per 50 carbon atoms for 2 functionalized graphene.
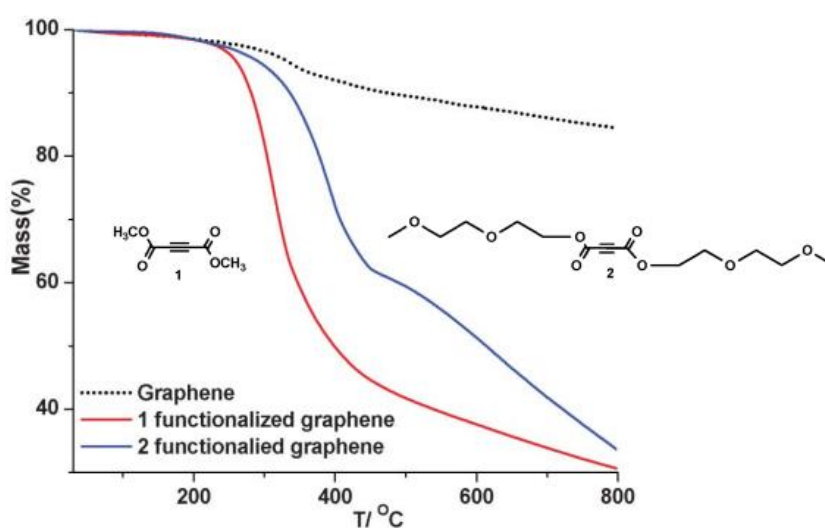
Figure 1.19 TGA analyses of graphene, **1** and **2** functionalized graphene. (ref. 61)

1.4 Chemical functionalization of graphene

Chemical functionalization of graphene is one of the key topics in graphene research which enables it to be processed by solvent-assisted techniques.[62] Chemical functionalization not only prevents the aggregation of graphene layers and maintains the inherent properties of graphene, but also improve the solubility of the graphene-based materials leading to better operability in producing devices. In addition, organic functional groups, such as chromophores, offer new properties that could be combined with the properties of graphene. The functionalization of graphene can be performed by several methods which can generally be classified into covalent and noncovalent modification techniques. It has been found that both the covalent and noncovalent modification techniques are very effective in the preparation of processable graphene.[62]

1.4.1 Covalent functionalization of graphene

Covalent functionalization of graphene is the attachment of chemical moieties to the graphene structure.[63] In most cases, when (in)organic molecules are covalently attached to the graphene surface, its extended aromatic character is perturbed, enabling, potentially, the tuning of graphene electronic properties. The reactions to graphene that will be considered in this section will be radical addition reactions, nucleophilic addition reactions, cycloadditions and electrophilic reactions. [64]

1.4.2.1 Addition of free radicals to sp^2 carbon atoms of graphene

Free radical additions are among the most common reaction to covalently functionalize carbon nanostructures.[65] In this Thesis work, aryl radicals, generated from the corresponding diazonium salts, were added to graphene. Reduction of the diazonium salt induces nitrogen extrusion, leaving an aryl radical that further reacts, in a manner similar to that shown in Figure 1.20,[66] with a carbon surface, leaving an adjacent radical that may further react or be quenched by solvent. The propensity of the initial aryl radical to dimerize or abstract a hydrogen atom from the solvent is minimized by the fact that the radical is generated at the carbon surface where reaction is desired.
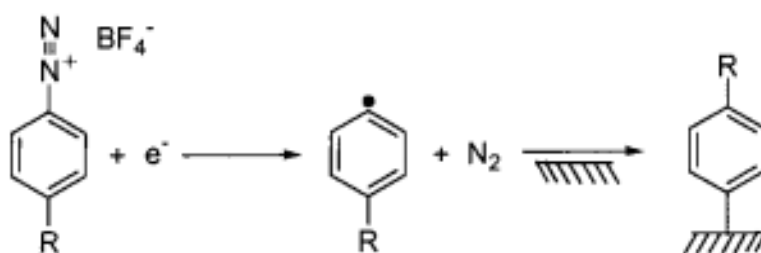
Figure 1.20 Electrochemical reduction of an aryl diazonium salt, giving a reactive radical that covalently attaches to a carbon surface. (ref. 66)

This method was introduced by J. M. Tour and coworkers for the functionalization of SWNT and then further applied to functionalize graphene. [67] As shown in Figure 1.21, functionalization of a SWNT might start through an electron transfer from the SWNT to the arenediazonium salt to form a SWNT-radical cation and a nearby aryl radical with evolution of nitrogen. Radical-radical coupling would afford the aryl–SWNT cation, which could react further with any nucleophile in solution.[67a] J. M. Tour extended this functionalization method to a surfactant-wrapped graphene sheet; the reaction most likely involves an electron transfer from graphene to the diazonium ion, as in the case of SWNT, followed by extrusion of N_2 and a subsequent addition of the aryl radical to the oxidized graphene layer. [67b]
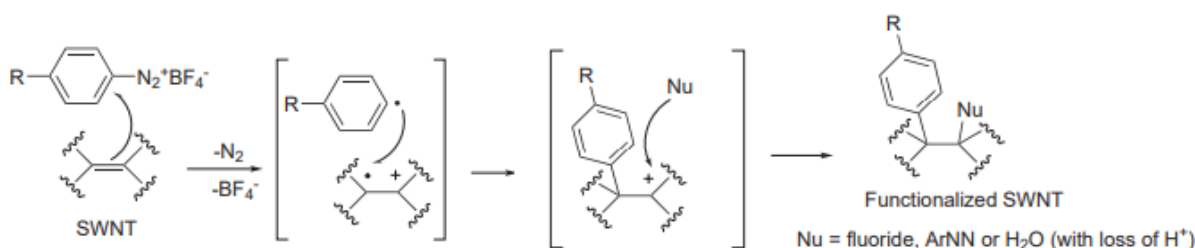
Figure 1.21 Functionalization of SWNTs by diazonium species could arise by electron addition from the SWNT to the arenediazonium. [ref. 67b]

With 4-nitrobenzene diazonium tetrafluoroborate, [67c] the 4-nitrobenzene units were successfully attached on single/bi/multi-layers graphene. Through Raman spectroscopy, single graphene sheets were found to be almost 10 times more reactive than bi- or multilayers of graphene, which is attributed to an effect of electron and hole puddles whereby the Dirac point deviates spatially.
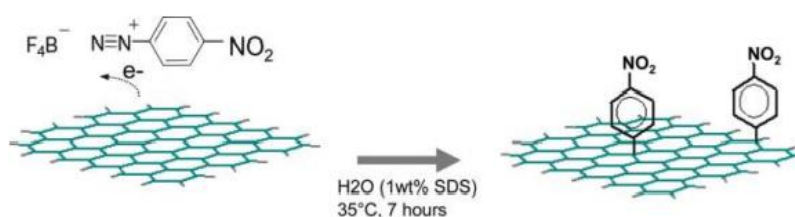
Figure1.22 Schematic of the electron transfer chemistry between graphene and 4-nitrobenzene diazonium tetrafluoroborate. [ref 67c]

1.4.1.2 Nucleophilic addition reactions

An alternative way to functionalize graphene materials is through nucleophilic addition onto GO. Amines add readily to GO, being the main reactive sites the epoxy groups of GO. An example of nucleophilic addition to graphene was developed by Yu Chen and coworkers; [68] they developed a new synthetic method for grafting polymers on reduced graphene oxide (rGO). The study describes the functionalization of thermally-reduced GO with the anion poly (Nvinyl-carbazole).
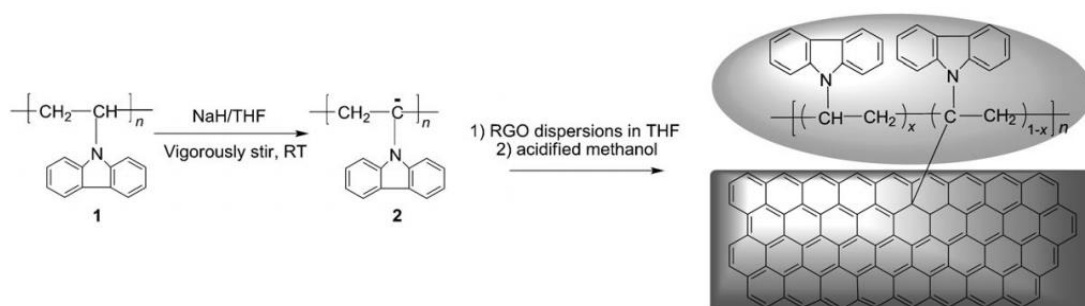
Figure. 1.23 Functionalization of rGO with the anion of PVK. (ref. 68)

1.4.1.3 Cycloaddition reactions

Extensively used reactions to functionalize carbon nanostructures are the cycloaddition reactions, which are favored at the tips and defects of carbon surfaces due to the pronounced curvature. [68] Among the cycloaddition reactions used to functionalize graphene, the 1,3-dipolar cycloaddition reaction of in-situ generated azomethine ylides is a versatile method. Trapalis and coworkers [69] prepared a functionalized graphene sheet by 1,3 dipolar cycloadditions of azomethine ylide. A decisive factor for the successful accomplishment of the reaction was the miscibility of the graphene dispersion in pyridine with DMF, a commonly used solvent for 1,3 dipolar cycloadditions on nanocarbons. (Figure 1.24).
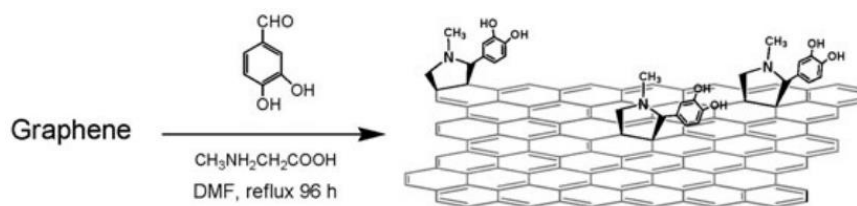
Figure 1.24 Schematic representation of the 1,3 dipolar cyclo-addition of azomethine ylide on graphene. [ref. 69]

1.4.1.4 Electrophilic substitution reactions

The Friedel–Crafts reaction is a well-known electrophilic aromatic substitution reaction in synthetic chemistry; it has previously been successfully employed for the chemical modification of fullerene and carbon-nanotubes.[70] Chun Kiang Chua and Martin Pumera extended the scope of the Friedel–Crafts reactions to rGO.[71] High-resolution X-ray photoelectron spectroscopy (HRXPS) and FTIR spectroscopic analyses were used to confirm the success of the functionalization reaction. The Raman spectra showed a lower I_D/I_G ratio for modified graphene with 4-aminobenzoic acid (Figure 1.25) and the non-destructive nature of the functionalization towards the integrity of the sp^2 sheets.
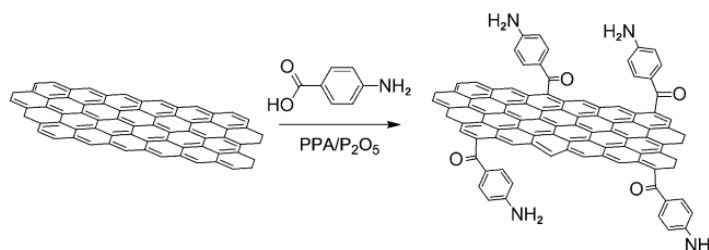
Figure 1.25 Friedel–Crafts reaction on graphene by using 4-aminobenzoic acid with PPA/P_2O_5. (ref. 71)

1.4.2 Non-covalent functionalization of graphene

Unlike covalent functionalization which creates defects on the graphene sheet, non-covalent functionalization does not disrupt the conjugated sp^2 hybridized carbon network of graphene on the graphene surface, hence retaining its superior intrinsic electron and thermal conductivity. [72] The non-covalent functionalization of graphene can take place via π–π stacking, hydrophobic interaction, Van der Waals forces and electrostatic attraction.[73] Decorating graphene with polycyclic aromatic hydrocarbons are frequently used due to their π-π stacking interactions with graphene. In this context, frequently used

anchoring groups are naphthalene, anthracene, pyrene, coronene, porphyrin and their derivatives. [74] However, the supramolecular hybrids that these compounds form with graphene are often unstable in solvents where the molecular binding groups are highly soluble. Considering these stability aspects, Dichtel and co-workers designed a multivalent tripod capable of binding graphene through three pyrene units, which enhanced the overall stability.[75]
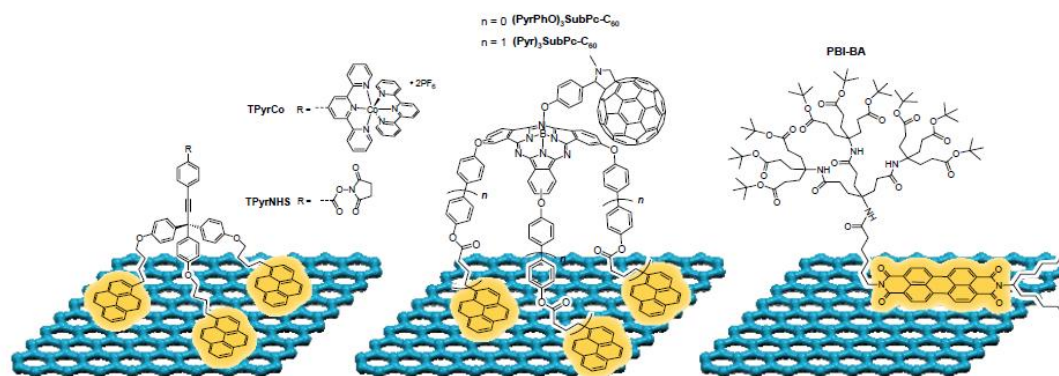
Figure 1.26 Representative examples of graphene-based hybrids with tripodal pyrene derivatives. (ref 75)

Stable dispersions of graphene sheets in water and organic solvents can also be obtained through non-covalent functionalization with a wide range of polymers.[74] Different non-ionic and ionic polymers have been used to disperse and stabilize graphene and, in general, it has been observed that nonionic polymers significantly outperform their ionic counterparts.[76a] Yoon and co-workers produced stable graphene dispersions by simply sonicating graphite with four different polymers based on either poly(vinyl alcohol) or dextran (Figure 1.27).[76b] The water-soluble polymers with phenyl- and pyrenyl-functionalized side chains facilitated the formation of stable aqueous dispersions of graphene without degrading its sp^2 hybridized structure.
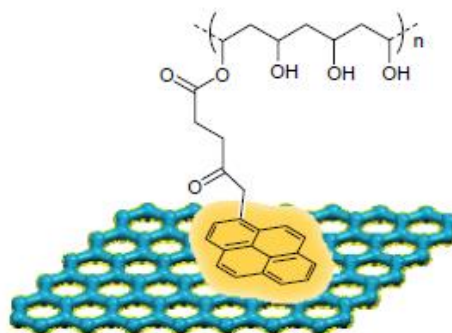
Figure 1.27 Molecular structure of graphene/polymer hybrid in ref. 76b.

1.5 Graphene-based Donor-Acceptor Systems

The band structure of graphene is that of a 0-gap semiconductor. This is a limit for the development of electronic devices, since virtually every device nowadays is based on semiconductor technologies that exploit band gaps. This feature, however, may offer an intriguing possibility for the development of donor-acceptor systems with donor/acceptor centers bound to a single sp^2 carbon backbone that provides them with an extended conjugation network. Recently, many researchers work on the graphene-based donor-acceptor systems [77], that can potentially facilitate photo-induced electron transfer interactions. With regard to energy conversion schemes, a few covalently linked graphene sheets with organic electron-donor moieties to facilitate photo-induced energy or electron-transfer processes have been synthesized by combining graphene and photo- and/or electro-active components.[78] In this respect, photo-induced excitation of the organic electron donor in the graphene-based hybrid materials results on the formation of the singlet-excited state of the organic component. Then, charge-separation takes place and the efficiency of the whole process is governed by how fast or slow the recombination of charges occurs. Jincai Zhao [79] developed a covalent donor-acceptor graphene-based hybrid via a very simple method, using a 1,3-dipolar cycloaddition with phenanthrene-9-carboxaldehyde (PCA). When this donor-acceptor graphene hybrid was transferred into an optoelectronic device, an enhanced photoelectrochemical performance was observed, if compared with its individual components. The performance was ascribed to the excellent electron-accepting and -transporting properties of graphene. Electron transfer from excited PCA to graphene was confirmed by the efficient fluorescence quenching of PCA.
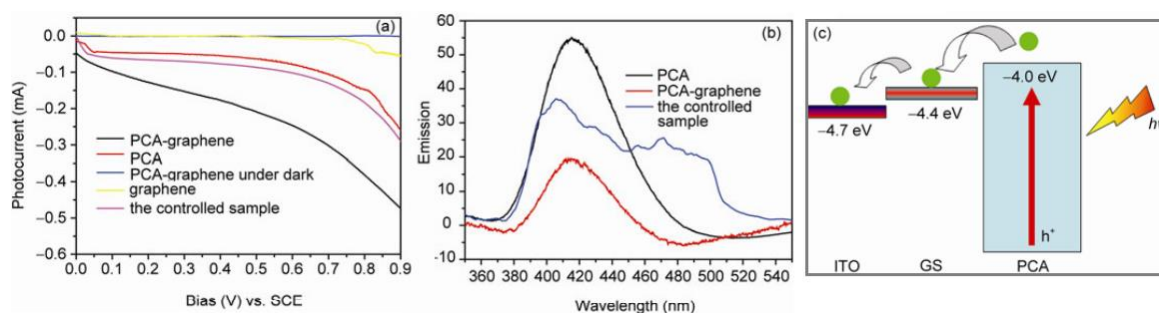
Figure 1.28 (a) Photoelectrochemical performance (b) steady-state fluorescence spectroscopic changes and (c) schematic energy-level diagram for the PCA-graphene (ref. 79).

Tomas Torres reported a highly exfoliated graphene covalently linked to electron accepting phthalocyanines (Figure 1.29). [80] The functionalization of the nanocarbon surface with alkyl sulfonyl phthalocyanines was attained by means of a "click" chemistry protocol. Notably, few-layered graphene was obtained by solvent-assisted exfoliation of graphite following a modification of a procedure recently reported by Tour and co-workers, which relies on the use of chlorosulfonic acid. In addition, a full-fledged and comprehensive assay regarding the electronic features of the resulting nanoconjugate was described.
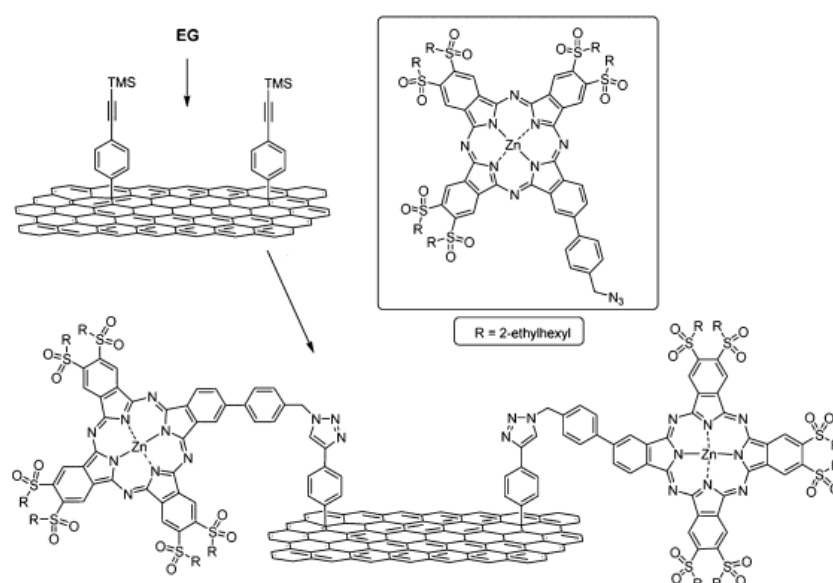
Figure 1.29 Procedure for the covalent functionalization of exfoliated graphene (ref. 90).

Complete microscopic and spectroscopic assays confirmed the structure of the resulting electron donor−acceptor conjugate and the electron transfer evolving from graphene to the photoexcited Pc component. In terms of electron transfer mechanism, charge separation with 1.0 ± 0.5 ps leads the authors to assume that a through-space pathway rather than a through bond pathway is operative before charge delocalization within few-layer graphene takes over. Implicit in such a mechanism is a close proximity of the Pcs relative to the basal plane of graphene. Covalent functionalization introduces sp³ centers within the basal plane of graphene, which are expected to impact the charge delocalization and electron donating behavior. F Bonaccorso and coworkers exploited graphene nanoflakes (GNFs) with controlled lateral size;[81] the functionalization was carried out through the attachment of an ethylenedinitrobenzoyl (EDNB) molecule to the

GNFs. Their idea originates from model calculations based on a density functional theory (DFT) approach that demonstrates the possibility to tune the GNF electronic properties in order to open a bandgap, achieving a fine tuning of both the highest occupied molecular orbital (HOMO) and lowest unoccupied molecular orbital (LUMO) energy values of the GNFs.
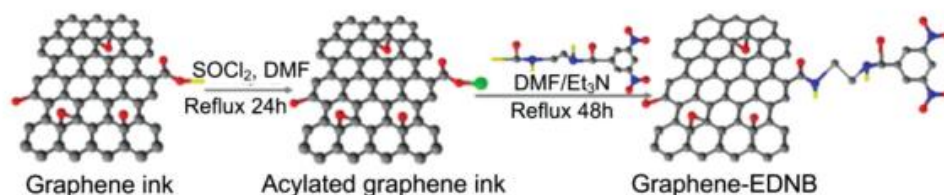
Figure 1.30 Schematic illustration of the graphene functionalization process in Ref. 81.

1.6 Diketopyrrolopyrrole (DPP) as Electron Acceptor to Functionalize Graphene

The above-mentioned studies reveal that by attaching organic moieties (acting as donors or acceptors) to graphene, the electronic characteristics of graphene can be improved and multifunctional nanometer-scale materials for optical and/or optoelectronic applications may be generated. However, applications of donor-acceptor graphene in real photodevices is still limited, for the low optical absorption of the final conjugates. To increase the conjugate performance, one should increase either the absorption efficiency or the lifetime of the photo-excited carriers. Here, we focus on an outstanding π-conjugated building block, diketopyrrolopyrrole (DPP), which is a strong electron acceptor with high visible-light absorption and strong fluorescence.[82] Coupling the DPP unit with electron donor units to form a donor–acceptor (D–A) motif is a common strategy to tune the frontier molecular orbital positions and increase effective conjugation length.[83] The molecular frame of DPP (Figure 1.31) has many reactive centers such as (i) the aryl rings that undergo electrophilic and nucleophilic reactions and (ii) the bicyclic lactam chromophoric unit with three different functional groups: (1) –C=C– double bonds, (2) carbonyl, and (3) secondary amine (NH) groups that may potentially undergo structural modification for further derivatization (Scheme 1). The significant advantages of DPP derivatives are as follows: (a) they can undergo several synthetic modifications, (b) act as

strong acceptor units, (c) exhibit high fluorescence quantum yields, and (d) possess exceptional thermal and photostability, making them excellent building blocks for many applications.
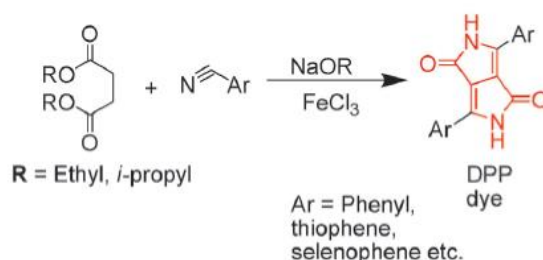
Figure 1.31 General synthetic route for DPP and its derivatives.

All DPP derivatives exhibit dual band absorption profiles common for compounds with a donor–acceptor primary structure. For example, Figure 1.32 present the UV-Vis spectra of TDPP derivatives, the absorption profiles show intense low energy bands at approximately 500 nm and weaker high energy bands at around 340 nm attributed to strong intramolecular interactions from the thiophene donor to the DPP acceptor and π–π transitions localized on either the donor or the acceptor, respectively. [84]
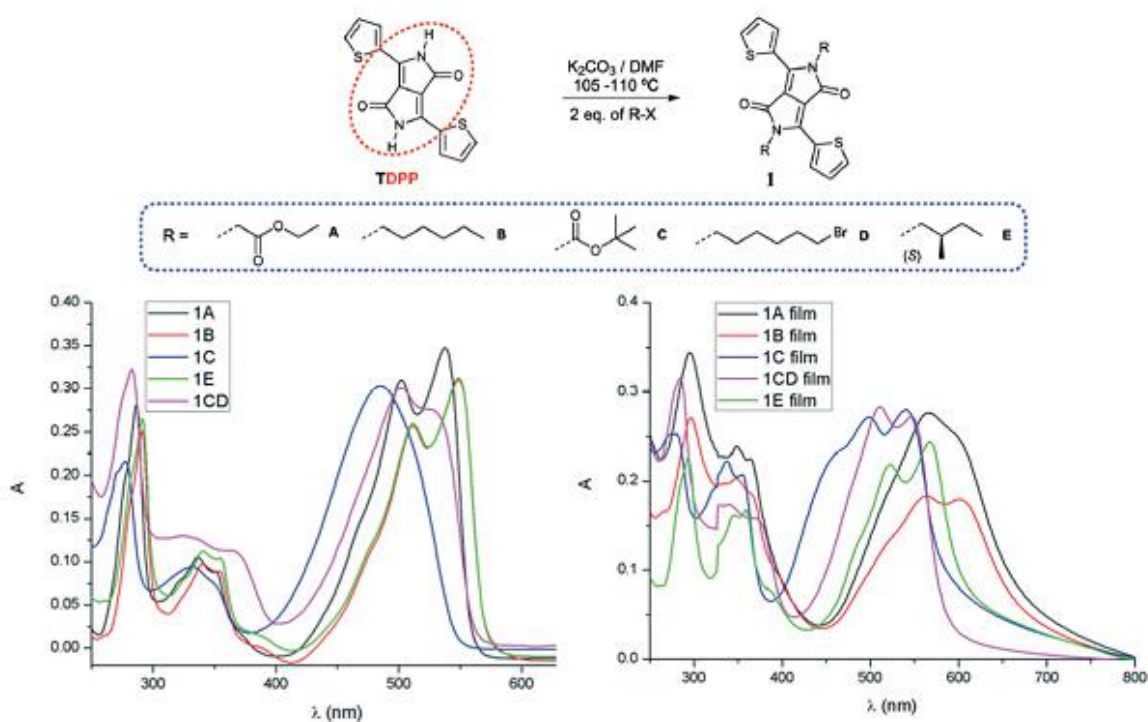
Figure 1.32 Absorption spectra of compounds 1A–C, E and 2A–C, E in solution (CH_2Cl_2 10^{-5} M, left) as film (right) in Ref [84].

In all derivatives, the absorption peaks of the solids (film) are broader and red shifted by about 50 nm compared to the solution state bands, which is indicative of increased intermolecular interactions in the solid state. In the absorption spectra of the films the low energy regions show shoulder peaks that result from vibrionic coupling of adjacent molecules. The emerging shoulder of the lower energy band has been associated to the formation of H-type aggregates and the red shift of the lower energy band to the formation of J-type aggregation. These results are particularly pertinent given the very recent report on the geometry dependence of singlet fission in TDPP derivatives, an effect which is promising for the application of these materials in optoelectronic devices.

As reported by W. J. Yang,[85] the emission spectra of DPP derivatives are all of the same shape, but the red-shift emission bands of ~10 nm can be observed for different group ended DPP derivatives. The solution fluorescence quantum yields (Ø) of DPP derivatives are also relative to the substituents at the benzene ring, and Ø values of mDPP-Br, mDPP-Cl and mDPP-Me in THF measured by the dilute solution method using rhodamine B as the reference are 0.56, 0.52 and 0.61, respectively. Overall, they are all strongly fluorescent molecules, and the substituents at the benzene ring of DPP, even if simple methyl, chloride and bromide, could affect the intramolecular charge transfer (ICT) effect of the DPP core and modify moderately the optical properties of DPP derivatives.
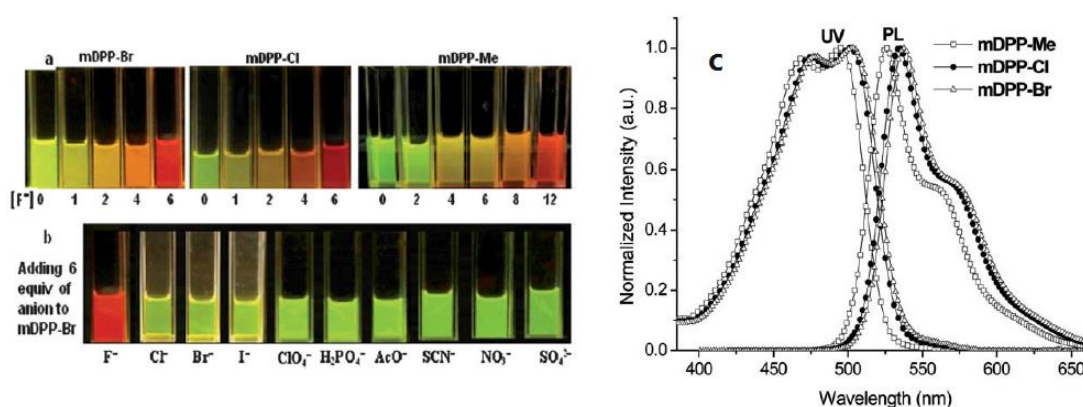
Figure 1.33 a) Fluorescence photographs under illumination of mDPP-X in THF with different equivalents of fluoride anions and b) mDPP-Br in THF with other anions of 6 equiv. c) Absorption and emission spectra in Ref [85].

Y. S. Wu [86] first functionalized graphene with diketopyrrolopyrrole derivatives (TDPP, TTDPP) to enhance the light absorption of graphene hybrid systems for high performance

visible-light photodetectors. In their research, the DPP derivatives were non-covalently attached to rGO nanosheets through self-assembly (Figure 1.34).
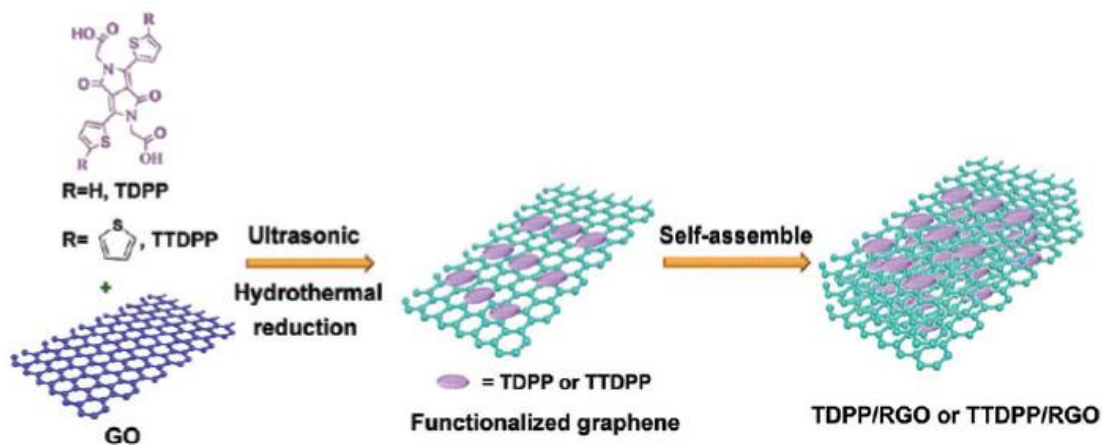
Figure 1.34 Schematic illustration of preparation of the TDPP(TTDPP)/RGO hybrids.

The hybrid TTDPP/rGO photodetector exhibits excellent visible-light photo response characteristics (34.2 A W^{-1} and the on/off ratio was 282) as shown in Figure 1.35, owing to the broad absorption and large extinction of TTDPP molecules and the excellent electronic conductivity of rGO that acts not only as a superior supporting matrix for anchoring the sensitizer molecules but also as an excellent electron mediator to adjust electron transfer.
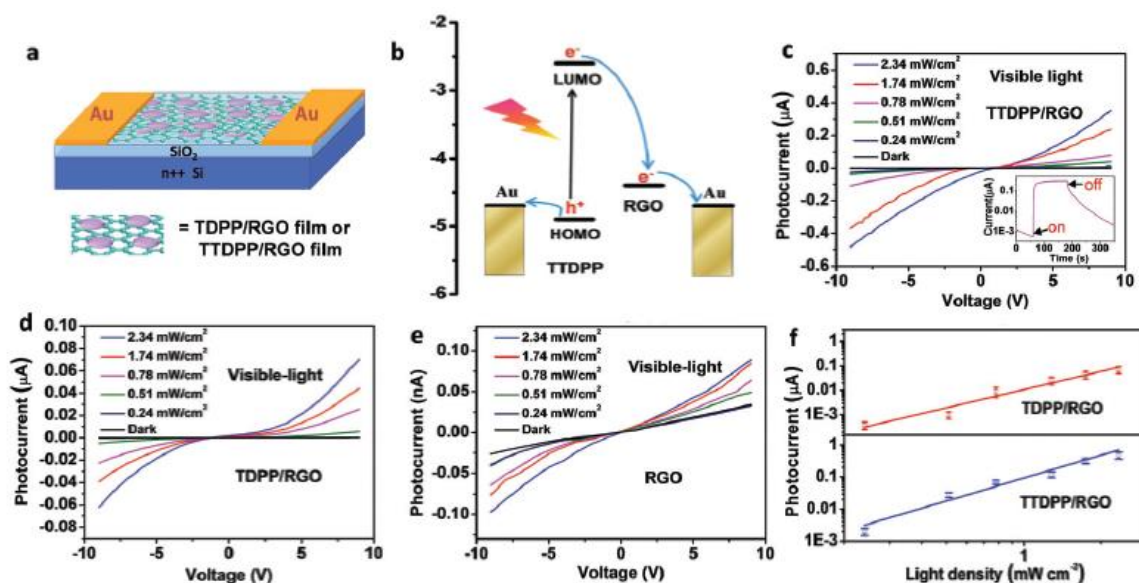
Figure 1.35 a) Schematic diagram of the photodetector based on the hybrid composites. b) Schematic diagram of the charge-transfer process in TTDPP/RGO hybrids. Photocurrents versus light densities upon visible illumination of (c) TTDPP/RGO, (d) TDPP/RGO and (e) RGO. (f) Photocurrents versus light densities of TDPP/RGO and TTDPP/RGO

1.7 Aim of The Thesis and Outline

The research described in this Thesis is aimed at the preparation and characterization of novel graphene-based materials that support organic chromophores. The extended conjugation provided by the network of sp^2 carbon atoms of the graphene scaffold should provide a direct electronic link between electron-donating or electron-accepting groups, opening the road to a new class of distributed D-A junctions. Chromophores linked to graphene typically experience a redshift in their absorption and emission spectra, due to the extension of their own π-systems, together with changes in their excited state lifetimes. On this basis, we explore a new covalent graphene system with electron trapping units diketopyrrolepyrrole (**DPP**) which has large extinction coefficient in the visible-light region. DPP derivatives can be easily attached covalently to electron-rich units to adjust the HOMO/LUMO energy levels and obtain low bandgap organic semiconductors. Therefore, it is expected that, by combining 2D nanometer-scale graphene with DPP molecules, multifunctional nanometer-scale materials for optoelectronic/electro-chemical applications may be generated.

This thesis is composed of 4 Chapters:

Chapter **1** gives an overview on the main characteristics of graphene, including the production, characterization, functionalization and graphene-based donor-acceptor systems.

Chapter **2** shows the method that we wrote to prepare exfoliated few layers graphene (EXG). These EXG flakes were used to prepare functionalized graphene hybrids.

Chapter **3** describes the synthesis and characterization of a graphene hybrid with the diketopyrrolopyrrole (DPP).

Chapter **4** reports the conclusive remarks and perspectives of this thesis research work.

Each Chapter is followed by its own list of references, and the NMR spectra in experimental section were listed in the appendix part.

1.8 Bibliography

[1] A. K. Geim and K. S. Novoselov, Nature Materials, 2007, 6, 183-191.

[2] a) P. R. Wallace, Phys. Rev., 1947, 71, 622-634; b) J.W. McClure, Phys. Rev., 1956, 104, 666-671; c) J.C. Slonczewski, P.R. Weiss, Phys. Rev. 1958, 109, 272-279.

[3] E. Fradkin, Phys. Rev. B, 1986, 33, 3263-3268.

[4] K. S. Novoselov, A. K. Geim, S. V. Morozov, D. Jiang, Y. Zhang, S. V. Dubonos, I. V. Grigorieva and A. A. Firsov, Science, 2004, 306, 666–669.

[5] a) A. H. Castro Neto, Reviews of modern physics, 2009, 81(1), 109-163; b) C. Riedl, C. Coletti, J. Phys. D: Appl. Phys., 2010, 43(37), 374009-374026.

[6] a) D. R. Cooper, B. D'Anjou, N. Ghattamaneni, B. Harack, M. Hilke, A. Horth, N. Majlis, M. Massicotte, L. Vandsburger, E. Whiteway, V. Yu. ISRN Condensed Matter Physics, 2012, 2012, 1-56; b) A. H. Castro Neto, F. Guinea, N. M. R. Peres, K. S. Novoselov, A. K. Geim, Rev. Mod. Phys., 2009, 81, 109–162; c) S. Das Sarma, A. K. Geim, P. Kim, A. H. MacDonald, Solid State Commun., 2007, 143, 1–2; d) M. D. Stoller, S. Park, Y. Zhu, J. An, R. S. Ruoff, Nano Lett., 2008, 8, 3498–3502.

[7] Novoselov, K. S.; Falko, V. I.; Colombo, L.; Gellert, P. R.; Schwab, M. G.; Kim, K. Nature 2012, 490, 192.

[8] K. I. Bolotin, K. J. Sikes, Z. Jiang, M. Klima, G. Fudenberg, J. Hone, P. Kim, H. L. Stormer, Solid State Communications, 2008, 146, 351-355.

[9] D. A. C. Brownson, D. K. Kampouris, C. E. Banks. Chem. Soc. Rev., 2012,41, 6944-6976.

[10] D. Akinwande, C. J. Brennan, J. S. Bunch, P. Egberts, J. R. Felts, H. Gao, R. Huang, J. Kim, T. Li, Y. Li, K. M. Liechti, N. Lu, H. S. Park, E. J. Reed, P. Wang, B. I. Yakobson, T. Zhang, Y. Zhang, Y. Zhou, Y. Zhu, Extreme Mechanics Letters, 2017, 13, 42–77.

[11] a) F. Liu, P. Ming, J. Li. Phys. Rev. B, 2007, 76, 064120; b) C. Lee, X. Wei, J. W. Kysar, J. Hone. Science, 2008, 321, 385–388.

[12] R. R. Nair, P. Blake, A. N. Grigorenko, K. S. Novoselov, T. J. Booth, T. Stauber, N. M. R. Peres, A. K. Geim. Science, 2008,320, 1308-1308.

[13] A. A. Balandin, S. Ghosh, W. Bao, I. Calizo, D. Teweldebrhan, F. Miao, C. N. Lau. Nano Lett., 2008, 8 (3), 902–907.

[14] a) G. W. Semenoff, Phys. Rev. Lett. 1984, 53, 2449–-2452; b) F. D. M. Haldane, Phys. Rev. Lett., 1988, 61, 2015–-2018.

[15] Y. Zheng, T. Ando, Phys. Rev. B, 2002, 65, 245420; b) K. S. Novoselov, A. K. Geim, S. V. Morozov, D. Jiang, M. I. Katsnelson, I. V. Grigorieva, S. V. Dubonos, A. A. Firsov. Nature, 2005, 438,197-200.

[16] Y. Zhang, Y. W. Tan, H. L. Stormer, P. Kim, Nature, 2005, 438, 201–204.

[17] a) Tour, J. M. Chemistry of Materials 2004, 26(1), 163-171; b) Keith R. Paton, Eswaraiah Varrla, Jonathan N. Coleman. Nature Materials 2014, 13, 624–630; c) John Texter, Current Opinion in Colloid & Interface Science, 2014, 19, 163-174.

[18] M. Lotya, P. J King, U. Khan, S. De, J. N. Coleman. ACS Nano 2010, 4, 3155-3162.

[19] C. Y. Su, A. Y. Lu, Y. P. Xu, F. R. Chen, A. N. Khlobystov, L. J. Li. ACS Nano 2011, 5, 2332-2339.

[20] a) Y. Hernandez, V. Nicolosi, M. Lotya, F. M. Blighe, Z. Sun, S. De, I. T. McGovern, B. Holland, M. Byrne, Y. K. Gun'ko, K. Yurii, J. J. Boland, P. Niraj, G. Duesberg, S. Krishnamurthy, R. Goodhue, J. Hutchison, V. Scardaci, A. C. Ferrari, J. N. Coleman, Nature Nanotechnology, 2008, 3, 563-568; b) C. E. Hamilton, J. R. Lomeda, Z. Sun, J. M. Tour and A. R. Barron, Nano Letters, 2009, 9, 3460-3462. c) Michio Matsumoto,YusukeSaito, Chiyoung Park, Takanori Fukushima and Takuzo Aida. Nature Chemistry, 2015, 7, 730-736.

[21] C. Vallés, C. Drummond, H. Saadaoui, C. A. Furtado, M. S. He, O. Roubeau, L. Ortolani, M. Monthioux, A. PénicaudV. J. Am. Chem. Soc., 2008, 130, 47, 15802-15804.

[22] Y. Hernandez, V. Nicolosi, M. Lotya, F. M. Blighe, Z. Y. Sun, S. De, I. T. McGovern, B. Holland, M. Byrne, Y. K. Gun'Ko, J. J. Boland, P. Niraj, G. Duesberg, S. Krishnamurthy, R. Goodhue, J. Hutchison, V. Scardaci, A. C. Ferrari, J. N. Coleman. Nature Nanotechnology, 2008, 3, 563–568.

[23] W. C. Du, J. Lu, P. P. Sun, Y. Y. Zhu, X. Q. Jiang, Chemical Physics Letters, 2013, 568-569, 198-201.

[24] R. Singha, D. Kumar, C. C. Tripathi, Procedia Computer Science. 2015, 70, 565 – 571

[25] a) B. C. Brodie, Ann. Chim. Phys. 1860, 59, 466; b) C. Schafhaeutl, Phil. Mag. 1840, 16, 570–590; c) L. Staudenmaier, Ber. Deut. Chem. Ges. 1898, 31, 1481; d) W. S. Hummers, R. E. Offeman, J. Am. Chem. Soc. 1958, 80, 1339.

[26] A. Buchsteiner, A. Lerf, J. Pieper, J. Phys. Chem. B, 2006, 110, 22328-22338.

[27] I. Jung, M. Pelton, R. Piner, D. A. Dikin, S. Stankovich, S. Watcharotone, M. Hausner, R. S. Ruoff. Nano Lett., 2007, 7, 3569-3575.

[28] S. V. Tkachev, E. Y. Buslaeva, S. P. Gubin. Inorganic Materials, 2011, 47, 1-10.

[29] a) S. Stankovich, R. D. Piner, X. Q. Chen, N. Q. Wu, S. T. Nguyen, R. S. Ruoff. J Mater Chem, 2006; 16:1558–65; b) S. Z. Zu, B. H. Han. J Phys Chem C, 2009, 113, 13651–13657; c) C. Shan, H. Yang, D. Han, Q. Zhang, A. Ivaska, L. Niu. Langmuir 2009, 25, 12030–12033; d) J. Guo, L. Ren, R. Wang, C. Zhang, Y. Yang, T. Liu. Compos B, 2011, 42, 2130–2135.

[30] L. Sun, B. Fugetsu. Materials Letters, 2013, 109, 207-210.

[31] S. N. Alam, N. Sharma, L. Kumar. Graphene, 2017, 6, 1-18.

[32] A. Ambrosi, C. K. Chua, N. M. Latiff, A. H. Loo, C. H. A. Wong, A. Y. Sheng, A. Bonanni, M. Pumera. Chem. Soc. Rev., 2016, 45,2458-2493.

[33] a) A. J. Cooper, N. R. Wilson, I. A. Kinloch and R. A. W. Dryfe, Carbon, 2014, 66, 340–350; b) J. Wang, J. Huang, R. Yan, F. Wang, W. Cheng, Q. Guo and J. Wang, J. Mater. Chem. A, 2015, 3, 3144–3150; c) K. Parvez, Z.-S. Wu, R. Li, X. Liu, R. Graf, X. Feng and K. Mu¨llen, J. Am. Chem. Soc., 2014, 136, 6083–6091; d) A. Ambrosi and M. Pumera, Chem. – Eur. J., 2016, 22, 153–159; e) K. S. Rao, J. Sentilnathan, H.-W. Cho, J.-J. Wu and M. Yoshimura, Adv. Funct. Mater., 2015, 25, 298–305; f) S. Yang, et al., J. Am. Chem. Soc., 2015, 137, 13927–13932

[34] G. Wang, B. Wang, J. Park, Y. Wang, B. Sun and J. Yao, Carbon, 2009, 47, 3242–3246.

[35] a) Y. L. Zhong and T. M. Swager, J. Am. Chem. Soc., 2012, 134, 17896–17899; b) P. Yu, Z. M. Tian, S. E. Lowe, J. C. Song, Z. R. Ma, X. Wang, Z. J. Han, Q. L. Bao, G. P. Simon, D. Li, Y. L. Zhong. Chem. Mater., 2016, 28, 22, 8429-8438.

[36] a) L. Y. Jiao, L. Zhang, X. R. Wang, G. Diankov, H. J. Dai. Nature, 2009, 458(7240), 877–880; b) A. L. Elias, A. R. Botello-Mendez, D. Meneses-Rodriguez, V. J. Gonzalez, D. Ramirez-Gonzalez, L. Ci, E. Muñoz-Sandoval, P. M. Ajayan, H. Terrones and M. Terrones. Nano Lett, 2010, 10(2), 366–372.

[37] D. V. Kosynkin, A. L. Higginbotham, A. Sinitskii, J. R. Lomeda, A. Dimiev, B. K. Price, J. M. Tour. Nature, 2009, 458, 872-876.

[38] a) J. L. Li, K. N. Kudin, M. J. McAllister, R. K. Prud'homme, I. A. Aksay, R. CarPhys. Rev. Lett. 2006, 96, 176101; b) P. M. Ajayan, B. I. Yakobson, Nature, 2006, 441, 818–819.

[39] C. S. Tiwary, B. Javvaji, C. Kumar, D. R. Mahapatra, S. Ozden, P. M. Ajayan, K. Chattopadhyay. Carbon, 2015, 89, 217-224.

[40] S. Mondal, S. Ghosh, C. R. Raj. ACS Omega 2018, 3, 622–630.

[41] H. Huang, S. Chen,A. T. Wee, W. Chen, Graphene, 2014, 3–26.

[42] A. J. V. Bommel, J. E. Crombeen, A. V. Tooren, Surf. Sci., 1975, 48, 463.

[43] a) W. A. De Heer, C. Berger, M. Ruan, M. Sprinkle, X. Li, Y. Hu, B. Zhang, J. Hankinson, E. Conrad, PNAS 2011, 108, 16900–16905; b) K. V. Emtsev, A. Bostwick, K. Horn, J. Jobst, G. L. Kellogg, L. Ley, J. L. McChesney, T. Ohta, S. A. Reshanov, J. R€ohrl, Nature Mater. 2009, 8, 203–207; c) B. Gupta, M. Notarianni, N. Mishra, M. Shafiei, F. Iacopi, and N. Motta, Carbon, 2014, 68, 563–572; d) B. Gupta, E. Placidi, C. Hogan, N. Mishra, F. Iacopi, N. Motta, Carbon, 2015, 91, 378–385.

[44] N.Mishra, J. Boeckl, N. Motta, F. Iacopi, Phys. Status Solidi A, 2016, 213, 2277-2289.

[45] a) Q. K. Yu, J. Lian, S. Siriponglert, H. Li, Y. P. Chen, S. S. Pei, Appl. Phys. Lett. 2008, 93, 113103; b) L. G. De Arco, Y. Zhang, A. Kumar, C. Zhou, IEEE Trans. Nanotechnol. 2009, 8, 135–138; c) A. Reina, X. Jia, J. Ho, D. Nezich, H. Son, V. Bulovic, M. S. Dresselhaus, J. Kong, Nano Lett. 2009, 9, 30–35.

[46] a) Y Zhang, L. Y. Zhang, C. W. Zhou. Accounts of chemical research, 2013, 46, 2329–2339; b) R. Muñoz, C. Gómez-Aleixandre. Chem. Vap. Deposition, 2013, 19, 297–322.

[47] D. Jiang, H. Zhu, W. Yang, L. Cui and J. Liu, Sens. Actuators B Chem., 2017, 239, 193–202.

[48] a) A. F. Tran-Van, H. A. Wegner. Top Curr Chem, 2014, 349, 121-157; b) F. Morgenroth, C. Kubel, M. Muller. Carbon, 1998, 36, 833–837; c) J. Sakamoto, J. van Heijst, O. Lukin, A. D. Schluter, Angew Chem Int Edit, 2009, 48, 1030–1069.

[49] M. C. Hu, Z. H. Yao, X. Q. Wang. AIMS Materials Science, 2017, 4(3), 755-788.

[50] X. D. Yang, Y. Zheng, J. Yang. W. Shi, J. H. Zhong, C. K. Zhang, X. Zhang, Y. H. Hong, X. X. Peng, Z. Y. Zhou, S. G. Sun, ACS Catal, 2017, 7, 139-145.

[51] a) H. Wang, W. Wei, Y. H. Hu. Catal Today, 2016, 274, 99–102. b) L. Rout, A. Kumar, R. S. Dhaka. G. N. Reddy, S. Giri, P. Dash. Appl Catal A-Gen, 2017, 538, 107–122.

[52] L. Lu, H. Tian, J. H. He, Q. W. Yang. J Phys Chem C, 2016, 120, 23660–23668.

[53] S. S. Nanda, M. J. Kim, K. S. Yeom. S. S. A. An, H. Ju, K. Yia. Trends Anal Chem, 2016, 80, 125–131.

[54] A. C. Ferrari, J. C. Meyer, V. Scardaci, C. Casiraghi, M. Lazzeri, F. Mauri, S. Piscanec, D. Jiang, K. S. Novoselov, S. Roth, A. K. Geim. Physical review letters, 2006, 97, 187401.

[55] a) D. Deng, X. L. Pan, L. Yu, Y. Cui, Y. P. Jiang, J. Qi, W. X. Li, Q. Fu, X. C. Ma, Q. K. Xue, G. Q. Sun, X. H. Bao. Chem Mater, 2011, 23, 1188–1193; b) M. Begliarbekov, O. Sul, S. Kalliakos. E. H. Yang, S. Strauf, Appl Phys Lett, 2010, 97, 031908.

[56] A. Milani, M. Tommasini, V. Russo, A. L. Bassi, A. Lucotti, F. Cataldo and C. S. Casari, Beilstein J. Nanotechnol, 2015, 6, 480–491.

[57] A. C. Ferrari, D. M. Basko, Nat Nano, 2013, 8, 235.

[58] Y. Zhou, Q. L. Bao, L. A. L. Tang, Y. L. Zhong, K. P. Loh. Chem Mater, 2009, 21, 2950–2956.

[59] a) L. Rout, A. Kumar, R. S. Dhaka, G. N. Reddy, S. Giri, P. Dash. Appl Catal A-Gen. 2017, 538, 107–122; b) M. Hu, K. S. Hui, K. N. Hui. Chem. Eng. J, 2014, 254, 237–244; c) H. Einaga, S. Futamura, J. Catal, 2004, 227, 304–312.

[60] B. L. Ou, Z. H. Zhou, Q. Q. Liu, B. Liao, S. J. Yi, Y. J. Ou, X. Zhang, D. X. Li, Polym. Chem., 2012, 3, 2768-2775.

[61] K. Yao, G. C. Zhang, Y. C. Lin, J. Gong, H. Na, T. Tang, Polym. Chem., 2015, 6, 389-396.

[62] a) T. Kuila, S. Bose, A. K. Mishra, P. Khanra, N. H. Kim, J. H. Lee, Progress in Materials Science, 2012, 1061–1105; b) A. Hirsch, J. M. Englert, F. Hauke. Accounts of Chemical Research, 2013, 87–96; c) D. W. Boukhvalov, M. I. Katsnelson. J. Phys.: Condens. Matter, 2009, 21, 344205-344217.

[63] a) M. B. Smith, March's Advanced Organic Chemistry: Reactions, Mechanisms, and Structure. 1992, ISBN: 0-471-60180-2. b) G. L. Miessler, D. A. Tarr, Inorganic Chemistry. Prentice Hall. 2004, ISBN: 0-13-035471-6.

[64] J. Park, M. Yan. Accounts of Chemical Research, 2012, 46(1), 181–189.

[65] A. Sinitskii, A. Dimiev, D. A. Corley, A. A. Fursina, D. V. Kosynkin, J. M. Tour, ACS Nano, 2010, 4, 1949–1954.

[66] a) J. M. Tour, C. A. Dyke, M. P. Stewart, F. Maya, Synlett, 2004, 1, 155–160; b) J. R. Lomeda, C. D. Doyle, D. V. Kosynkin, W. F. Hwang, J. M. Tour, J Am Chem Soc, 2008, 130(48), 16201–16206. c) R. Sharma, J. H. Baik, C. J. Perera, Nano Letters, 2010, 10(2), 398–405.

[67] P. P. Li, Y. Chen, J. H. Zhu, M. Feng, X. D. Zhuang, Y. Lin, H. B. Zhan. Chem – Eur J 2011, 17(3), 780–785.

[68] H. C. Wu, X. L. Chang, L. Liu, F. Zhao, Y. L. Zhao, J. Mater. Chem., 2010, 20, 1036–1052.

[69] V. Georgakilas, A. B. Bourlinos, R. Zboril, T. A. Steriotis, P. Dallas, A. K. Stuboscd, C Trapalis. Chem. Commun., 2010, 46(10), 1766–1768.

[70] a) G. A. Olah, I. Bucsi, D. S. Ha, R. Aniszfeld, C. S. Lee, G. K. S. Prakash, Fullerene Sci. Technol. 1997, 5, 389 – 405. b) T. S. Balaban, M. C. Balaban, S. Malik, F. Hennrich, R. Fischer, H. Rçsner, M. M. Kappes, Adv. Mater. 2006, 18, 2763 – 2767.

[72] a) D. Tasis, N. Tagmatarchis, A. Bianco, M. Prato. Chem Rev, 2006, 106(3), 1105–36; b) K. E. Riley, M. Pitoňák, P. Jurečka, P. Hobza. Chem Rev, 2010, 110(9), 5023–5063; c) D. A. Dougherty. Acc Chem Res, 2013, 46(4), 885–993; d) E. C. Lee, D. Kim, P. Jurečka, P. Tarakeshwar, P. Hobza, K. S. Kim. J Phys Chem A, 2007, 111(18), 3446–3457; e) S. Grimme S. Chem – Eur J, 2004, 10(14), 3423–3429; f) P. Tarakeshwar, H. S. Choi, K. S. Kim. J Am Chem Soc 2001, 123(14), 3323–3331.

[73] V. Georgakilas, J. N. Tiwari, K. C. Kemp, J. A. Perman, A. B. Bourlinos, K. S. Kim, R. Zboril, Chem. Rev., 2016, 116(9), 5464–5519.

[74] J. A. Mann and W. R. Dichtel, Phys. Chem. Lett., 2013, 4, 2649–2657.

[75] A. Ciesielski and P. Samori, Adv. Mater., 2016, 28, 6030–6051

[76] a) I. U. Unalan, C. Y. Wan, S. Trabattoni, L. Piergiovanni and S. Farris, RSC Adv., 2015, 5, 26482–26490; b) H. W. Shim, K.-J. Ahn, K. Im, S. Noh, M.-S. Kim, Y. Lee, H. Choi and H. Yoon,Macromolecules, 2015, 48, 6628–6637.

[77] A. Stergiou, G. Pagona, N. Tagmatarchis, Beilstein Journal of Nanotechnology, 2014, 5, 1580–1589.

[78] a) M.-E. Ragoussi, G. Katsukis, A. Roth, J. Malig, G. de la Torre, D. M. Guldi, T. Torres, J. Am. Chem. Soc. 2014, 136, 4593–4598. b) B. Xiao, X. Wang, H. Huang, M. Zhu, P. Yang, Y. Wang, Y. Du, J. Phys. Chem. C 2013, 117, 21303–21311. c) L. Brinkhaus, G. Katsukis, J. Malig, R. D. Costa, M. Garcia-Iglesias, P. Vasquez, T. Torres, D. M. Guldi, Small 2013, 9, 2348–2357.

[79] G. L. Liu, C. L. Yu, C. C. Chen, W. H. Ma. H. W. Ji, J. C. Zhao, Sci. China Chem. 2011, 54, 1622-1526.

[80] M. E. Ragoussi, G. Katsukis, A. Roth, J. Malig, G. de la Torre, D. M. Guldi, T. Torres. J. Am. Chem. Soc., 2014, 136, 4593–4598.

[81] F. Bonaccorso, N. Balis, M. M. Stylianakis, M. Savarese, C. Adamo, M. Gemmi, V. Pellegrini, E. Stratakis, E. Kymakis. Adv. Mater. 2015, 25, 3870-3880.

[82] a) S. Qu, H. Tian, Chem. Commun. 2012, 48, 3039–3051. b) Y. Li, P. Sonar, L. Murphy, W. Hong, Energy Environ. Sci. 2013, 6, 1684–1710. c) P. Sonar, G. M. Ng, T. T. Lin, A. Dodabalapur, Z. K. Chen. J. Mater. Chem. 2010, 20, 3626–3636. d) A. Tang, C. Zhan, J. Yao, E. Zhou. Adv. Mater. 2017, 29, 1600013.

[83] J. Dhar, N. Venkatramaiah, A. A, S. J. Patil. J. Mater. Chem. C 2014, 2, 3457–3466. b) S. P. Senanayak, A. Z. Ashar, C. Kanimozhi, S. Patil, K. S. Narayan. Phys. Rev. B: Condens. Matter Mater. Phys. 2015, 91, 115302. c) Y. P. Zhang, L. C. Chen, Z. Q. Zhang, J. J. Cao, C. Tang, J. Liu, L. L. Duan, Y. Huo, X. Shao, W. Hong, H. L. Zhang. J. Am. Chem. Soc. 2018, 140, 6531–6535.

[84] F. Pop, W. Lewisa, D. B. Amabilino. CrystEngComm, 2016, 18, 8933-8943.

[85] C. Yang, M. Zheng, Y. P. Li, B. L. Zhang, J. F. Li, L. Y. Bu, W. Liu, M. X. Sun, H. C. Zhang, Y. Tao, S. F. Xue, W. J. Yang. J. Mater. Chem. A, 2013, 1, 5172-5178.

[86] H. T. Lin, Z. C. Xu, L. N. Zhang, X. C. Yang, Q. Ju, L. Xue, J. Zhou, S. P. Zhuo, Y. S. Wu. NewJ.Chem., 2017, 41, 4302-4307.

CHAPTER 2

FEW LAYERS GRAPHENE BASED ON SOLVENT EXFOLIATION OF GRAPHITE

We prepared a series of few layer-graphene samples from graphite, through rotor-stator homogenizer using N-Cyclohexyl-2-Pyrrolidone *(NCP)* as solvent. After centrifugation at different rounds per minute (rpm), three kinds of exfoliated graphene flakes *(EXG800*, *EXG1500* and *EXG3000)* with different qualities were obtained. They were characterized by TEM, TGA and Raman spectroscopy.

2. FEW LAYERS GRAPHENE BASED ON SOLVENT EXFOLIATION OF GRAPHITE

2.1 Introduction

Among the production methods of few layer-graphene, aforementioned in the previous chapter, liquid exfoliation of graphite using an organic solvent and a high-speed homogenizer is a convenient way to give scalable, defect-free graphene sheets. It is a low-cost method since commercial graphite powder is used as starting material. As reported by James Tour, [1] this approach is also more energy efficient than the sonication route, making few layers graphene solutions to be industrially accessible, with a productivity up to 100 g h^{-1}[2].

2.2 Basis

The exfoliation of graphite is achieved by breaking the van der Waals interactions among adjacent carbon layers, whose distance is 0.335 nm. We consider a system made of two infinite graphene layers as described by Rafael Tadmor; [3] the force over the radius corresponds to the energy per unit area E_A between the two infinite layers, which can be derived from equation (1):

$$E_A = -\frac{A}{12\pi}\left(\frac{1}{d^2} + \frac{1}{(d+h_1+h_2)^2} - \frac{1}{(d+h_1)^2} - \frac{1}{(d+h_2)^2}\right) \cdot$$

....(1)

Equation (1) gives the energy per unit area between a planar wall of thickness h_1 and a planar wall of thickness h_2 when separated by a distance d, as shown in figure 2.1.; A is the Hamaker constant of graphite (A = 2:38 × 10^{-19} J).
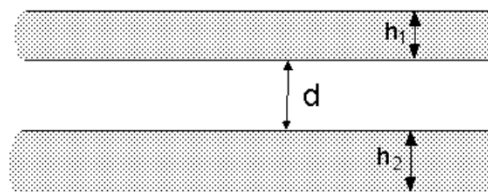
Figure 2.1. A cross-section of two parallel walls of finite thickness and infinite lateral dimensions. (ref 3)

For graphite exfoliation, the thickness of the second plate h_2 was held constant at 4 µm, which is equal to the mean of the initial size of a graphite particle. Figure 2.2 shows that on increasing the sheet thickness, the interaction energy between the two plates increases until a nearly constant energy is reached at a small thickness h_1, because $d<<h_1$, h_2. Hence, the mechanism of peeling only few layers from the graphite surface is energetically more likely. From the above analysis, it can be estimated that in order to shear off a complete sheet from a feed particle with an initial size of 4 µm, an interaction energy of about 90×10^{-14} J has to be overcome by the exfoliating medium.
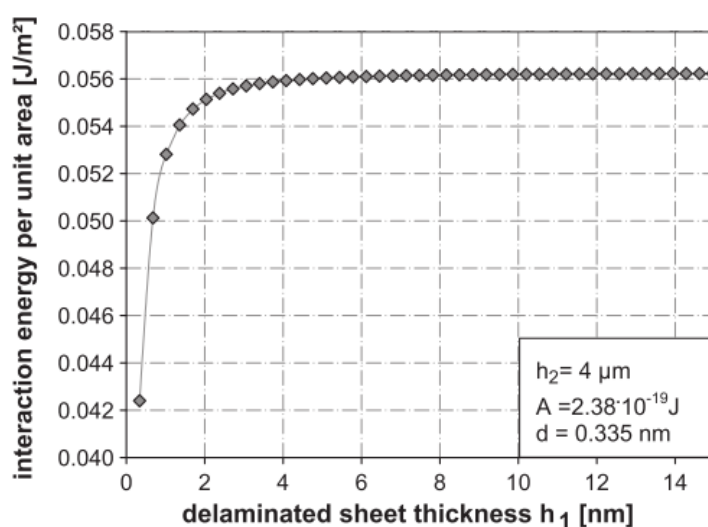
Figure 2.2. Interaction energies per unit area between two plates of finite thickness. (ref 3)

To understand the surface energy of graphene, it is helpful to refer to the surface energy of carbon nanotubes (CNT) because both are composed of sp^2-hybridized carbon atoms and have a similar surface.[4] A combination of experiments and theoretical modelling, gave the enthalpy of mixing CNT per volume of solvent:

$$\Delta H_{mix} / V \approx 4 \left(\sqrt{E_{S,NT}} - \sqrt{E_{S,Sol}} \right)^2 \phi / D$$

....(2)

Where Ø is the dispersed nanotube volume fraction, D is the dispersed nanotube diameter, $E_{S,NT}$, and $E_{S,Sol}$ are the nanotube and solvent surface energies respectively. This suggested that, successful solvents are those with surface energies close to that of the nanotubes. [5] It has been shown that the maximum dispersible concentration of rigid rods in a solvent is given by the following expression: [6]

$$\phi \approx K' \exp\left[-\frac{\bar{v}}{RT} \frac{\partial\left(\Delta H_{Mix}/V\right)}{\partial\phi} \right]$$ ....(3)

Where K' is a constant and $\bar{v}$ is the molar volume of rods. Applying this to nanotubes by inserting (2) into (3) we obtain:

$$\phi \approx K' \exp\left[-\frac{\pi DL}{4E_{S,NT}kT}\left(E_{S,NT} - E_{S,Sol}\right)^2 \right]$$ ....(4)

where L is the mean nanotube length. This expression represents a Gaussian function when Ø is plotted versus the solvent surface energy. Experimental data agrees well with this model confirming that nanotubes can be dispersed at high concentrations once the solvent and nanotube surface energies match. [6] Once the role of surface energy was known, it became clear that as graphite has a surface energy similar to carbon nanotubes, it might be possible to exfoliate graphite to form graphene in certain solvents. According to Keith R. Paton, [2] localized, turbulent, and highly dissipative regions are responsible for exfoliation. [7] Turbulent energy dissipation, however, is unnecessary while shear-mixing graphite and NMP in the complete absence of turbulence under high-shear laminar flow. The study showed that with a minimum shear rate of $\dot{\gamma}_{min} \approx 10^4$ s^{-1}, the production of graphene was confirmed. For the exfoliation process, considered as a shear-induced interlayer sliding in a solvent, a minimum shear rate can be evaluated:

$$\dot{\gamma}_{min} = \frac{\left[\sqrt{E_{S,G}} - \sqrt{E_{S,L}}\right]^2}{\eta L}$$ ....(5)

where $E_{S,G}$ and $E_{S,L}$ are the surface energies of graphene and the liquid ($E_{S,L}$=69 mJ m^{-2} for NMP [8]), η is the liquid viscosity (0.0017 Pa s for NMP) and L is the flake length. This equation shows the role of the solvent; for solvents with surface energies matching to that of graphene, the exfoliation energy is minimized, facilitating shear exfoliation at low shear rates. Given the flake size measured by TEM (~300–800 nm) and $\dot{\gamma}_{min}$ = 10^4 s^{-1}, equation (5) predicts, $E_{S,G} \approx$ 70.5–71 mJ m^{-2}, very close to the expected value. [8] In fact it tells us that a shear rate > 10^4 s^{-1} is required for exfoliation. On this basis, in the following section

a rotor-stator homogenizer, which offers the appropriate shearing rate, could be used to exfoliate graphite.

2.3 Materials, instruments and methods

Materials: Solvents were purified by standard methods. All commercially available reagents and solvents were purchased from Sigma–Aldrich and, Fluka or TCI chemicals if not otherwise specified and used as received. Graphite powder was purchased from SUPERIOR GRAPHITE and used as received.

Instruments and methods: TEM images were recorded on a Jeol 300 PX electron microscope. One drop of sample was placed on the sample grid and the solvent was allowed to evaporate. Thermogravimetric analysis (TGA) was run with ~1 mg sample using a Q5000 IR model TGA instrument using the method of starting from 100 °C and keeping isothermal conditions for 20 min. Followed by, ramping up to 10 °C / min to 1000 °C. 240 μL **EXG** suspension was loaded on the TGA pan, after which the NCP solvent was removed by heating it to 135 °C under vacuum for 20 min. Micro-Raman spectra were collected with an Invia Renishaw Raman micro spectrometer (X50 objective) using the 633 nm line of a He – Ne laser. Raman measurement for each sample was tested on 8 spots applying the principle of statistics.

The solvent-based exfoliation of graphite was carried out with a high-speed rotor-stators homogenizer (Figure 2.3 left, IKA digital ultra turrax model: T 25 D, speed range from 3,000 to 25,000 rpm). The shearing head used in this work was- model S 25 N-25 F, which offers maximum number of permissible revolutions to 24,000 min^{-1} with a working volume range 100 – 2,000 mL. The generator type homogenizer was developed to make dispersions and emulsions. [9] The fast-spinning inner rotor with a stationary outer stator constitutes a generator to homogenize the samples through mechanical shearing fluid forces. Figure 2.4 illustrates the procedure of how the homogenizer works on tearing biological tissues. The biological tissues are drawn up into the apparatus by a rapidly rotating rotor positioned within a static stator containing slots or holes.

Figure 2.3. High-speed homogenizer (left) and components of the assembled shearing head (right).

Here, the material is pushed outward to exit through the slots or holes. The high speed of the rotor ensures that the tissue is rapidly reduced in size by a combination of extreme turbulence, cavitation and scissor-like mechanical shearing occurring within the narrow shear gap between the rotor and the stator. Since most rotor-stator homogenizers have an open configuration, the product is repeatedly produced. The process is fast and desired results will usually be obtained in 15-120 seconds. [9]
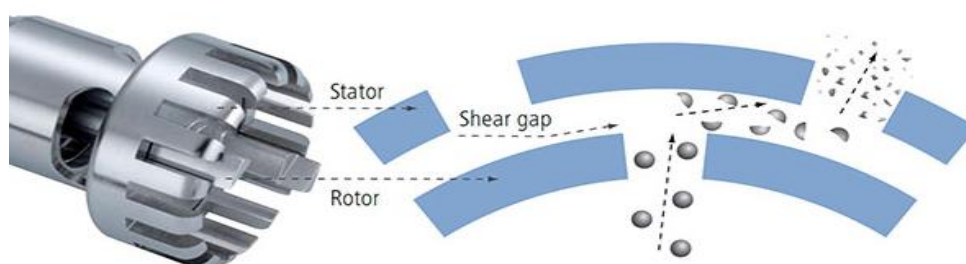
Figure 2.4. Illustration of biological tissues tearing by the homogenizer.

2.4 Production of exfoliated graphene (EXG) flakes

Our EXG flakes were produced with the homogenizer using the solvent, *N*-Cyclohexyl-2-pyrrolidone (**NCP**), the schematic diagram of the preparation procedure is shown in Figure 2.5.
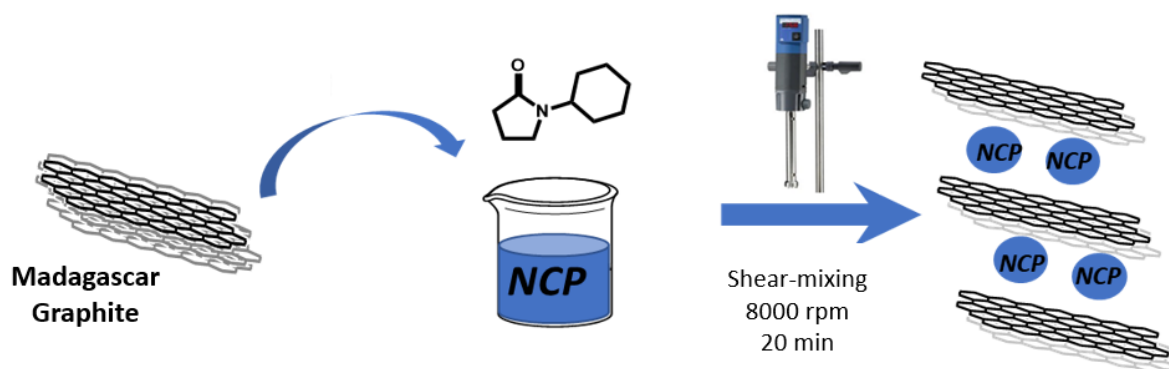
Figure 2.5. Production schematic diagram of EXG flakes through homogenizer.

Graphite powder (5 g, Figure 2.6) was inroduced into a 150 mL quartz cylinder with 100 mL **NCP** solvent. The quartz cylinder was cladded with ice to avoid rapid heat release during exfoliation. The high-speed homogenizer was set at a speed of 3000 rpm that was gradually increased to 8000 rpm. After shearing for 20 minutes at 8000 rpm, the suspended few layers graphene material was collected in a centrifuge tube.
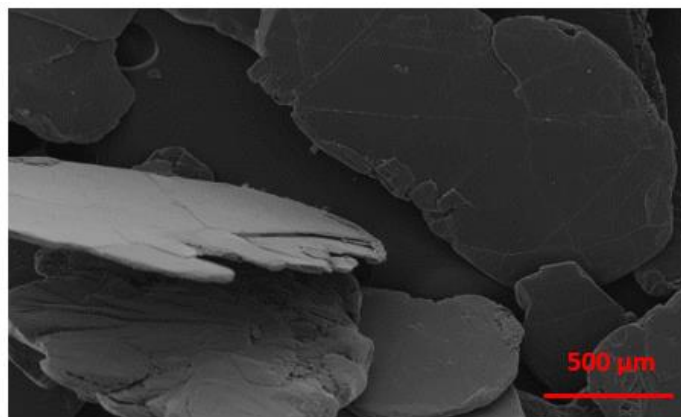
Figure 2.6. SEM image of the pristine Madagascar graphite.

It was demonstrated by Jonathan N. Coleman, [10] that controlled centrifugation can be used to separate graphene flakes by size. The suspended materials were centrifuged at different rpm to select different graphene flakes: the processing is as follows:

1) the dark suspension, after the homogenizer treatment of graphite described above, was introduced into a centrifuge tube and centrifuged at 800 rpm (83g) for 2 hours. The mixture was then left in the tube overnight to allow sedimentation. The upper suspension was separated from the precipitate and transferred to another tube, while the precipitate was discarded.

2) The suspension was centrifuged at 1500 rpm (293g). After 2 hours centrifugation,

the solid residue was separated from the supernatant and re-suspended in 20 mL of NCP. This suspension was marked as EXG 800.

3) The supernatant after removing **EXG800** (step 2) was further centrifuged at 3000 rpm (1170g). The solid residue was separated from the supernatant and re-suspended again in 20 mL **NCP** solvent. This suspension was marked as **EXG 1500**.

4) The supernatant after removing **EXG 1500** (step 3) was marked as **EXG3000**.
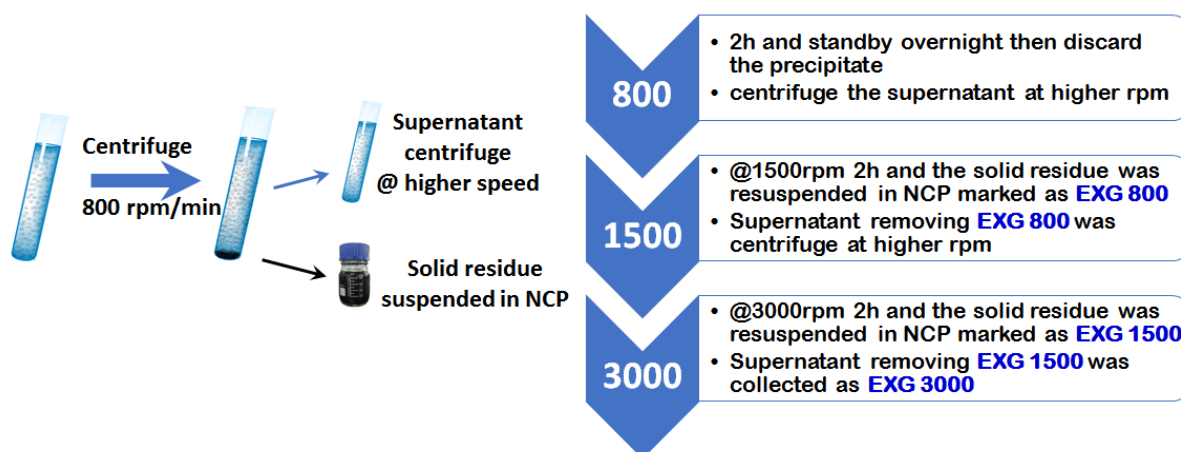
Figure 2.7. Centrifugation of EXG samples at different rpm to achieve different qualified few layer graphene flakes.

2.5 Characterization of exfoliated graphite sheets

The exfoliated graphene (**EXG**) flakes were characterized by Raman spectroscopy, TEM and TGA. The Raman source used here was a 636 nm laser. According to Ferrari, [11] the electronic structure of graphene is reflected by its Raman spectrum that clearly evolves with the number of layers (Figure 2.8 b and c). When the numbers of graphene layers increase, a Raman shift (about 30 cm^{-1}) to higher frequency can be observed from the 2D band shown in Figure 2.8 (b) and (c). Also, the shape of 2D band changes depend on the numbers of stacked graphene layers. Figure 2.8a shows that the characteristic 2D-band peak of **EXG 3000** is visible around 2660 cm^{-1}, while the characteristic 2D-band peak of **EXG 800** and **EXG 1500** samples appear around 2860 cm^{-1}. On this basis, comparing the 2D band shape and shift of the three **EXG** samples (Figure 2.8 a) with the literature data of ref. 11 (Figure 2.8 b and c), we can conclude that the **EXG 3000** samples mainly contain 2~5 graphene layers, while the **EXG 800** and **EXG 1500** samples mainly contain 5~10 graphene layers.
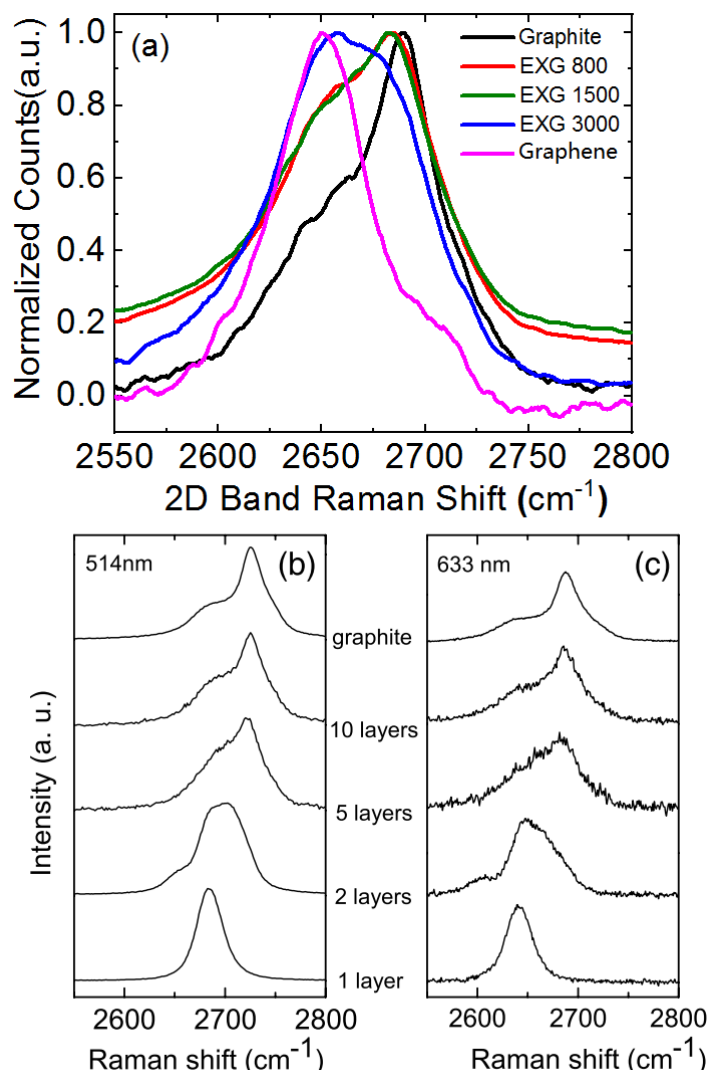
Figure 2.8. Raman spectra showing a) 2D band of exfoliated few layers graphene samples b) and c) Raman shift in ref. 11 using Laser 514 nm and 633 nm.

Thermogravimetric analysis (TGA) revealed a thermal stability under air. The blue curves, corresponding to the mass loss derivative, indicate a mass loss for the different **EXG** flakes, using the method of linear extrapolation, we can subsequently infer that the initiative burning temperature at the peak of the dashed curves (derivative peak) correspond to lower temperatures. The increasing thermal decomposition temperatures (derivative peak temperature 590 ℃, 690 ℃ and 710 ℃) indicate that the **EXG3000** was the most exfoliated sample that is easier to decompose, because it contains fewer layers of graphene. This means that less heat is needed to break intermolecular forces. A slight weight loss can also be observed before the temperature reaches 300 °C, which is due to defects caused during exfoliation, and also residual solvents.

43
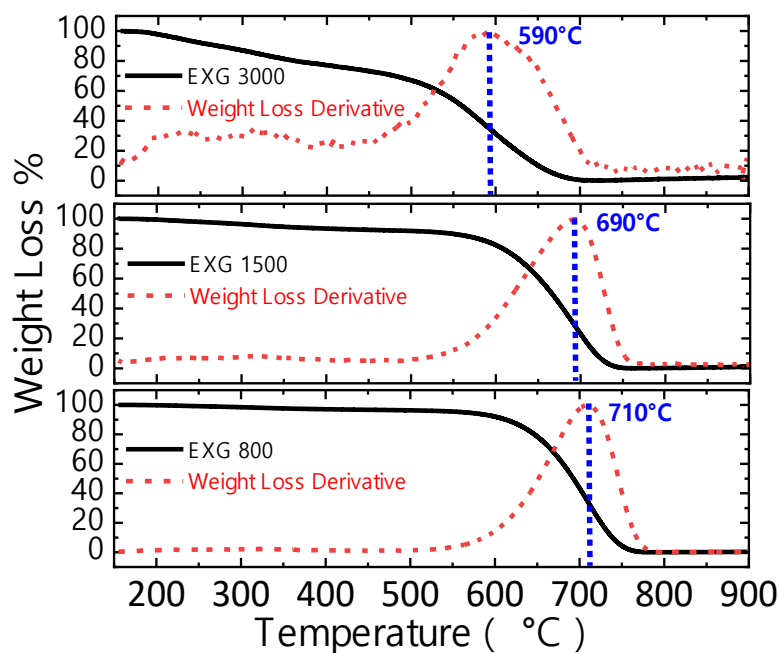
Figure 2.9. TGA spectra of 3 kinds of exfoliated few layers graphene samples.

The concentration of EXG samples were summarized in table 2.1, using the calculation of mass weight divided by the volume (240 µL) given by the TGA test.

Samples	Mass Weight (mg)	Concentration (mg/µL)
EXG 800	464	1.93
EXG 1500	236	0.98
EXG 3000	61	0.25

Table 2.1. The concentration of **EXG** samples.

TEM was performed for the three **EXG** samples as seen in Figure 2.10. After exfoliation, one can see that the **EXG 800** suspension (Figure 2.10 a) contains few layers graphene as well as non-exfoliated graphene. TEM images of **EXG3000** sample (Figure 2.10 c) indicate that, big flakes of high quality few layer-graphene sheets can be achieved by exfoliation and high-speed centrifugation.
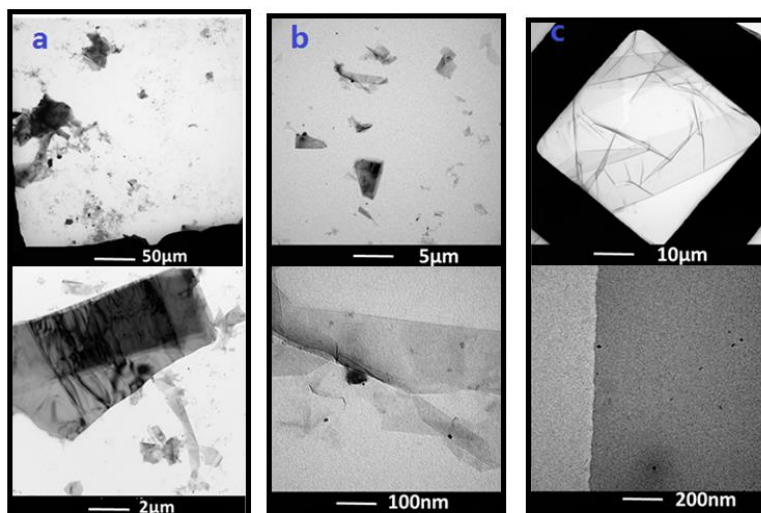
Figure 2.10. TEM images of a) **EXG 800** b) **EXG 1500** and c) **EXG 3000** showing the achievement of big flakes of few layers' graphene sheets after centrifuge.

2.6 Conclusion

EXG800, **EXG1500** and **EXG3000** were obtained after graphite exfoliation and centrifugation. TEM, TGA and Raman spectra confirm that **EXG3000** were the most exfoliated graphene flakes (2~5 layers), the flakes of **EXG3000** will be functionalized with organic chromophores.

2.7 bibliography

[1] J. M. Tour, Nature Materials, 2014, 13, 545–546.

[2] K. R. Paton, E. Varrla, C. Backes, R. J. Smith, U. Khan, A. O'Neill, C. Boland, M. Lotya, O. M. Istrate, P. King, T. Higgins, S. Barwich, P. May, P. Puczkarski, I. Ahmed, M. Moebius, H. Pettersson, E. Long, J. Coelho, S. E. O'Brien, E. K. McGuire, B. M. Sanchez, G. S. Duesberg, N. McEvoy, T. J. Pennycook, C. Downing, A. Crossley, V. Nicolosi, J. N. Coleman. Nature Materials, 2014, 13, 624–630.

[3] Ra. Tadmor. J. Phys.: Condens. Matter, 2001, 13, L195–L202

[4] J. N Coleman, Accounts of Chemical Research, 2013, 46, 14-22.

[5] a) S. D. Bergin, V. Nicolosi, P. V. Streich, S. Giordani, Z. Y. Sun, A. H. Windle, P. Ryan, N. P. P. Niraj, Z. T. T. Wang, L. Carpenter, W. J. Blau, J. J. Boland, J. P. Hamilton, J. N.

Coleman. Advanced Materials, 2008, 20, 1876; b) S. D. Bergin, Z. Y. Sun, D. Rickard, P. V. Streich, J. P. Hamilton, J. N. Coleman, ACS Nano 2009, 3, 2340–2350.

[6] J. M. Hughes, D. Aherne, S. D. Bergin, P. V. Streich, J. P. Hamilton, J. N. Coleman, Nanotechnology. 2012, 23(26), 265604-265611.

[7] S. M. Kresta, R. S. Brodkey, in Handbook of Industrial Mixing: Science and Practice (eds Paul, E. L., Atiemo-Obeng, V. A. & Kresta, S. M.) 19–87 (John Wiley, 2004).; b) Alhassan, S. M., Qutubuddin, S. & Schiraldi, D. A. Graphene arrested in laponite-water colloidal glass. Langmuir 28, 4009–4015 (2012).

[8] Y. Hernandez, V. Nicolosi, M. Lotya, F. M. Blighe, Z. Y. Sun, S. De, I. T. McGovern, B. Holland, M. Byrne, Y. K. Gun'Ko, J. J. Boland, P. Niraj, G. Duesberg, S. Krishnamurthy, R. Goodhue, J. Hutchison, V. Scardaci, A. C. Ferrari, J. N. Coleman, Nature Nanotech, 2008, 3, 563–568.

[9] P. Dhankhar, IOSR Journal of Engineering, 2014, 04, 01-08.

[10] U. Khan, A. O'Neill, H. Porwal, P. May, K. Nawaz, J. N. Coleman. Carbon, 2012, 50, 470-475.

[11] A. Ferrari, J. Meyer, V. Scardaci, C. Casiraghi, M. Lazzeri, F. Mauri, S. Piscanec, D. Jiang, K. Novoselov, S. Roth, A. Geim, Physical Review Letters, 2006, 97, 187401(1-4).

CHAPTER 3

NOVEL COVALENT FEW LAYERS GRAPHENE HYBRIDS WITH DIKETOPYRROLOPYRROLE DYE EXHIBITING RED-NIR ABSORPTION FEATURES

In this chapter, the preparation of two graphene hybrids containing a diketopyrropyrrole dye is described. They are both soluble in chloroform, toluene, acetone and DMF, and they both improve NIR absorption features ranging from 500 to 800 nm. Solvatochromism was observed in this system, showing hypochromic shift of the absorption band with increasing solvent polarity. These new materials might be interesting to test as a third component in a P3HT: PCBM BHJ blend for OPV, partially allowing light harvesting in the deep-red/NIR as well as possible positive interactions with both P3HT and PCBM.

3. NOVEL COVALENT FEW LAYERS GRAPHENE HYBRIDS WITH DIKETOPYRROLOPYRROLE DYE EXHIBITING RED-NIR ABSORPTION FEATURES

3.1 Introduction

As we know, graphene nanosheets only absorb 2.3% of incident visible light which is a drawback for optoelectronic devices. [1] Through inducing electron trapping centers or creating a bandgap on graphene, the absorbance of a graphene layer can be greatly enhanced up to nearly 70%. [2] 3,6-Di(thiophen-2-yl)pyrrolo[3,4-c]pyrrole-1,4(2H,5H)-dione (**TDPP**) is a brilliant red and strongly fluorescent high performance pigment, with exceptional light and heat stability. [3] Also, **TDPP** derivatives have been used to produce highly luminescent, electroactive and photoactive materials for opto-lectronic devices. [4]

In this work, we explore a new covalent graphene system with TDPP derivatives with a large extinction coefficient in the visible-light region. [5] TDPP derivatives can be easily attached to various electron-rich units via a D–A covalent linkage strategy to tune the HOMO/LUMO energy levels and obtain low bandgap organic semiconductors. Therefore, it is expected that, by combining 2D nanometer-scale graphene with TDPP molecules, multifunctional nanometer-scale materials for optoelectronic/electro-chemical applications may be generated. As shown in Figure 3.1, two different frameworks **EXG-TDPP** (mono) and **c-EXG-TDPP** (crosslink) were created.
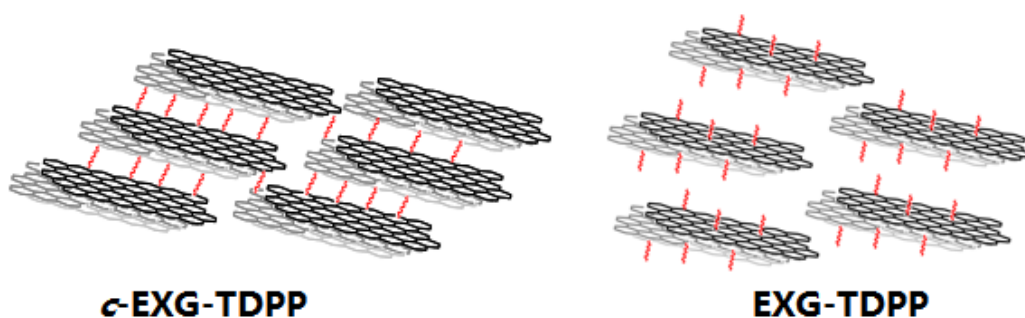
Figure 3.1 Schematic diagrams of structures of the two different EXG hybrids. The red tails are the DPP relative units.

3.2 Results and Discussion

The two different frameworks **EXG-TDPP** (mono-functionalized) and **c-EXG-TDPP** (crosslinked structure) were shown as Figure 3.2; a benzene chain (octan-3-yloxyl) was attached to improve the solubility of the frameworks. Both the graphene-diketopyrrolopyrrole hybrids were obtained through in-situ direct arylations starting from **EXG 3000** and the corresponding **TDPP** aniline derivatives using the method by **J. M. Tour** through free radical addition reaction. [6]
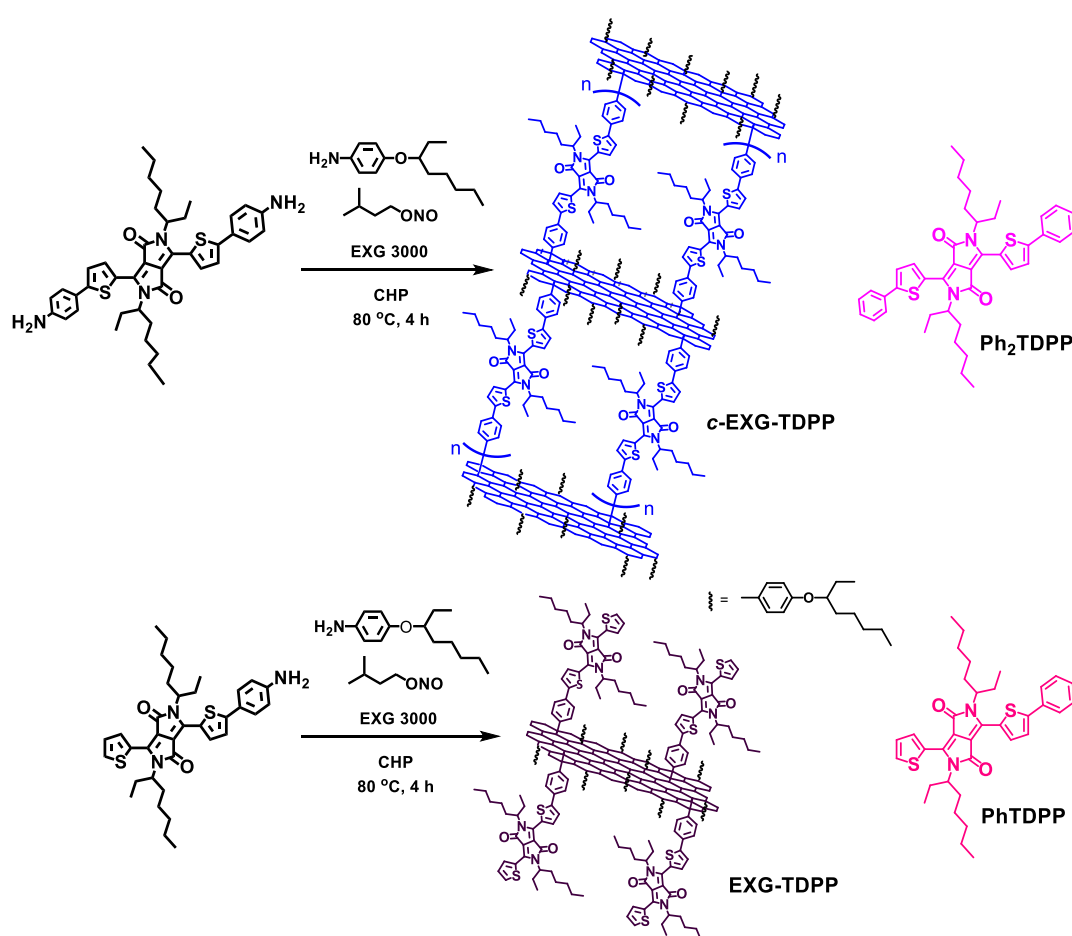
Figure 3.2 Synthesis of the cross-linked graphene-diketopyrrolopyrrole hybrid (**c-EXG-TDPP**) and of the reference material lacking cross-linking (**EXG-TDPP**).

3.2.1 Scanning Probe Microscopy

Figure 3.3 shows TEM images at different magnifications of a sample deposited from solution on the grid. Through TEM images of **c-EXG-TDPP** and **EXG-TDPP** hybrids, we can

see widespread aggregation. This fact suggests the formation of crosslinked hybrids, where the presence of bigger dark blocks implied a higher degree of aggregation.
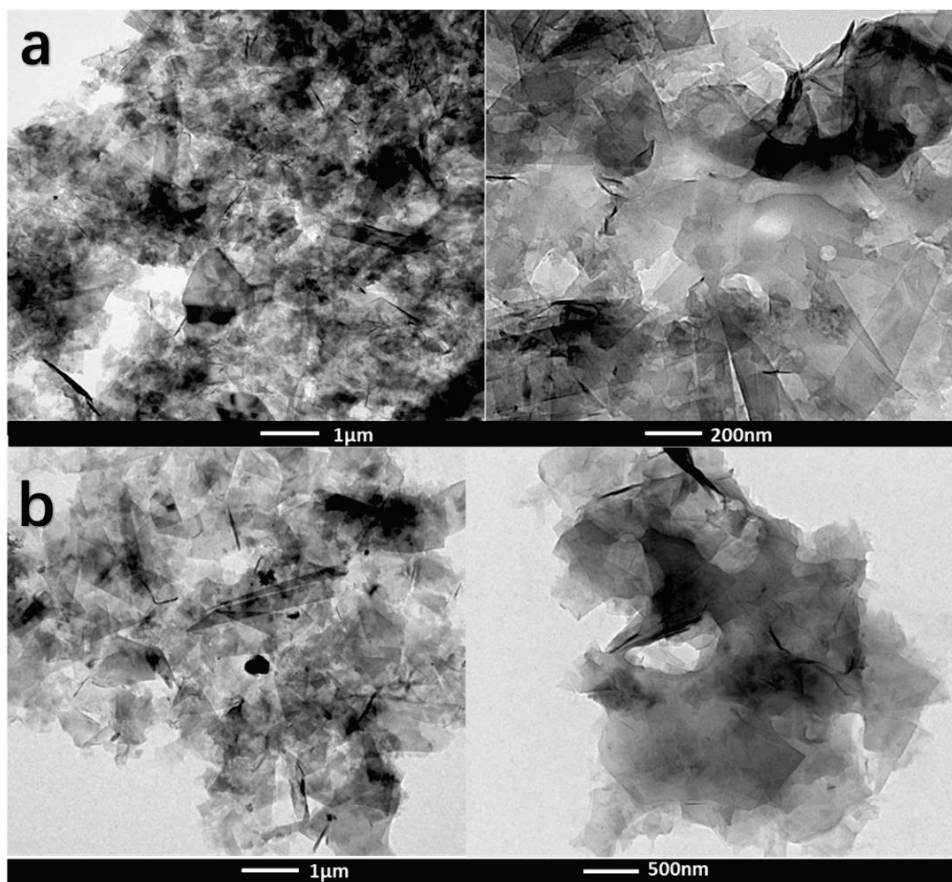
Figure 3.3 TEM images of the *c*-**EXG-TDPP** (a) and **EXG-TDPP** (b) hybrids.

As we proposed, the *c*-**EXG-TDPP** hybrid was crosslinked (Figure 3.1 left) by the **Ph₂TDPP** molecules. The **EXG** flakes were linked together through the **Ph₂TDPP** dye resulting in a net structure. Aggregation of **EXG-TDPP** hybrid could be due to the interlinking between molecules caused by the presence of long alkyl chain. At the higher magnification (200 nm), large aggregates of the *c*-**EXG-TDPP** hybrid were observed. Compared with the crosslinked *c*-**EXG-TDPP** hybrid, the TEM images of mono functionalized **EXG-TDPP** hybrid showed less aggregation and more transparency. Figure 3.4 show the SEM images of a spin-coated film of *c*-**EXG-TDPP** hybrid on a conductive indium tin oxide glass slide. Figure 3.4b is the comparison between the secondary electron image (left) and the back-scattered electron image (right) of the same sample as in Figure 3.4a.
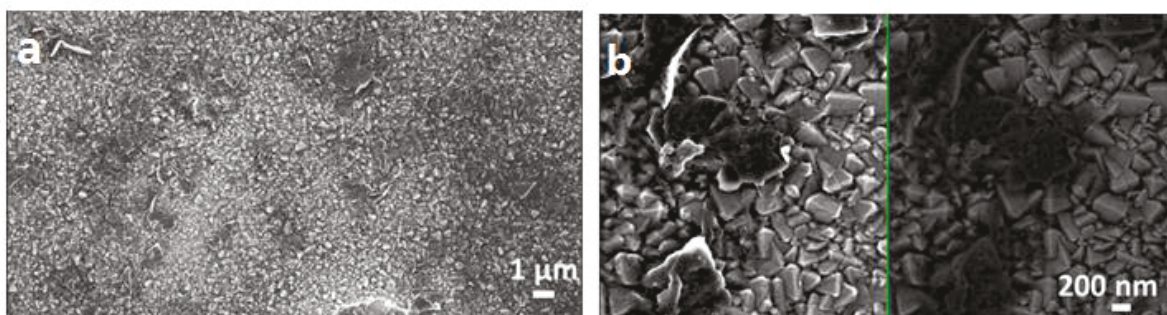
Figure 3.4 SEM image of of the cross-linked graphene-diketopyrrolopyrrole hybrid (*c*-**EXG-TDPP**).

The different structures are also confirmed by Dynamic light scattering (DLS) with diluted solution ($\sim 10^{-6}$ M) in DMF filled in optical cuvettes. Figure 3.5 states that the *c*-**EXG-TDPP** particles in DMF solution are bigger in size (613.8 nm, size distribution by volume) than **EXG-TDPP** (406.1 nm).
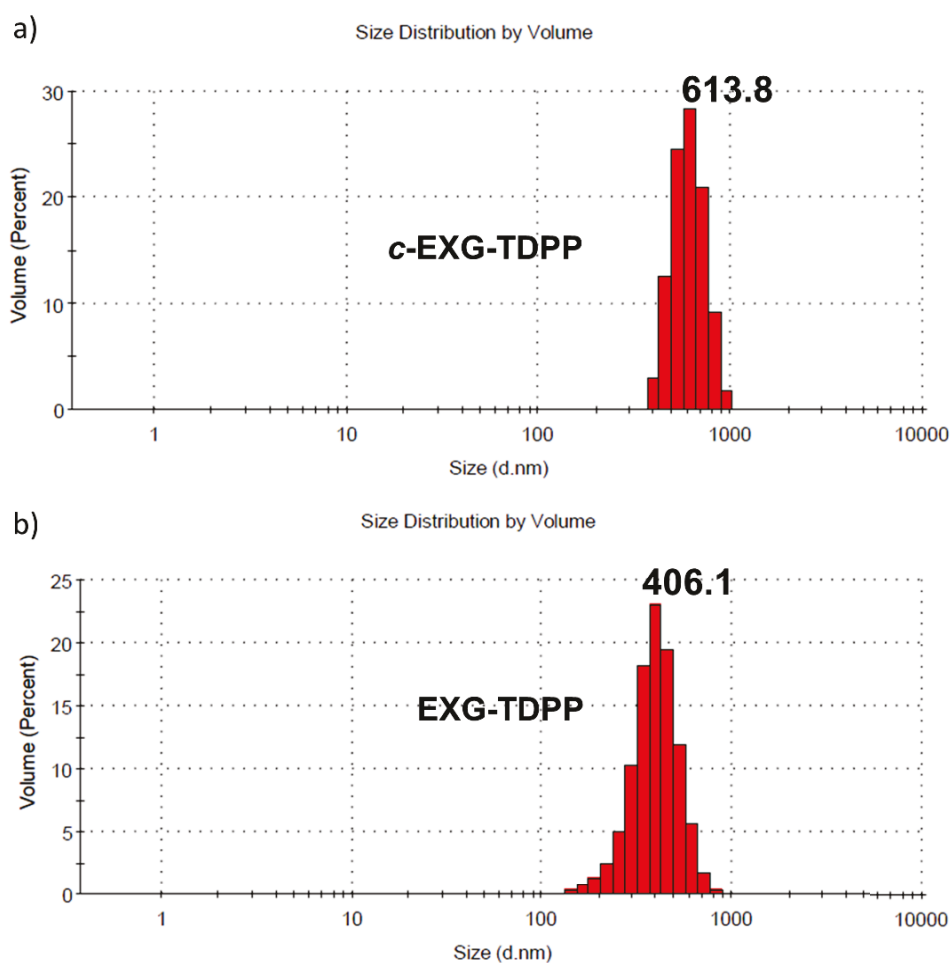
Figure 3.5 Dynamic light scattering showing different size distribution by volume in solution of DMF.

3.2.2 Thermal Properties

Figure 3.6 is the TGA of **EXG-TDPP** & *c*-**EXG-PhTDPP** hybrids and the corresponding free dyes. The black line is the starting material **EXG3000** sample on which TDPP dyes were functionalized. The green line is the functionalized **EXG-TDPP** hybrids attached with single aniline-ended **PhTDPP** dye to give a mono-functionalized structure. The red line corresponds to **PhTDPP** dye with single phenyl ring (compound **4**). The blue line is the functionalized *c*-**EXG-TDPP** hybrids attached with single aniline-ended **PhTDPP** dye to give crosslink-functionalized structure, and the pink line is the corresponding **Ph₂TDPP** dye with double phenyl rings (compound **6**). The dashed lines in corresponding colors with the solid lines showed the first derivatives of the weight loss of each structure. Comparing the maximum peak of the dashed curves, we can infer that, lower the temperature at the derivative peak, lower is the thermal stability.
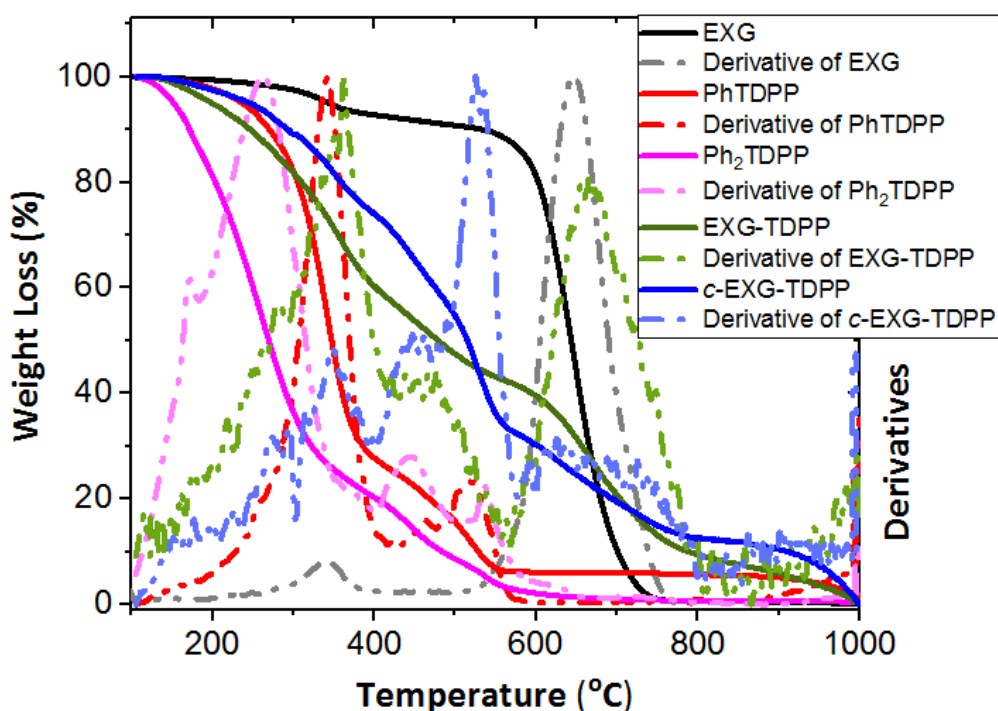
Figure 3.6 TGA of the **EXG-TDPP** & *c*-**EXG-TDPP** hybrids.

Through TGA, we can see that the main mass loss of the **PhTDPP** & **Ph₂TDPP** dye occurring before 500 °C, which was caused by the complete burning of the dyes. These burning features fit the weight loss of functionalized **EXG** hybrids at the area of lower than 500 °C. This indicates that mass loss at that stage came from the burning of the attached

dye on the **EXG** layers. Due to the covalent binding with the **EXG** flakes, the procedure of dye burning was extended to the temperature area around 600 °C, because it needed more heat to break the interlinking between the dye and the graphene layers. Compared with **EXG3000** (the black line), the mass loss happened after reaching 600 °C, this was due to the burning of the graphene structures. Compare with **EXG-TDPP**, the higher temperature of *c*-**EXG-TDPP** at derivative peak showing higher initiative burning temperature, indicates that the *c*-**EXG-TDPP** framework is more complicated (graphite-like polymer) that need more heat to break its structure.

3.2.2 Fourier Transform Infrared (FTIR) Spectroscopy

The presence of organic functional groups in the functionalized graphene products is further confirmed by FTIR spectroscopy. Figure 3.7 shows the FTIR spectra of the cross-linked graphene-diketopyrrolopyrrole hybrid (*c*-**EXG-TDPP**, Figure 3.7a) and of the reference material lacking cross-linking (**EXG-TDPP**, Figure 3.7b).
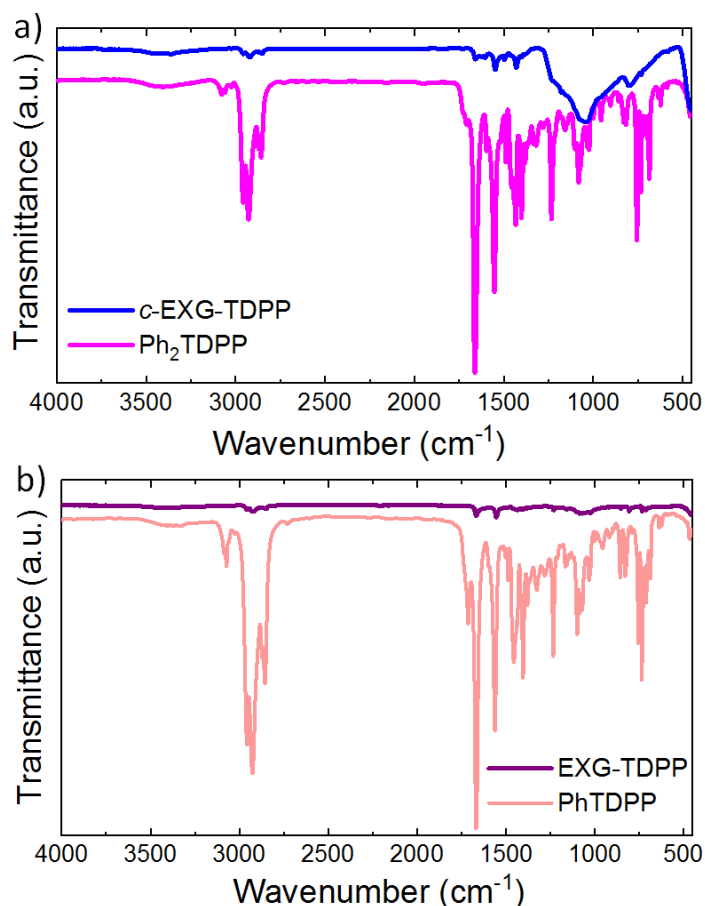
Figure 3.7 FT-IR spectra of the a) *c*-**EXG-TDPP** & b) **EXG-TDPP** hybrids.

52

Both of the **Ph₂TDPP** and **PhTDPP** show significant FTIR peaks. It indicates clear identification of C–H stretching (2900~3100 cm^{-1}), C=O stretching (~1720 cm^{-1}), C=C stretching (~ 1600 cm^{-1}), and the single band stretching at the region from 500 cm^{-1} to 1300 cm^{-1} through stretching vibrations from C-N, C-S and C-C. As reported in ref. [7], there is no significant functional groups in FTIR of graphene, but for graphene-based materials there are the characteristic peaks of the functional groups. Through Figure 3.7, it is easy to observe that the intensities of stretching vibrations were significantly reduced for both graphene-diketopyrrolopyrrole hybrids *c*-**EXG-TDPP** and **EXG-TDPP**, this is due to energy transfer from the **PhTDPP** molecules to the graphene surface after functionalization, indicating the successful functionalization of **EXG** with the **PhTDPP** chromophores.

3.2.3 Absorption and Solvatochromism Properties

Figure 3.8 shows the optical characterization of the graphene-diketopyrrolopyrrole hybrids. Figure 3.8a is the UV-Vis-NIR absorption spectra of the hybrids and of the corresponding reference dyes in DMF solutions. The spectrum of the exfoliated graphene used for their synthesis (**EXG 3000**) in DMF is also reported for comparison. In the inset, a zoom on the absorption maximum is reported. Figure 3.8b shows the appearance of the DMF solutions of the graphene-diketopyrrolopyrrole hybrids and of their reference dyes. As seen in the UV-Vis spectra, the band of the free dye (**Ph₂TDPP**) is strongly red-shifted in the case of the covalent hybrid when compared to graphene. We see this as a combination of electronic effects due to the covalent bond with graphene and to the formation of J-type aggregates within the molecular units. On the other hand, the hybrid species missing crosslinking (**EXG-TDPP**) has very small red shift compared to the corresponding free dye (**PhTDPP**). In addition, the presence of graphene ensures residual absorption in the NIR.

Moreover, the UV-Vis absorption of the cross-linked graphene-diketopyrrolopyrrole hybrids in spin-coated thin films on glass slides confirmed the successful functionalization of the graphene, an approximately 80nm red shift of the crosslinked hybrid *c*-**EXG-TDPP** was obtained form the corresponding reference dye **Ph₂TDPP**. The pictures of these films were also reported in Figure 3.8d. As we supposed, this hybrid can be seen as sort of

polymer. Indeed, it has very nice filming properties (showed in Figure 3.8d) compared to pristine graphene.
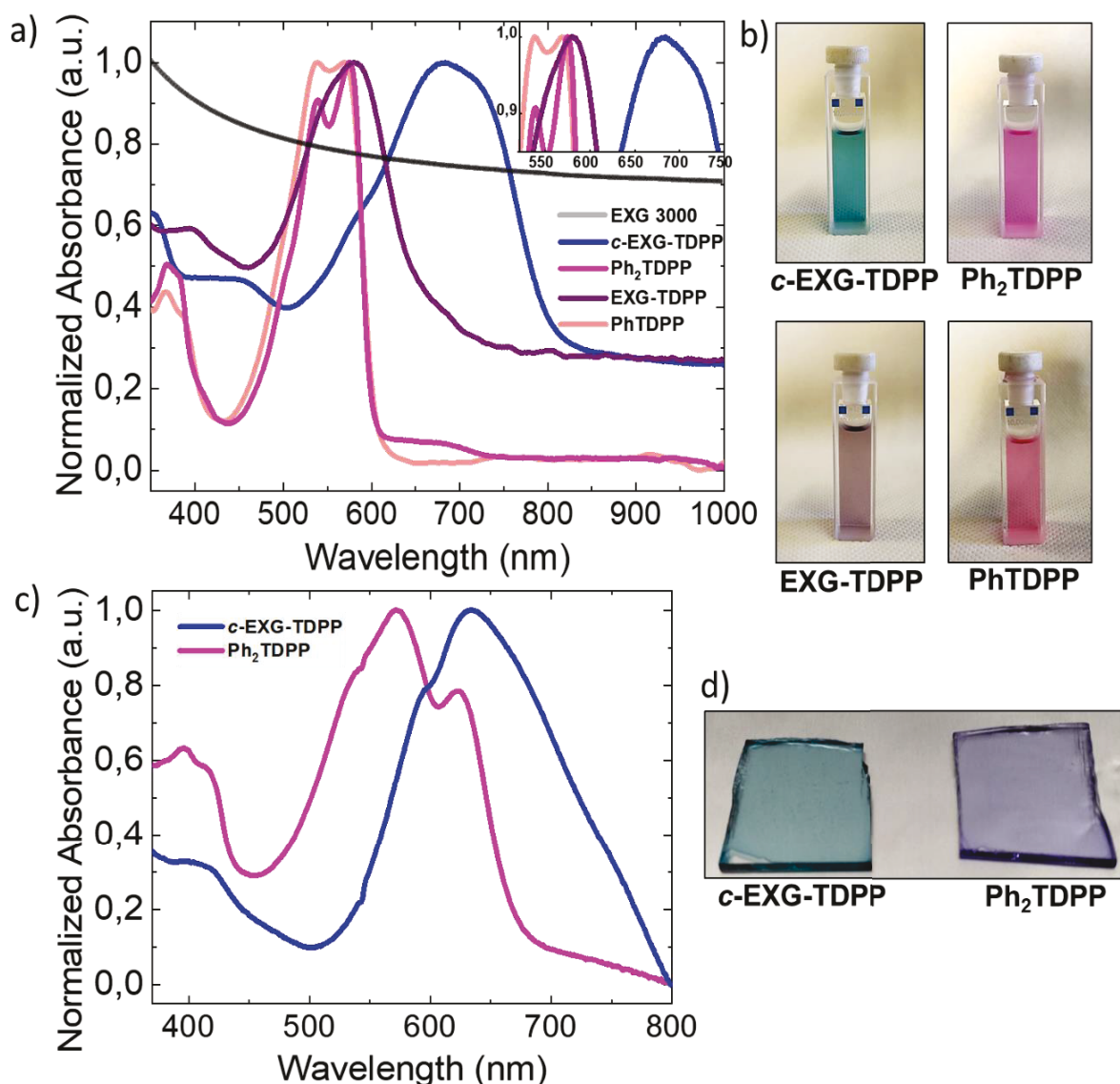
Figure 3.8 a) UV-Vis-NIR absorption spectra of the hybrids and of the corresponding reference dyes in DMF solutions. b) Photos of the DMF solutions of the graphene hybrids and of their reference dye. c) Film UV-Vis absorption spectra of the cross-linked graphene hybrids and of its reference dye. d) The pictures of these films.

Solvatochromism was carried out using solvents like DMF, toluene, chloroform, acetone, acetonitrile and methanol. From the UV-Vis spectra (Figure 3.9), we can observe that there was hypochromic shift of the absorption band with increasing solvent polarity. Along with this shift, the shapes of the absorbance curves also changed in different solvents with different polarity.
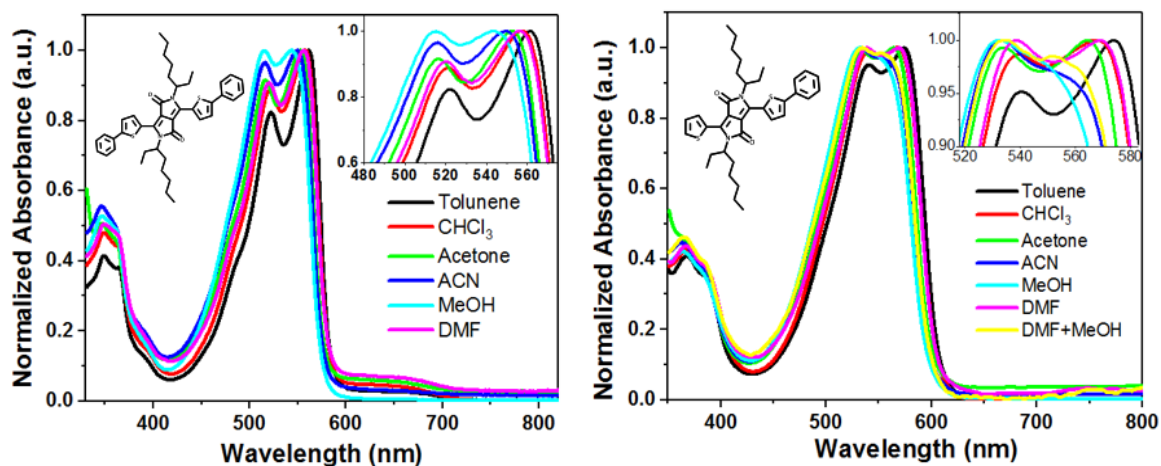
Figure 3.9 UV-Vis spectra of the a) **Ph₂TDPP** and b) **PhTDPP** in different solvents showing negative Solvatochromism.

The maximum absorption band λ_{max} and the wavelength variation $\Delta\lambda_{max}$ were summarized in Table 3.1, we observe that **PhTDPP** molecule exhibits larger extent of hypochromic shift than the **Ph₂TDPP** molecule, which is explained by the more conjugated and symmetric structure of the **Ph₂TDPP** molecule. This is also visible in the images of the solutions showed in Figure 3.10. Through these images, we can observe **Ph₂TDPP** dye exhibiting purple color in different solvent, and the color changed slightly but visible in the solvents with different polarities.

		λ_{max} (nm)						$\Delta\lambda_{max}$
	band	Toluene	CHCl3	Acetone	DMF	ACN	MeOH	(nm)
PhTDPP	~570	573.93	567.04	564.04	568.99	549.92	547.97	25.96
	~530	539.98	538.93	533.95	538.92	533.04	531.99	7.99
Ph₂TDPP	~570	578.04	573.99	569.93	572.94	566.92	560.94	17.1
	~530	539.01	537.95	532.95	537.04	532.95	532.02	6.99

Table 3.1 Solvatochromism of TDPP chromophores in different solvents.
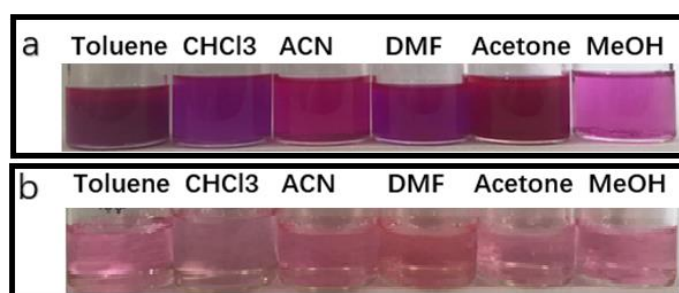
Figure 3.10 Images of the **DPP** chromophores and functionalized EXG hybrids in different solvents. a) **Ph₂TDPP** and b) **PhTDPP**

The solvatochromism was studied in the functionalized **EXG** samples, Figure 3.11 shows the UV-Vis spectra of the functionalized **EXG** hybrid with corresponding free dyes in different solvents, the maximum absorption band λ_{max} and the wavelength variation $\Delta\lambda_{max}$ were summarized in Table 3.2.
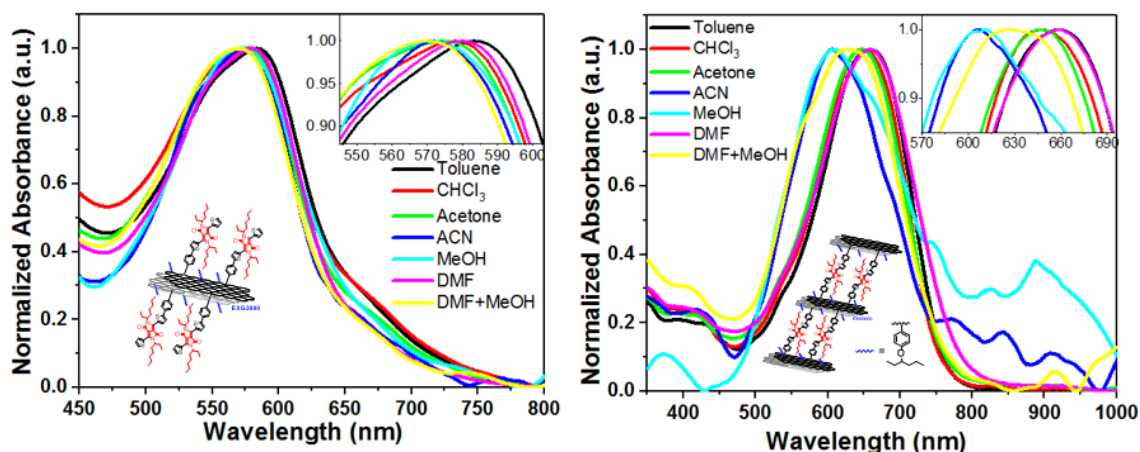
Figure 3.11 UV-Vis spectra of the hybrids in different solvents.

	λ_{max} (nm)				$\Delta\lambda_{max}$ (nm)
	Toluene	CHCl3	Acetone	DMF	
EXG-TDPP	583.04	577.96	573.93	580.05	9.11
c-EXG-TDPP	658.96	647.98	645.93	658.96	13.05

Table 3.2 Solvatochromism of functionalized EXG hybrids in different solvents.

Although the wavelength variation $\Delta\lambda_{max}$ were lower after functionalization, the Solvatochromism was still visible in **EXG** hybrids. Figure 3.12 shows the soluble features of functionalized **EXG** hybrids, where the color slashed in the solvent of ACH and MeOH, caused by the insolubilities in these two kinds of solvents.
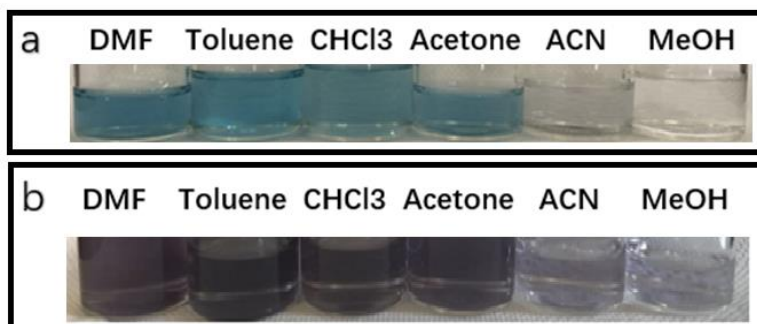
Figure 3.12 Images of the TDPP chromophores and EXG hybrids in different solvents. a) *c-EXG-TDPP* and b) **EXG-TDPP**.

However, the color difference was more obvious between the two **EXG** hybrids, the crosslinked *c*-**EXG-TDPP** series exhibit blue color in different organic solvent while the mono functionalized **EXG-TDPP** exhibit purple color. This phenomenon can contribute to the development of solution-processable device applications.

3.2.4 Emission Properties

Another approach to confirm the covalently bonded **DPP** molecules on **EXG 3000** flakes is the fluorescent spectroscopy. Figure 3.13 shows the fluorescent spectra of **Ph₂TDPP** dye and the crosslinked *c*-**EXG TDPP**. The significant quenching of fluorescence intensity after functionalization indicates that strong fluorescent resonance energy transfer (FRET) happened between the **Ph₂TDPP** dye and the **EXG 3000** surface. The normalized fluorescent spectra exhibit both shift of wavelength and changes of shape; this is due to the movement of charge from **Ph₂TDPP** dye to the graphene layer. In order to examine electronic interaction between **Ph₂TDPP** unit and graphene in the hybrid, we measured fluorescence spectroscopic of the **EXG 3000** + **Ph₂TDPP** sample in which the **EXG 3000** and the **Ph₂TDPP** dye were merely mixed.
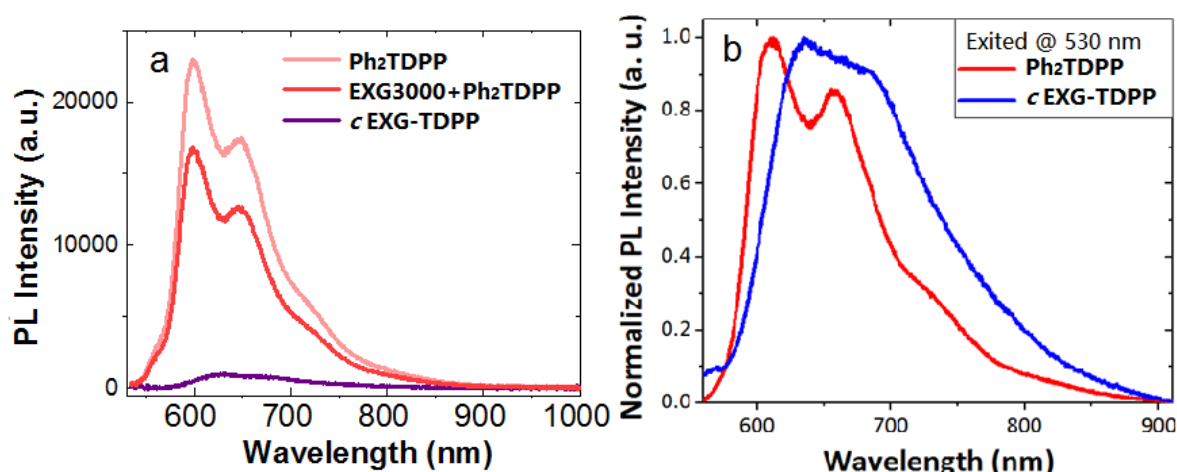
Figure3.13 Fluorescent spectra (excited at 530 nm) of **Ph₂TDPP** dye and the functionalized *c*-**EXG-TDPP** hybrid. (a) Fluorescence significant quenched after functionalization; (b) Fluorescent shape and shift changed after functionalization.

Through Figure 3.13a, the fluorescence emission of the mixed sample in DMF is quenched about 25%, while a much stronger quenching (95%) is observed for the hybrid *c*-**EXG-TDPP**, which indicates that there is a strong interaction between the excited state of **Ph₂TDPP** and **EXG 3000** flakes in the hybrid. Similar luminescence quenching has been

observed for the hybrids of carbon nanotubes with fullerene, and a photoinduced electron transfer mechanism has been demonstrated for these hybrids.[8] Figure 3.13b shows the normalized fluorescence between **Ph₂TDPP** dye and the functionalized *c*-**EXG-TDPP** hybrid. It reveals that the emission band of **Ph₂TDPP** dye at 675 nm trend to disappear in the *c*-**EXG-TDPP** hybrid, and the emission band of **Ph₂TDPP** dye at 610 nm shifted to 635 nm after functionalization with **EXG 3000**, which indicates the strong interaction between the **PhTDPP** and **EXG 3000** flakes in the hybrid. The emission properties provide another piece of evidence for the successful functionalization.

Figure 3.14a reveals the normalized 2D excitation/emission maps of the cross-linked graphene-diketopyrrolopyrrole hybrids and of its reference dye in DMF solution. Two different emission were excited at λ_{em} = 690 nm (Figure 3.14b left) and λ_{exc} = 456 nm (Figure 3.14b right), both of the graphene-diketopyrrolopyrrole hybrids and of its reference dye were diluted in DMF solution.
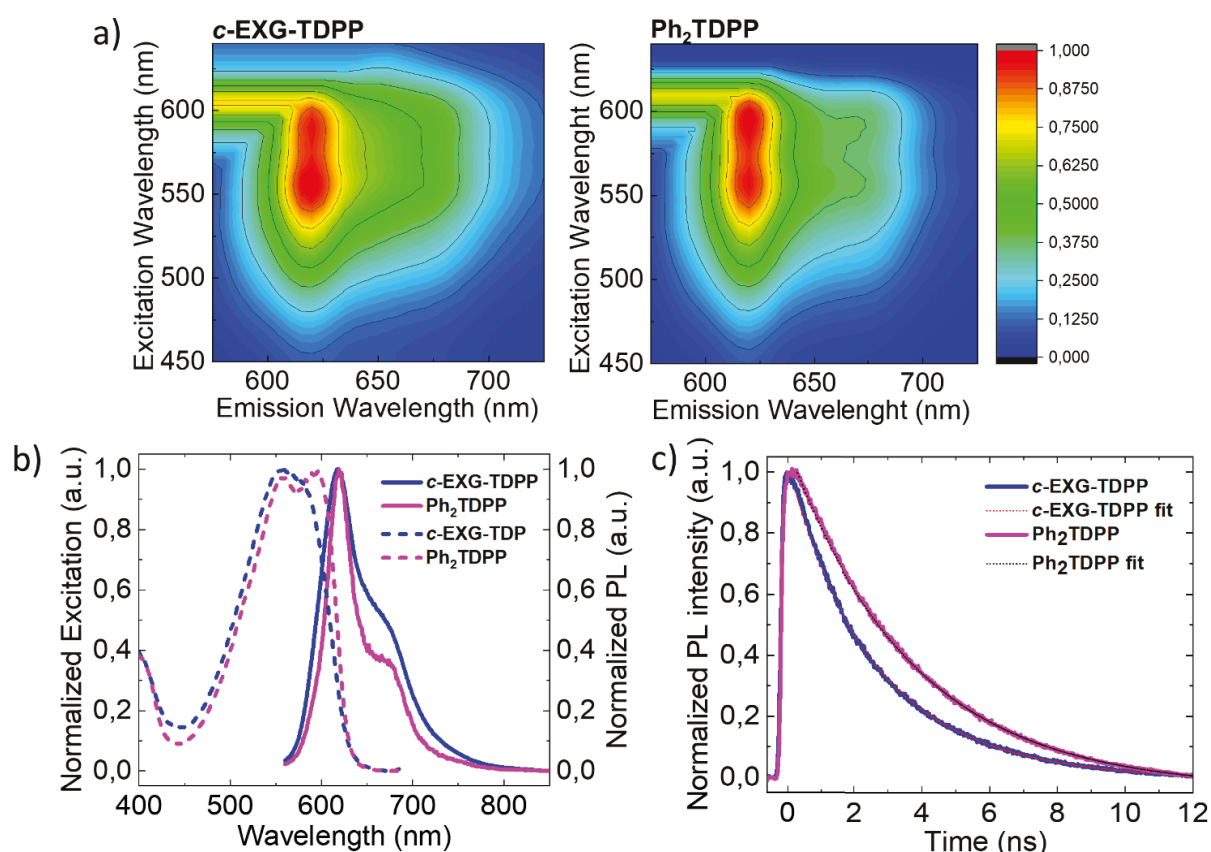
Figure 3.14 Characterization of the emissive properties of the cross-linked graphene-diketopyrrolopyrrole hybrid (*c*-**EXG-TDPP**).

As reported in Figure 3.14c, TRPL decay of the graphene-diketopyrrolopyrrole hybrids and of its reference dye in DMF solution were probed at 690 nm (λ_{exc} = 456 nm). The fits of the two decays are also reported. For *c*-**EXG-TDPP** two lifetimes are found, namely τ1 = 1.7 ns (A1 = 52%) and τ2 = 3.8 ns (amplitude = 48%). For the free dye **Ph₂TDPP**, only one lifetime is detected, τ1 = 3.8 ns.

3.2.5 Raman Spectroscopy

Raman spectroscopy is widely used to study the structural and electronic properties of graphitic materials.[9] The typical Raman bands for graphitic materials are: a disorder-induced D band at about 1350 cm^{-1}, a doubly degenerate zone centre E$_{2g}$ mode at about 1580 cm^{-1} (G band, indicative to sp^2 carbon bonds), and a two phonon double resonance Raman process at about 2700 cm^{-1} (2D band).[9] The intensity ratio I$_D$/I$_G$ between the D band and G band is often used to quantify the defects in graphitic materials. Attachment of organic functional groups changes some carbon atoms from sp^2 to sp^3 and therefore results in an increased I$_D$/I$_G$ ratio, which indicates successful covalent functionalization.

Figure 3.15 shows Raman spectra of **EXG3000**, the hybrid of **EXG-TDPP** & *c*-**EXG-TDPP** and also their reference dyes **PhTDPP** & **Ph₂TDPP.** Through Figure 3.15a, after functionalization with **Ph₂TDPP**, the I$_D$/I$_G$ ratio changes from 0.44 in **EXG-3000** to 0.55 in *c*-**EXG-TDPP** stating the success of the functionalization. And, the *c*-**EXG-TDPP** arise new Raman band appering from 1350~1550 cm^{-1}, which belong to the characteristic band of **Ph₂TDPP.** Meanwhile, the D and G band of *c*-**EXG-TDPP** shifted to lower frenquency region, the inset of Figure 3.15a shows the 2D band area of the Raman spectra, the intensity of the 2D band was decreased after functionalization. All the above features state that the energy transfer occurs between the dye and graphene, indicating that the *c*-**EXG-TDPP** was covalently functionalized with **Ph₂TDPP.**

Interestingly, the mono-functionalized **EXG-TDPP** show different Raman features from the crosslinked *c*-**EXG-TDPP.** Through Figure 3.15b), the I$_D$/I$_G$ ratio changes from 0.44 in **EXG-3000** to 0.34 in **EXG-TDPP** and the 2D band cannot be observed, which may be caused by the high fluorescent **PhTDPP** unit. But the Raman band shifted to lower frenquency area

(from 1333 cm^{-1} to 1328 cm^{-1}, 1439 cm^{-1} to 1428 cm^{-1}, 1528 cm^{-1} to 1517cm^{-1}), indicates the **EXG-TDPP** was a covalent graphene hybrid.
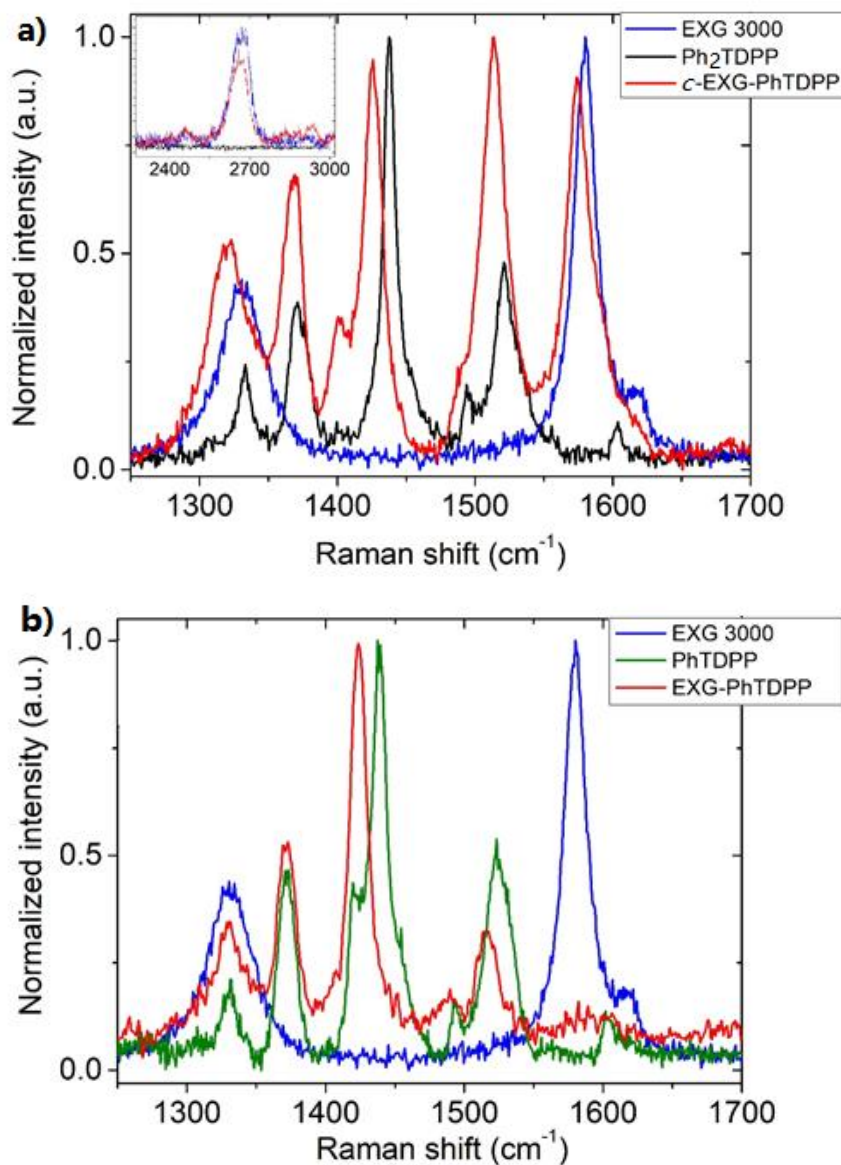
Figure 3.15 Raman spectra of a) cross-linked and b) mono-functionalized graphene-hybrids, of their reference dyes and **EXG-3000**.

3.3 Conclusion

Two different functionalized **EXG** hybrids were synthesized, TEM images, TGA measurements, FTIR tests confirm the covalent functionalization of the graphene. The synthesized **EXG** hybrids both dissolve well in organic solvents, such as chloroform, dichloromethane, DMF, toluene, acetone, and so on. With the **DPP** electron trapping

centers, the band gap of functionalized **EXG** hybrids were broadened with an improvement of light absorbance from 500 nm to 800 nm, the unique absorption properties of **DPP** were also introduced to the **EXG** hybrids through covalent bounding with interesting solvatochromism phenomenon. The electron transfer from **DPP** chromophores to **EXG** flakes was confirmed by the efficient fluorescence quenching of **DPP** chromophores. This material might be interesting to test as third component in a **P3HT: PCBM** bulk heterojunction (BHJ) blend for Organic Photovoltaics (OPV), partially allowing light harvesting in the deep-red/NIR as well as possible positive interactions with both **P3HT** and **PCBM**.

3.4 Experimental Section

3.4.1 Materials and instruments and methods

Materials: Solvents were purified by standard methods. All commercially available reagents and solvents were purchased from Sigma–Aldrichand, Fluka or TCI chemicals if not otherwise specified and used as received. Graphene powder was purchased from SUPERIOR GRAPHITE and used as received. Procedures for the exfoliated graphene were given in Chapter 2. TLC analyses were performed using Merck 60 F 254 precoated silica gel glass plates. Column chromatography under constant pressure was carried out on Macherey-Nagel silica gel 60 (70-230 mesh, 63 – 200 μm), flash column chromatography was carried out on Macherey-Nagel silica gel 60M (230-400 mesh, 40 – 63 μm). The dry method was used to prepare a column.

Instruments and methods: NMR spectra were recorded using a Bruker AV III 500 spectrometer operating at 500 MHz for ^{1}H, 125 MHz for ^{13}C (301 K) and a Bruker Avance 300 spectrometer operating at 300 MHz for ^{1}H, 75 MHz for ^{13}C (301K). Chemical shifts are reported relative to internal Me$_4$Si. Multiplicity is given as follow: s = singlet, d = doublet, t = triplet, q =quartet, m = multiplet. ESI-MS mass spectra were obtained with Agilent Technologies 1100 Series system equipped with a binary pump (G1312A) and MSD SL Trap mass spectrometer (G2445D SL). The eluent used were MeOH or ACN, both with 0.5% formic acid. TEM images were recorded on a Jeol 300 PX electron microscope. One drop of sample was placed on the sample grid and the solvent was allowed to evaporate. SEM

characterization was carried on an ultra-high vacuum Zeiss Supra 40 with GEMINI column FE-SEM. An electron Energy of 3–5 kV, a distance from the sample around 4 mm and a magnification between 20 and 200 k were employed. A high efficiency In-Lens secondary electron detector was used during the images acquisition. UV-Visible spectra were recorded on Varian Cary 5000 spectrophotometer equipped with diluted solution in different solvent at 10^{-6} M. Thermogravimetric analysis (TGA) was run on ~1 mg sample using a Q5000 IR model TA instrument with the method of starting at 100 ℃ and kept isothermal for 20 min then ramping to 10 ℃/ min upto 1000 ℃.

Fluorescence spectra were recorded on Perkin Elmer LS50B fluorescence spectrometer with diluted solution in DCM solvent at 10^{-6} M. Solid state-PL measurements were carried out by exciting samples with the second harmonic (about 400 nm) of a mode locked Ti-Sapphire laser (Mira 900, Coherent) delivering 150 fs pulses at a repetition rate of 76 MHz in reflection geometry. The excitation beam was spatially limited by an iris and focused onto a spot of about 50 μm by a 150 mm focal length lens. The power was adjusted using neutral density filters. Solid state-PL spectra were collected by a spectrograph with a grating of 30 lines mm1 and further recorded by a Hamamatsu em-CCD camera sensitive in the visible region. The same pulsed excitation was used for TR-PL measurements but PL decays were instead collected with a Hamamatsu streak camera unit working in Synchroscan mode (time resolution ~2 ps) with a cathode sensitive in the visible region. All spectra were corrected for the response of the instrument using a calibrated lamp. Micro-Raman spectra were collected with an Invia Renishaw Raman micro spectrometer (X50 objective,) using the 633 nm line of a He − Ne laser.

3.4.2 Synthesis of TDPP dyes

The synthesis of the TDPP dyes and their functionalization on EXG flakes were given in Figure 3.15. Compound **1** ~ **4** and **6** were prepared as literature methods,[10] the Compound **5** and **7** were synthesized through Suzuki coupling, all the structures were confirmed by ^{1}H-NMR,^{13}C-NMR, Elemental Analysis and ESI-MS characterization.
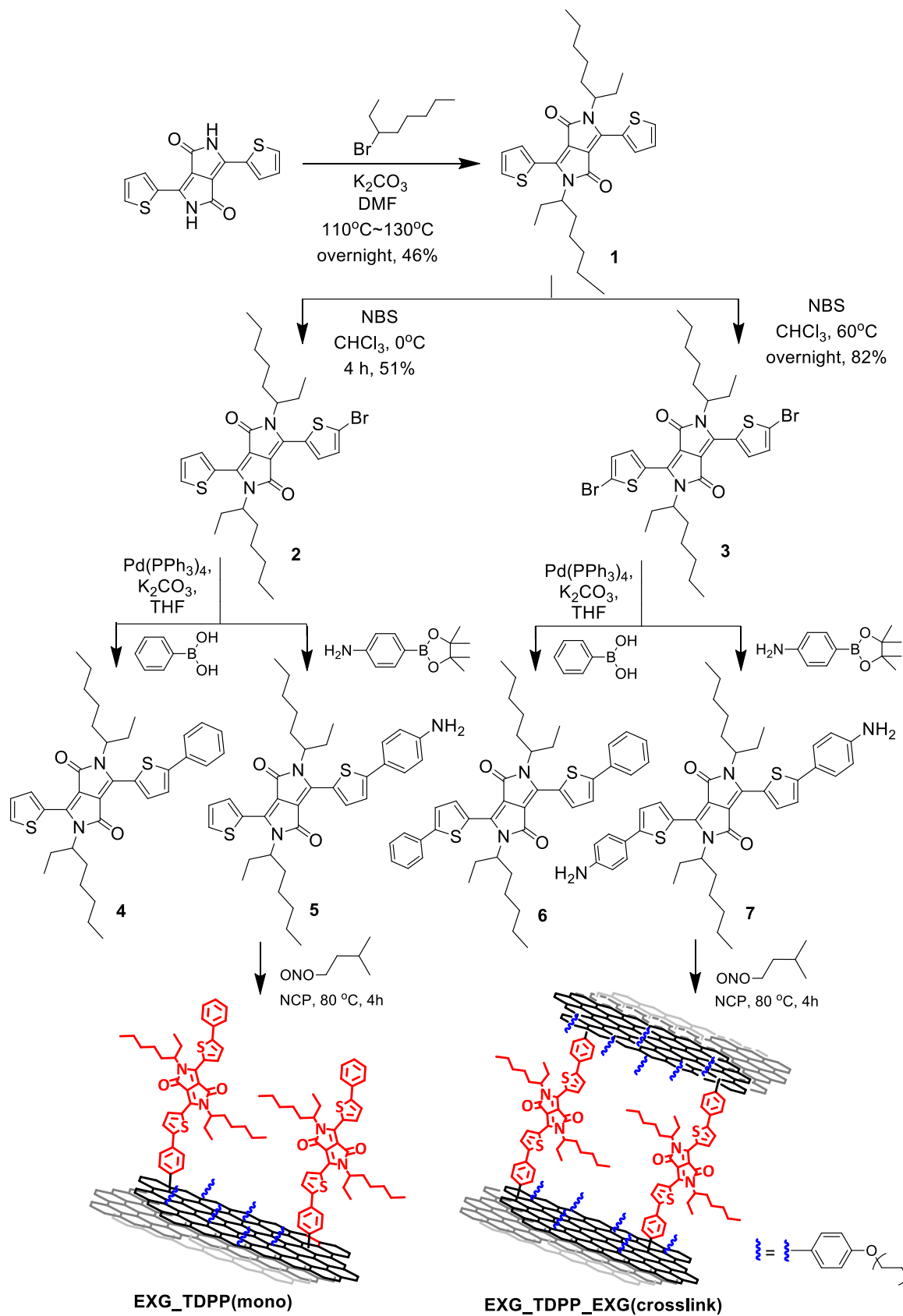
Figure 3.15. Synthesis route of the TDPP derivatives and functionalized on EXG flakes.

Synthesis of 2,5-di(octan-3-yl)-3,6-di(thiophen-2-yl)pyrrolo[3,4-c]pyrrole-1,4(2H, 5H)-dione (compound 1)

Under inert atmosphere, 3,6-di(thiophen-2-yl)pyrrolo[3,4-c]pyrrole-1,4(2H,5H)-dione (3.90 g, 13 mmol) was dissolved in 200 ml DMF in a 500 mL double neck flask. K_2CO_3 (5.38 g, 39 mmol) was added to the flask and the mixture was heated to 110 ^{o}C for 30 min. Then 2-Ethylhexyl bromide (5.76 mL, 32.5 mmol) was added dropwise in 2 h, the mixture was keep stirring at 110 ^{o}C for 1 h then heated to 130 ^{o}C and refluxed overnight. The reaction contents were cooled to room temperature and poured into 200 mL DCM, after washed by water for 5 times, the organic phase was dried with anhydrous $MgSO_4$ and solvent was removed under vacuum to give a dark taupe oil. The crude compound was purified by silica column-chromatography eluting with ethyl acetate: hexane = 1:10 ∼ 1:5 (*v/v*), a dark red solid was obtained after the solvent was removed under vacuum. (3.1 g, yielded ∼ 46%).

^{1}H-NMR and ^{13}C-NMR characterization were given as followed: ^{1}H-NMR (CDCl3, 300MHz) δ (ppm): 8.88 (d, 3Hz, 2H), 7.62 (d, 3Hz, 2H), 7.25 (m, 2H), 4.04 (m, 2H), 1.89~1.25 (m, 20H), 0.89~0.94 (m, 12H). ^{13}C-NMR (CDCl$_3$, 75 MHz) δ (ppm): 162.10, 140.77, 135.57, 130.83, 130.18, 128.75, 108.30, 46.30, 39.44, 28.72, 23.91, 23.40, 18.31,14.34, 10.83. Elem. Anal. Calcd for C30H40N2O2S2 (%): C, 68.66; H, 7.68; N, 5.34; O, 6.10; S, 12.22. Found: C, 68.82; H, 7.43; N, 5.44; O, 6.08; S, 12.23. ESI-MS Calcd for: 525.25. Found: 525.41

Synthesis of 3-(5-bromothiophen-2-yl)-2,5-di(octan-3-yl)-6-(thiophen-2-yl)pyrrolo[3,4-c]pyrrole-1,4(2H,5H)-dione (compound 2)

Under inert atmosphere, in a 500 mL double neck flask compound **1** (1.36 g, 2.6 mmol) was dissolved in 100 mL CHCl$_3$, NBS (1.16 g, 6.5 mmol) in 50 mL CHCl$_3$ was added dropwise in dark at 0 ^{o}C. The reaction was stirred for 4 h then quenched with 100 mL water, the mixture was extracted with CHCl$_3$. The organic phase was collected and dried over anhydrous $MgSO_4$, after filtered and evaporated to dryness, the crude product was purified by column chromatography on silica gel eluting with ethyl acetate / petroleum ether = 1 / 10 (*v / v*) to give dark red solid (0.8 g, yield ∼ 51%).

^{1}H-NMR and ^{13}C-NMR characterization were given as followed: ^{1}H-NMR (CDCl3, 300MHz) δ (ppm): 8.89 (d, 3Hz, 1H), 8.62 (d, 6Hz, 1H), 7.63 (d, 6Hz, 1H), 7.26 (m, 1H), 7.21

(m, 1H), 4.06 (m, 2H), 1.83 ~1.26 (m, 20H), 0.97 (m, 12H).^{13}C-NMR (CDCl$_3$, 75 MHz) δ (ppm) =162.00, 161.83, 141.30, 141.23, 139.29, 135.86, 135.41, 131.72, 131.61, 131.15, 130.10, 128.82, 118.94, 108.69, 46.27, 39.47, 30.53, 28.69, 23.89, 23.37, 14.34, 10.82. Elem. Anal. Calcd for C30H39BrN2O2S2 (%): C, 59.69; H, 6.51; Br, 13.24; N, 4.64; O, 5.30; S, 10.62. Found: C, 59.81; H, 6.41; Br, 13.04; N, 4.69; O, 5.19; S, 10.86. ESI-MS Calcd for: 604.68. Found: 604.91

Synthesis of 3,6-bis(5-bromothiophen-2-yl)-2,5-di(octan-3-yl)pyrrolo[3,4-c]pyrrole-1,4(2H, 5H)-dione (compound 3)

Under inert atmosphere, in a 500 mL double neck flask compound **1** (1.36 g, 2.6 mmol) was dissolved in 100 mL CHCl$_3$, NBS (1.16 g, 6.5 mmol) in 50 mL CHCl$_3$ was added dropwise in dark at 0 °C. The reaction was stirred for 1 h then heated to 60 °C and stirred overnight. After cooling to room temperature, the mixture was extracted with CHCl$_3$ and water. The organic phase was collected and dried with anhydrous MgSO$_4$, after filtered and evaporated to dryness, the crude product was purified by column chromatography on silica gel eluting with ethyl acetate / petroleum ether = 1 / 15 (*v / v*) to give dark red solid (1.76 g, yield ~ 82%).

^{1}H-NMR and ^{13}C-NMR characterization were given as followed: ^{1}H-NMR (CDCl3, 300MHz) δ (ppm): 8.63 (d, 3Hz, 2H), 7.22 (m, 6Hz, 2H), 3.85~3.93 (m, 12Hz, 2H), 1.20~1.85 (m, 20H), 0.85~0.88 (m, 12H). ^{13}C-NMR (CDCl3, 75 MHz) δ(ppm): 161.76, 139.76, 135.70, 131.81, 131.52, 119.34, 108.38, 46.36, 39.45, 30.52, 28.67, 23.92, 23.36, 14.34, 10.80. Elem. Anal. Calcd for C30H38Br2N2O2S2 (%): C, 52.79; H, 5.61; Br, 23.41; N, 4.10; O, 4.69; S, 9.40. Found: C, 52.67; H, 5.82; Br, 23.11; N, 4.41; O, 4.78; S, 9.21. ESI-MS Calcd for: 683.57. Found: 683.78.

Synthesis of 2,5-di(octan-3-yl)-3-(5-phenylthiophen-2-yl)-6-(thiophen-2-yl)pyrrolo [3,4-c]pyrrole-1,4(2H,5H)-dione (compound 4)

In a 250 mL double neck flask, Compound **2** (0.32 g, 0.53 mmol), 4-phenylboronic acid (0.71 g, 0.58 mmol), Pd(PPh$_3$)$_4$ (0.013 g, 0.011 mmol) and 10 mL 2M K$_2$CO$_3$ solution were added into the mixture of THF (30mL) under nitrogen. The resulting mixture was refluxed under stirring and nitrogen protection overnight. After cooling down to room temperature,

100 mL of chloroform was added, and the organic phase was washed with water and dried over MgSO$_4$. The solvent was operated under vacuum to give a dark purple crude, the crude product was purified by column chromatography using silica gel eluting with ethyl acetate / petroleum ether = 1 / 5 ~ 1/3 (v / v) to give a dark red purple shiny crystalline solid. (0.11 g, ~ 35%).

^{1}H-NMR and ^{13}C-NMR characterization were given as followed: ^{1}H-NMR (CDCl3, 300MHz) δ (ppm): 8.96 (d, 6Hz, 1H), 8.88 (d, 3Hz, 1H), 7.25~7.69 (m, 8H), 4.02~4.10 (m, 2H), 1.92 (m, 2H), 1.89 (m, 4H), 1.25~1.36 (m, 14H), 0.85~0.93 (m, 12H). ^{13}C-NMR (CDCl3,75Hz) δ (ppm): 162.18, 162.03, 150.14, 140.71, 137.20, 136.13, 135.46, 133.53, 132.11, 130.26, 129.57, 129.11, 128.75, 126.51, 125.84, 113.84, 108.36, 46.25, 34.57, 31.92, 30.67, 23.40, 22.99, 14.44, 10.91. Elem. Anal. Calcd for C36H44N2O2S2 (%): C, 71.96; H, 7.38; N, 4.66; O, 5.33; S, 10.67. Found: C, 72.04; H, 7.43; N, 4.22; O, 5.08; S, 11.23. ESI-MS Calcd for: 601.88. Found: 601.91

Synthesis of 3-(5-(4-aminophenyl)thiophen-2-yl)-2,5-di(octan-3-yl)-6-(thiophen-2-yl)-pyrrolo[3,4-c]pyrrole-1,4(2H,5H)-dione (compound 5)

In a 250 mL double neck flask, Compound **2** (0.36 g, 0.53 mmol), 4-aminophenylboronic acid pinacol ester (0.26 g, 1.17 mmol), Pd(PPh$_3$)$_4$ (0.013 g, 0.011 mmol) and 10 mL 2M K$_2$CO$_3$ solution were added into the mixture of THF (30mL) under nitrogen. The resulting mixture was refluxed under stirring and nitrogen protection overnight. After cooling down to room temperature, 100 mL of chloroform was added, and the organic phase was washed with water and dried over MgSO$_4$. The solvent was operated under vacuum to give a dark purple crude, the crude product was purified by column chromatography on silica gel eluting with ethyl acetate / petroleum ether = 1 / 5 ~ 1/3 (v / v) to give a dark purple shiny crystalline solid. (0.14 g, ~ 40%).

^{1}H-NMR and ^{13}C-NMR characterization were given as followed: ^{1}H-NMR (DMSO, 500MHz) δ (ppm) =8.92 (d, 3Hz, 1H), 8.70 (d, 6Hz, 1H), 8.05 (d, 3Hz, 1H),7.75 (d, 3Hz, 1H) 7.50 (d, 6Hz, 2H), 7.37-7.39 (m, 1H), 6.65 (m, 2H), 5.73 (S, 2H), 3.94~4.00 (m, 2H), 1.73 (m, 2H), 1.20~1.31 (m, 18H), 0.80-0.83 (m, 12H). ^{13}C-NMR (DMSO, 125MHz) δ (ppm): 161.47, 160.92, 152.85, 150.98, 140.56, 138.26, 137.71, 134.34, 132.51, 129.81, 128.88, 127.66, 125.20, 122.27, 120.11, 114.46, 107.61, 106.37, 45.53, 30.22, 28.48, 28.19, 23.64, 22.90,

22.84, 14.28, 14.22, 10.77. Elem. Anal. Calcd for C36H45N3O2S2 (%): C, 70.20; H, 7.36; N, 6.82; O, 5.20; S, 10.41. Found: C, C, 70.34; H, 7.14; N, 6.77; O, 5.31; S, 10.44. ESI-MS Calcd for: 616.89. Found: 616.91.

Synthesis of 2,5-di(octan-3-yl)-3,6-bis(5-phenylthiophen-2-yl)pyrrolo[3,4-c]pyrrole-1,4(2H,5H)-dione (compound 6)

In a 250 mL double neck flask, Compound **3** (0.32 g, 0.53 mmol), 4-phenylboronic acid (0.14 g, 1.17 mmol), Pd(PPh3)4 (0.023 g, 0.02 mmol) and 10 mL 2M K2CO3 solution were added into the mixture of THF (30mL) under nitrogen. The resulting mixture was refluxed under stirring and nitrogen protection for 40 h. After cooling down to room temperature, 100 mL of chloroform was added, and the organic phase was washed with water and dried over MgSO4. The solvent was operated under vacuum to give a dark purple crude, the crude product was purified by column chromatography on silica gel eluting with ethyl acetate / petroleum ether = 1 / 5 ∼ 1/3 (v / v) to give a dark red purple shiny crystalline solid. (0.15 g, ∼ 42%).

^{1}H-NMR and ^{13}C-NMR characterization were given as followed: ^{1}H-NMR (CDCl3, 300MHz) δ (ppm): 8.96 (d, 6Hz, 2H), 7.69 (d, 9Hz, 2H), 7.35~7.47 (m, 10H), 4.09 (m, 2H),1.94 (m, 2H), 1.39-1.25 (m, 18H), 0.94-0.86 (m, 12H). ^{13}C-NMR (CDCl3, 75MHz) δ (ppm): 162.06, 149.98, 140.23, 137.12, 133.55, 129.50, 129.20, 129.14, 126.48, 124.82, 108.56, 46.35, 39.60, 30.72, 28.93, 24.07, 23.46, 14.41, 10.95. Elem. Anal. Calcd for C42H48N2O2S2 (%): C, 74.52; H, 7.15; N, 4.14; O, 4.73; S, 9.47. Found: C, 74.52; H, 7.15; N, 4.14; O, 4.73; S, 9.47. ESI-MS Calcd for: 677.97. Found: 677.53

Synthesis of 3,6-bis(5-(4-aminophenyl)thiophen-2-yl)-2,5-di(octan-3-yl)pyrrolo[3,4-c]pyrrole-1,4(2H,5H)-dione (compound 7)

In a 250 mL double neck flask, Compound **3** (0.34 g, 0.5 mmol), 4-aminophenylboronic acid pinacol ester (0.24 g, 1.1 mmol), Pd(PPh3)4 (0.023 g, 0.02 mmol) and 10 mL 2M K2CO3 solution were added into the mixture of THF (30mL) under nitrogen. The resulting mixture was refluxed under stirring and nitrogen protection for 48 h. After cooling down to room temperature, 100 mL of chloroform was added, and the organic phase was washed with water and dried over MgSO4. The solvent was operated under vacuum to give a dark

purple crude, the crude product was purified by column chromatography on silica gel eluting with ethyl acetate / petroleum ether = 1 / 5 ~ 1/3 (*v / v*) to give a dark purple shiny crystalline solid. (0.17 g, ~ 48 %).

^{1}H-NMR and ^{13}C-NMR characterization were given as followed: ^{1}H-NMR (DMSO, 500MHz) δ (ppm) : 8.86 (d, 3Hz, 2H), 7.53~7.48 (m, 6H), 6.65 (m, 4H), 5.70 (S, 4H), 3.99 (m, 2H), 1.84(m, 2H), 1.07~1.32 (m, 18H), 0.80~0.87 (m, 12H). ^{13}C-NMR (DMSO, 125MHz) δ (ppm): 161.16, 151.97, 150.82, 138.82, 136.94, 127.56, 125.53, 122.18, 120.26, 114.46, 106.79, 40.48, 39.07, 30.25, 28.50, 23.75, 22.92, 14.29, 10.80. Elem. Anal. Calcd for C42H50N4O2S2 (%): C, 71.35; H, 7.13; N, 7.92; O, 4.53; S, 9.07. Found: C, 71.35; H, 7.13; N, 7.92; O, 4.53; S, 9.07. ESI-MS Calcd for: 708.00. Found: 708.15.

3.4.3 Synthesis of functionalized EXG hybrids with TDPP dyes

EXG (10 mg, 0.84 mmol of C) was suspended in *N*-Cyclohexylpirrolidone (15 mL) in a 250 mL double neck flask under nitrogen. 260 mg(0.42 mmol) aniline compound **5 (7,** 300 mg) was then added to the stirring suspension of EXG and the mixture was heated up to 80 ℃. After reaching the desired temperature, isopentyl nitrite (55 µL, 0.42 mmol) was further added and the reaction mixture was left to stir for 4 h. After cooling down to room temperature, methanol (200 mL) was added and stirring was continued for 15 min. The functionalized EXG materials was then recovered by filtration (using Fluorophore TM membrane filters, 0.2 mm, Merck Millipore) and further washed with methanol (100 mL). After drying the material on the filter, the functionalized EXG was obtained.

3.5 Bibliography

[1] V. G. Kravets, A. V. Kabashin, W. L. Barnes, A. N. Grigorenko. Chemical Reviews. 2018, 118 (12), 5912-5951.

[2] a) B. Zhao, M. Zhao, Z. M. Zhang. Appl. Phys. Lett. 2014, 105, 031905. (b) B. Y. Zhang, T. Liu, B. Meng, X. Li, G. Liang, X. Hu, Q. J. Wang. Nat Commun. 2013, 4, 1811.

[3] a) S. Militzer, T. M. P. Tran, P. J. Mésini, A. Ruiz‑Carretero, Chem Nano Mat. 2018, 4, 790 − 795; b) S. Ghosh, S. Das, A. Saeki, V. K. Praveen, S. Seki, A. Ajayaghosh, Chem Nano Mat., 2018, 4, 831 − 836; c) M. Castelaí, H. Salavagione, J. L. Segura. Org. Lett., 2012, 14 (11), 2798–2801; d); e) A. Tang, C. Zhan, J. Yao, E. Zhou, Adv. Mater. 2017, 29, 1600013.

[4] a) S. Y. Qu, H. Tian. Chem. Commun., 2012,48, 3039-3051; b) H. Lin, Z. Xu, L. Zhang, X. Yang, Q. Ju, L. Xue, L. Zhou, S. Zhuo, Y. Wu, New J. Chem., 2017, 41, 4302.

[5] H. Lin, Z. Xu, L Zhang, X. Yang, Q. Ju, L. Xue, J. Zhou, S. Zhuo, Y W. New J. Chem., 2017, 41, 4302-4307.

[6] A. Sinitskii, A. Dimiev, D. A. Corley, A. A. Fursina, D. V. Kosynkin, J. M. Tour, ACS Nano, 2010, 4, 1949–1954.

[7] a) L. Rout, A. Kumar, R. S. Dhaka, G. N. Reddy, S. Giri, P. Dash. Appl Catal A-Gen. 2017, 538, 107–122; b) M. Hu, K. S. Hui, K. N. Hui. Chem. Eng. J, 2014, 254, 237–244; c) H. Einaga, S. Futamura, J. Catal, 2004, 227, 304–312.

[8] D. Souza, F. Chitta, R. Sandanayaka, A. S. D. Subbaiyan, N. K. D'Souza NK, L. Araki, Y. O. Ito. J Am Chem Soc, 2007, 129, 15865–15871.

[9] (a) A. C. Ferrari, J. C. Meyer, V. Scardaci, C. Casiraghi, M. Lazzeri, F. Mauri, S. Piscanec, D. Jiang, K. S. Novoselov, S. Roth, A. K.Geim, Phys. Rev. Lett., 2006, 97, 187401; (b) M. A. Pimenta, G. Dresselhaus, M. S. Dresselhaus, L. G. Cancado, A. Jorio, R. Saito, Phys. Chem. Chem. Phys., 2007, 9, 1276.

[10] C. H. Woo, P. M. Beaujuge, T. W. Holcombe, O. P. Lee, J. M. J. Fréchet. J. Am. Chem. Soc., 2010, 132 (44), 15547–15549.

3.6 Appendix
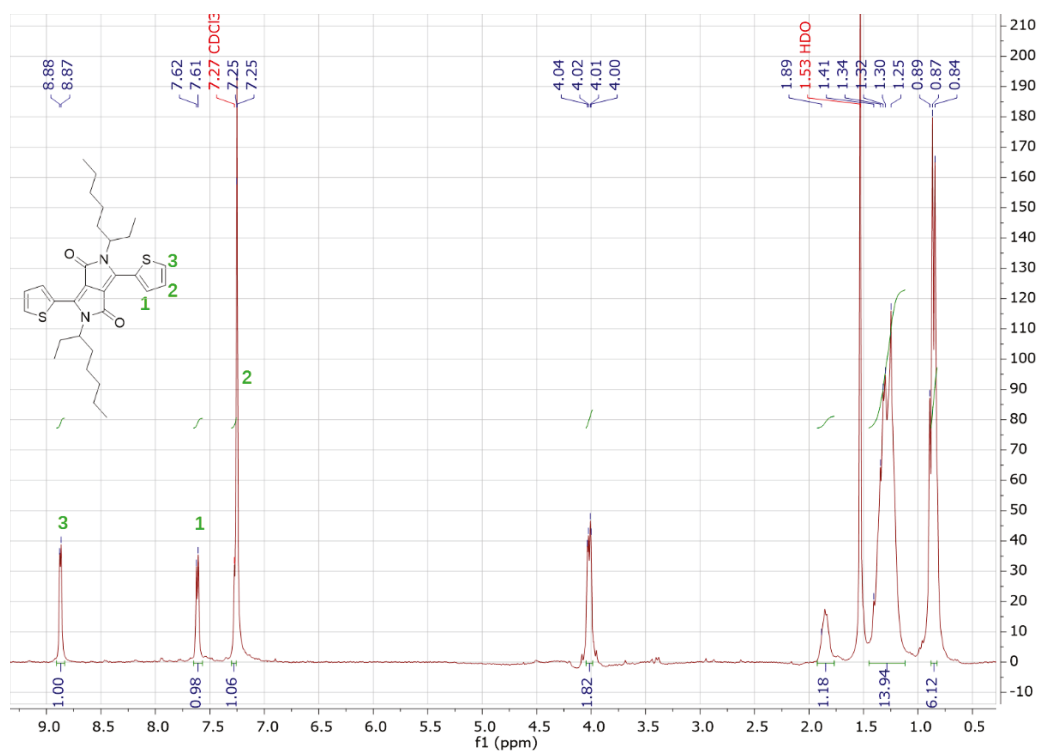
Figure 3.16. ^{1}H-NMR (CDCl$_3$, 300MHz) of compound **1**
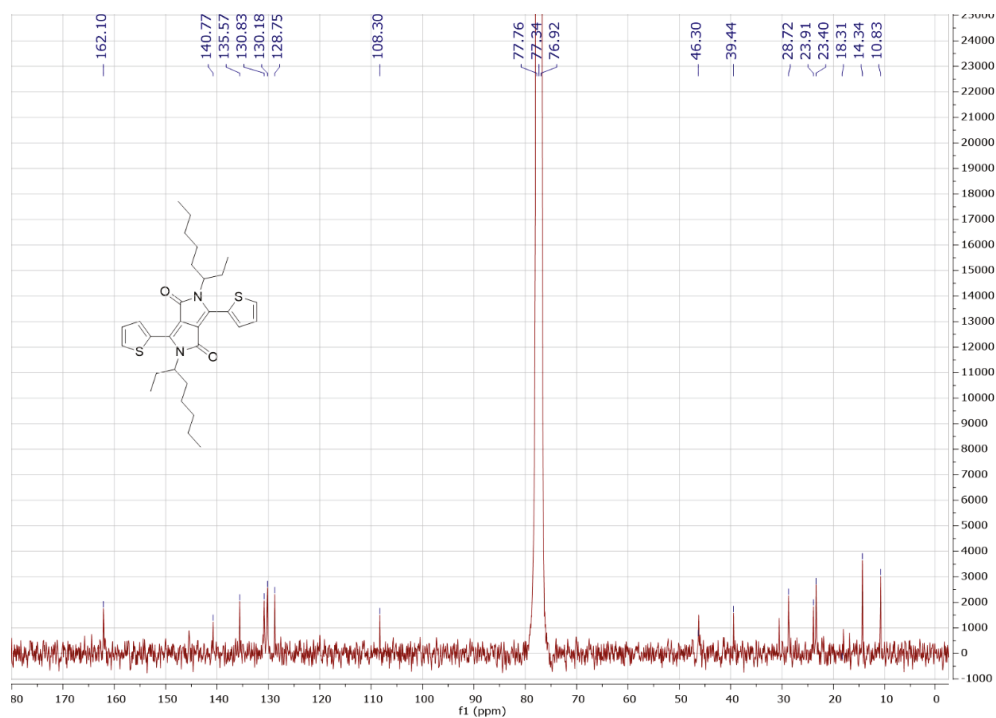
Figure 3.17. ^{13}C-N NMR (CDCl$_3$, 75MHz) of compound **1**
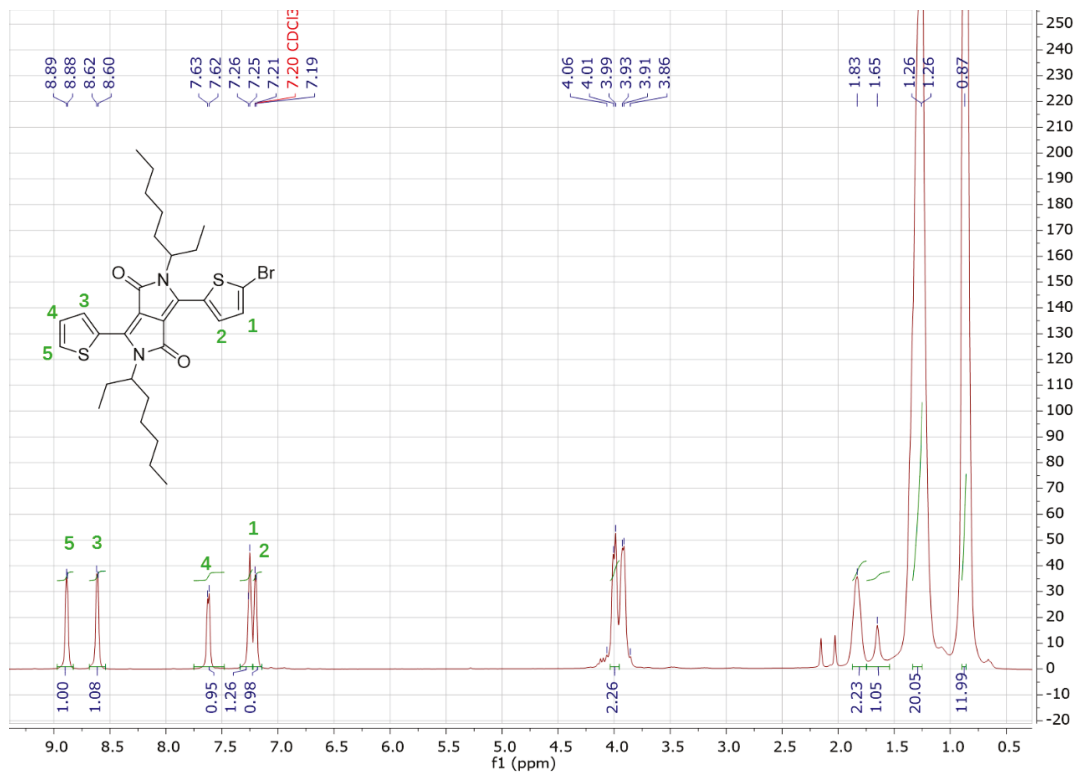
Figure 3.18. ^{1}H-NMR (CDCl$_3$, 300MHz) of compound **2**
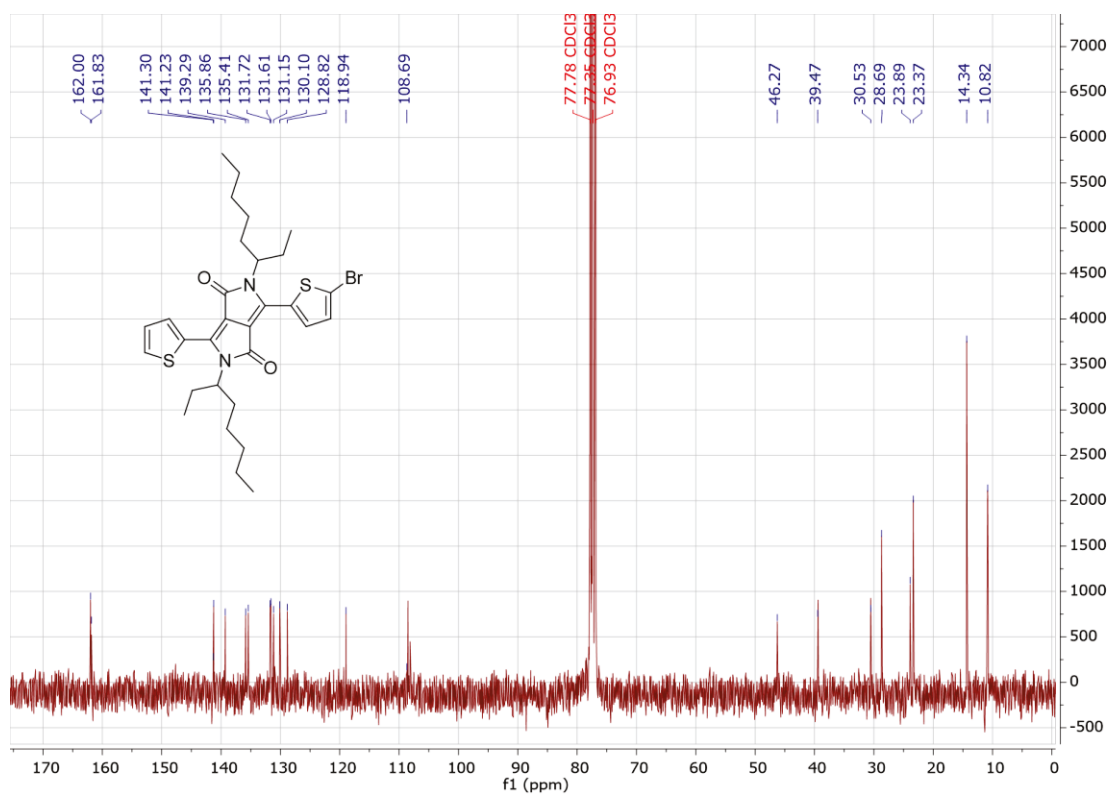
Figure 3.19. ^{13}C-NMR (CDCl$_3$, 75MHz) of compound **2**
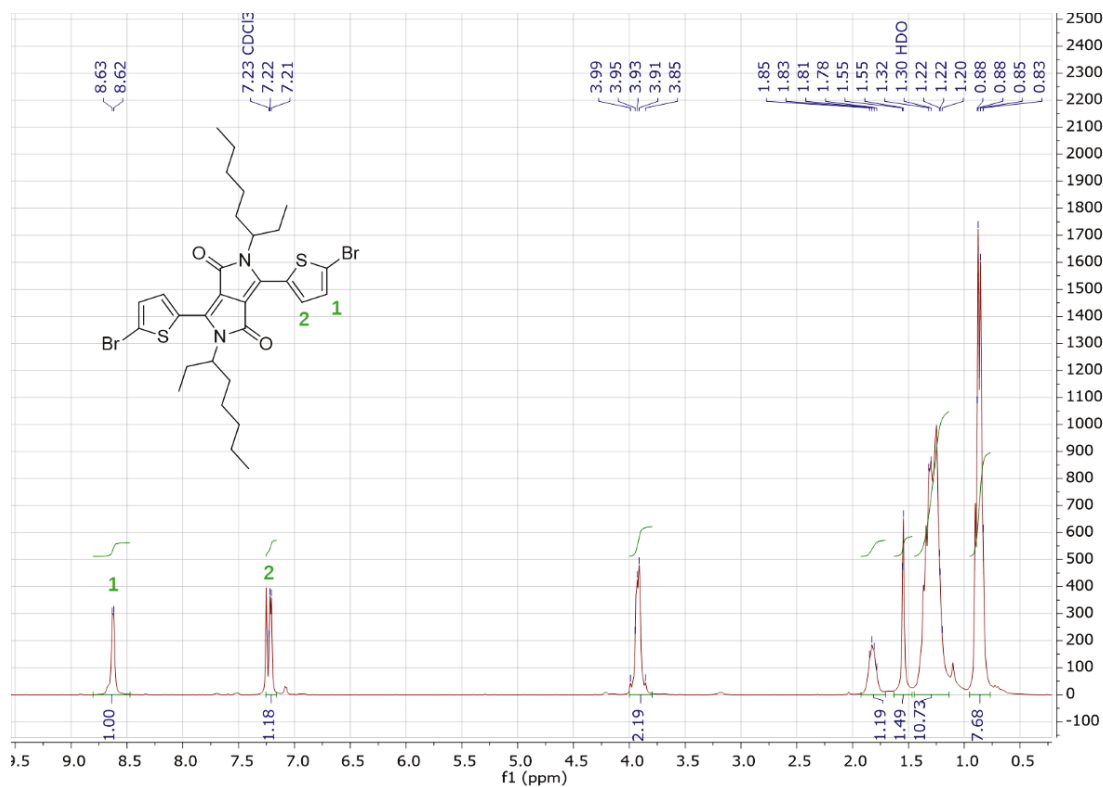
Figure 3.20. ^{1}H-NMR (CDCl$_3$, 300MHz) of compound **3**
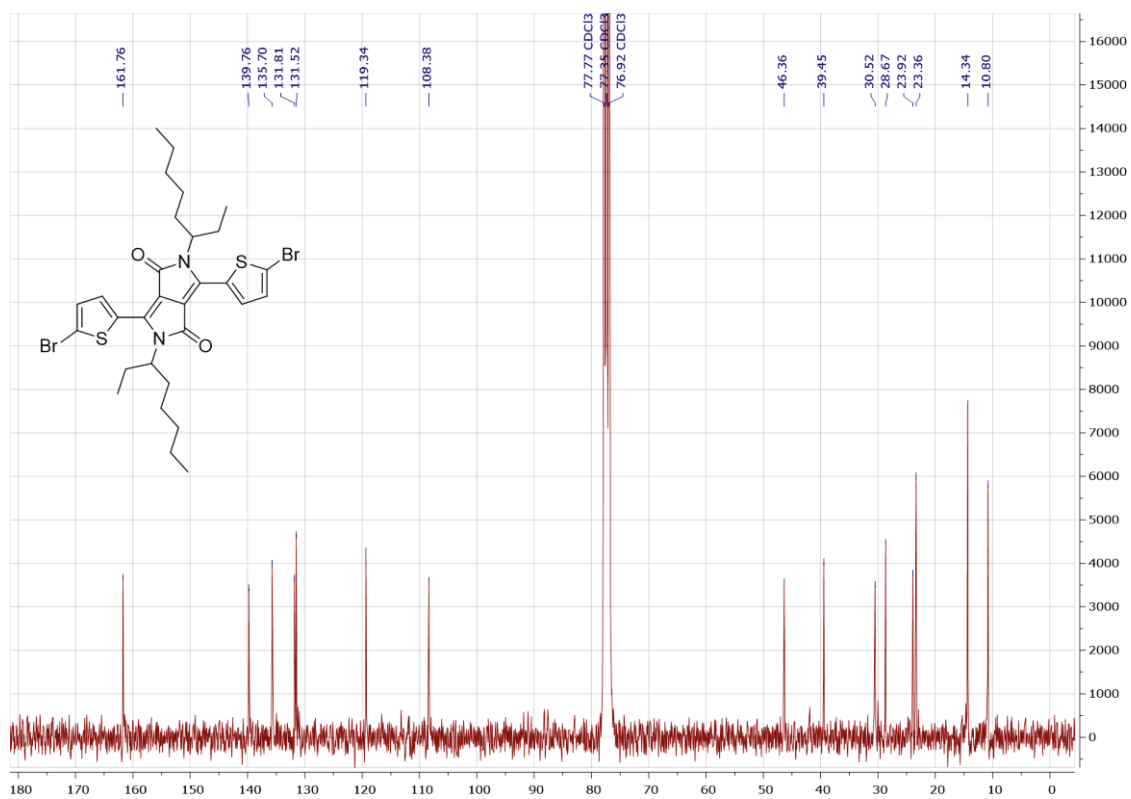
Figure 3.21. ^{13}C-NMR (CDCl$_3$, 75MHz) of compound **3**
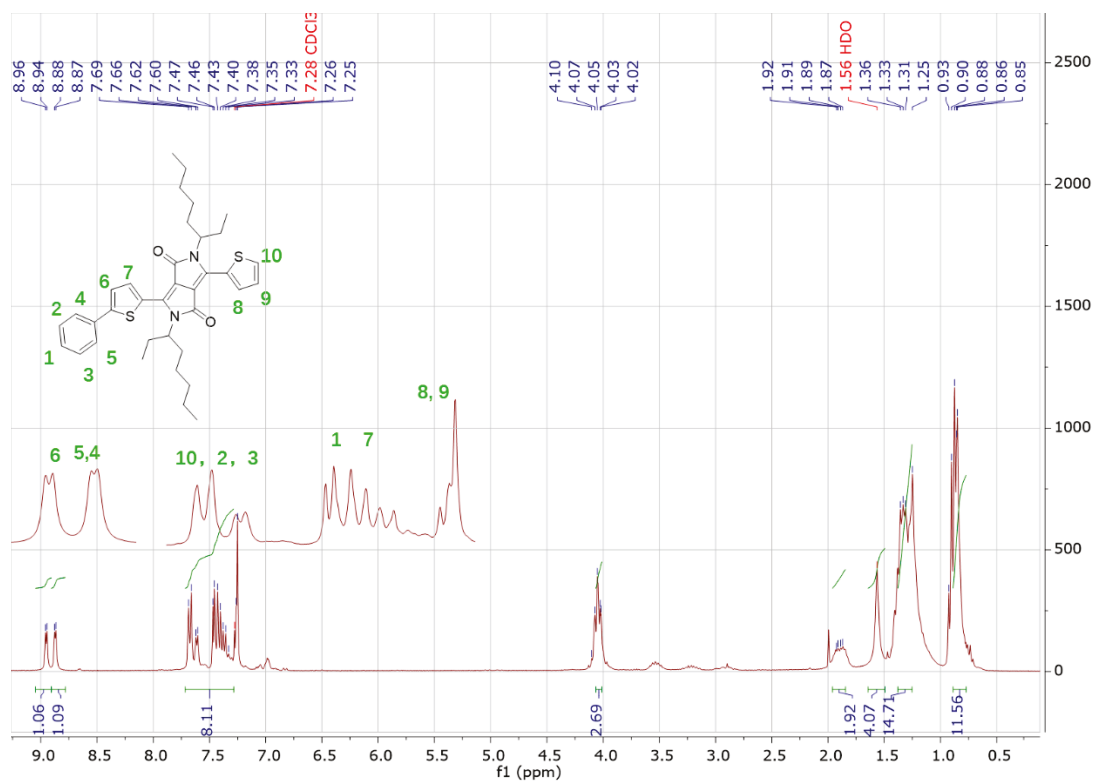
Figure 3.22. ^{1}H-NMR (CDCl$_3$, 300MHz) of compound **4**
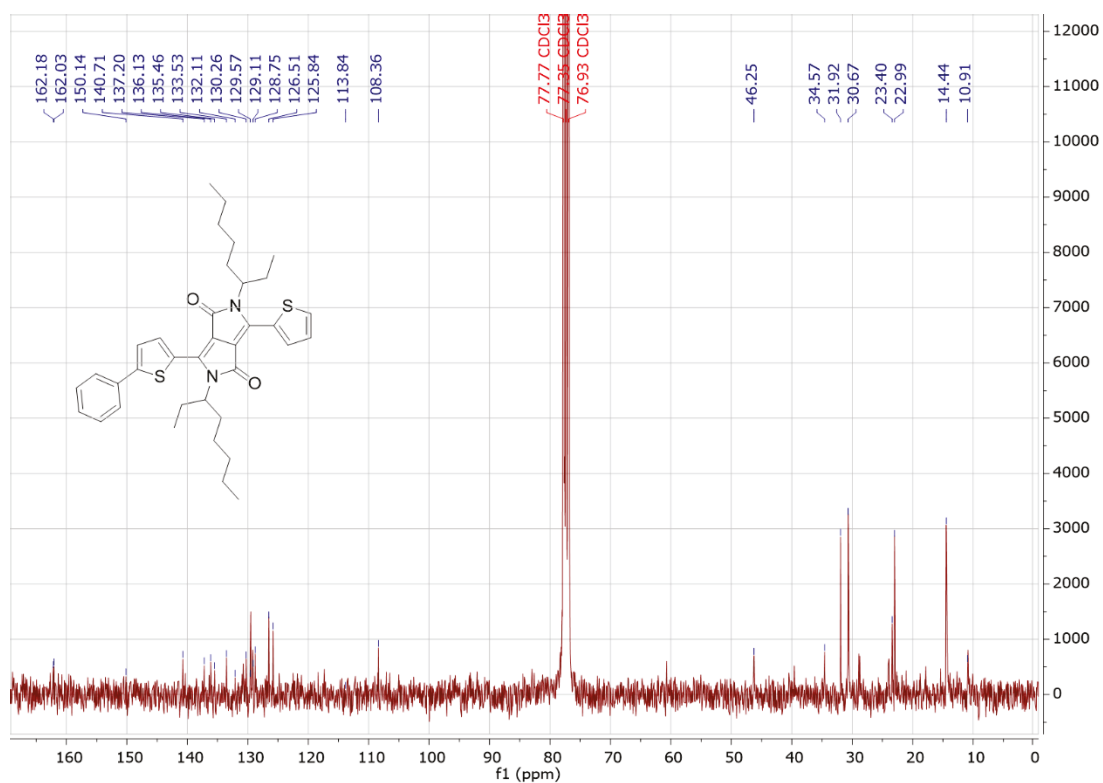
Figure 3.23. ^{13}C-NMR (CDCl$_3$, 75MHz) of compound **4**
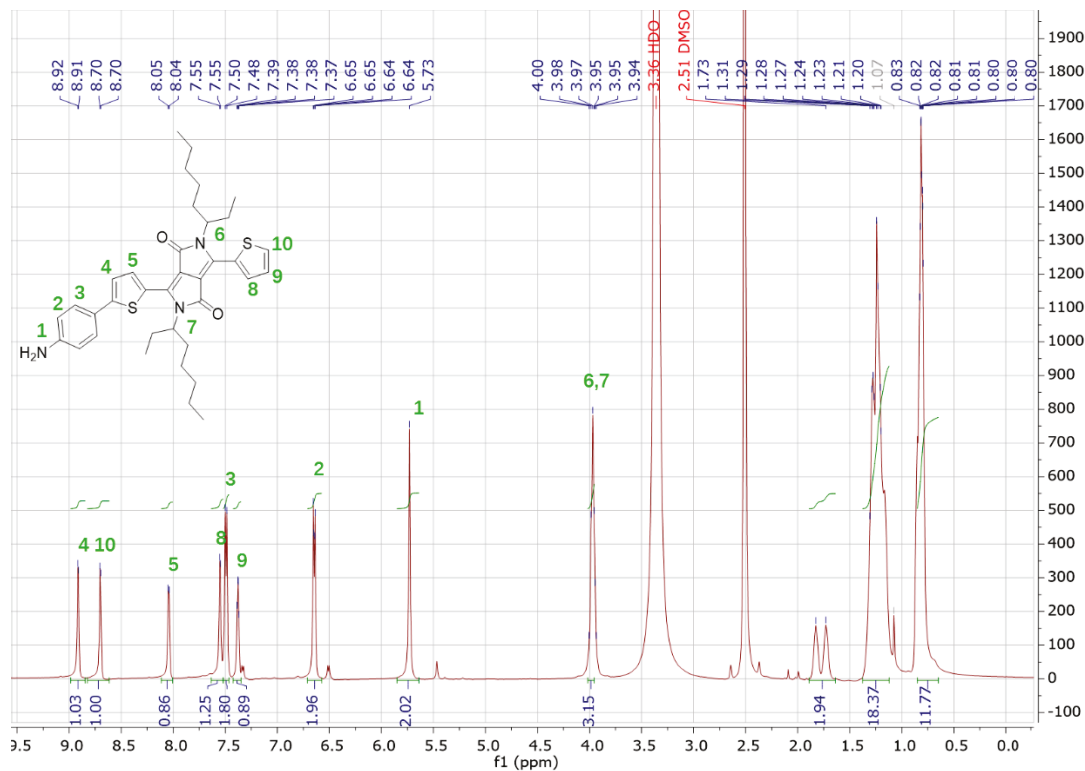
Figure 3.24. ^{1}H-NMR (DMSO, 500MHz) compound **5**
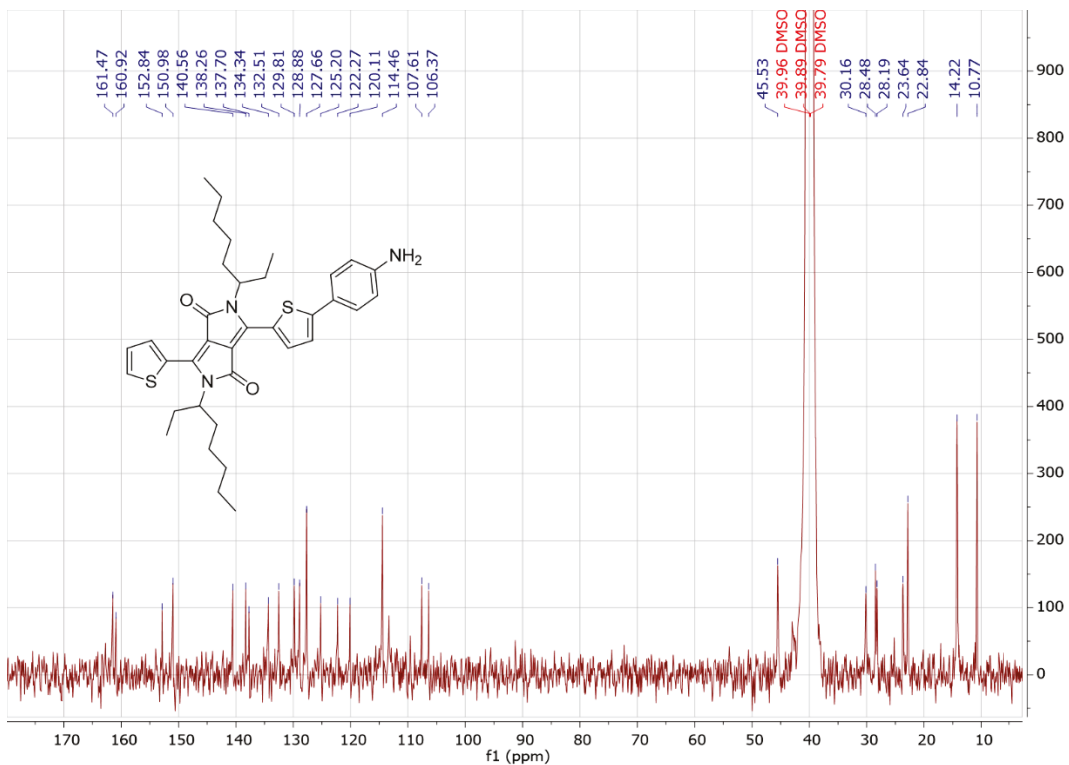
Figure 3.25. ^{13}C-NMR (DMSO, 125MHz) of compound **5**

74
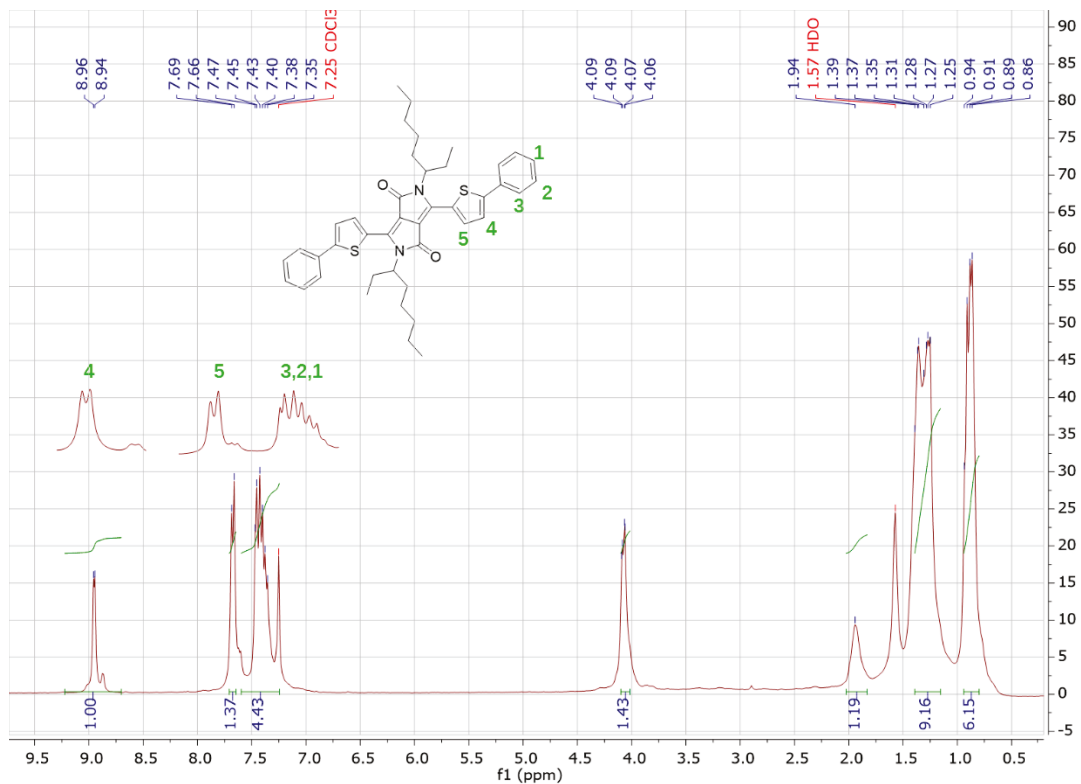
Figure 3.26 ^{1}H-NMR (CDCl$_3$, 300MHz) of compound **6**
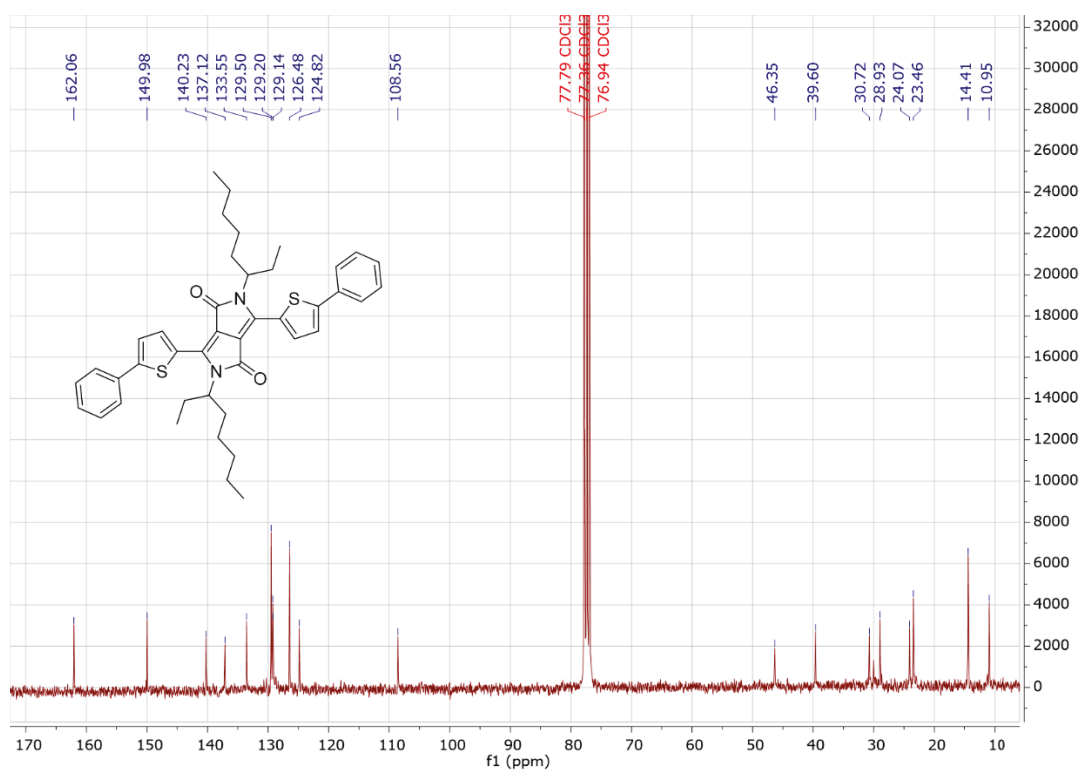
Figure 3.27. ^{13}C-NMR (CDCl$_3$, 75MHz) of compound **6**
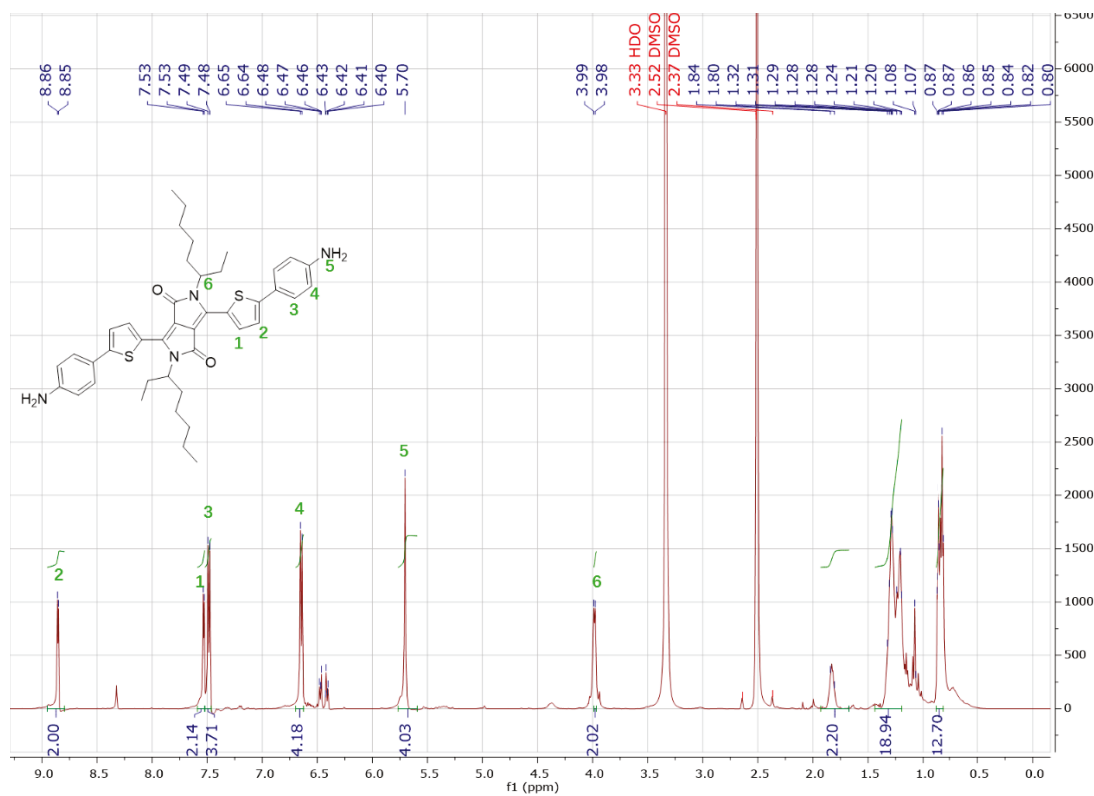
Figure 3.28. ^{1}H- NMR (DMSO, 500MHz) of compound **7**
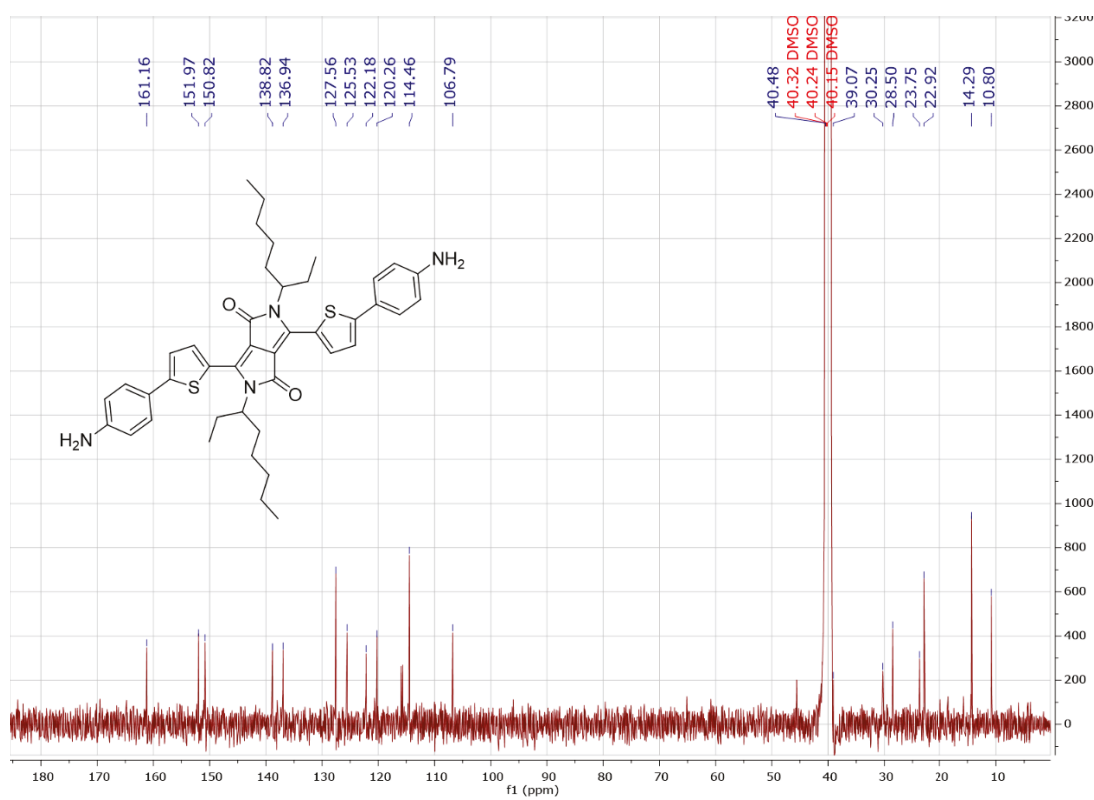
Figure 3.30. ^{13}C-N MR (DMSO, 125MHz) of compound **7**

CHAPTER 4

CONCLUSION

4.CONCLUSION

In this thesis, a facile, low-cost and efficient approach to generate few layers graphene was improved. After mechanical exfoliation and a few centrifugation steps, big flakes of few layers graphene (**EXG**) can be obtained. With appropriate centrifuge, while the EXG3000 flakes mainly contain 2~5 layers graphene which can be highly functionalized.

The as-prepared **EXG** flakes were functionalized with **DPP**-based molecules applying a cross-linking protocol. The resulting hybrid can be seen as graphite-like polymer with good filming properties and it has good solubility in organic solvents, such as DMF, toluene, DCM, chloroform and acetone. Also, a wide near infrared light absorption from 500 nm ~ 800 nm was improved through functionalization. Although the fluorescence was intensively quenched due to the strong fluorescent resonance energy transfer between the dye and graphene, this system is planned to be tested as third component in a **P3HT**: **PCBM** BHJ blend for OPVs.